STATUS OF THESIS

Title of thesis | Quantification and Classification of Microporosity in A Miocene Carbonate Platform of Central Luconia, Offshore Sarawak, Malaysia and Its Effects on Reservoir Properties.

I **MD HABIBUR RAHMAN**

hereby allow my thesis to be placed at the Information Resource Center (IRC) of Universiti Teknologi PETRONAS (UTP) with the following conditions:

1. The thesis becomes the property of UTP
2. The IRC of UTP may make copies of the thesis for academic purposes only
3. This thesis is classified as

[√] Confidential

[ ] Non-confidential

If this thesis is confidential, please state the reason:

The thesis is covered by a 'Confidentiality Agreement' with PETRONAS, established on 4th September, 2008.

The content of the thesis will remain confidential for 1 year.

Remarks on disclosure:

Signature of Author

Permanent Address:
17/8 K. M. Das Lane, Tikatuli;
Dhaka: 1203, Bangladesh

Date: 09 Sep 2011

Endorsed by

Signature of the Supervisor

Prof. Dr. Bernard J. M. Pierson

Date: 09/09/2011

UNIVERSITI TEKNOLOGI PETRONAS

QUANTIFICATION AND CLASSIFICATION OF MICROPOROSITY IN A MIOCENE CARBONATE PLATFORM OF CENTRAL LUCONIA, OFFSHORE SARAWAK, MALAYSIA AND ITS EFFECTS ON RESERVOIR PROPERTIES

by

MD HABIBUR RAHMAN

The undersigned certify that they have read, and recommend to The Postgraduate Studies Programme for acceptance this thesis for the fulfilment of the requirements for the degree stated.

Signature : _____

Main Supervisor : Professor Dr. Bernard J. M. Pierson

Signature : _____

Co-Supervisor : Assoc. Prof. Wan Ismail Wan Yusoff

Signature : _____

Head of Department : Assoc. Prof. Abdul Hadi Abd Rahman

Assoc. Prof. Dr Abdul Hadi B. Abd Rahman
Head
Faculty of Geosciences &
Petroleum Engineering
Universiti Teknologi PETRONAS

Date : 9-9-2011

QUANTIFICATION AND CLASSIFICATION OF MICROPOROSITY IN A MIOCENE CARBONATE PLATFORM OF CENTRAL LUCONIA, OFFSHORE SARAWAK, MALAYSIA AND ITS EFFECTS ON RESERVOIR PROPERTIES

by

MD HABIBUR RAHMAN

A Thesis
Submitted to the Postgraduate Studies Programme
as a Requirement for the Degree of

MASTER OF SCIENCE
GEOSCIENCE AND PETROLEUM ENGINEERING
UNIVERSITI TEKNOLOGI PETRONAS
BANDAR SRI ISKANDAR,
PERAK

SEPTEMBER 2011

DECLARATION OF THESIS

Title of thesis | Quantification and Classification of Microporosity in A Miocene Carbonate Platform of Central Luconia, Offshore Sarawak, Malaysia and Its Effects on Reservoir Properties.

I **MD HABIBUR RAHMAN**

hereby declare at the thesis is based on my original work except for quotations and citations which have been duly acknowledged. I also declare that it has not been previously or concurrently submitted for any other degree at UTP or other institutions.

Witnessed by

Signature of Author

Signature of the Supervisor

Prof. Dr. Bernard J. M. Pierson

Permanent Address:
17/8 K. M. Das Lane, Tikatuli;
Dhaka: 1203, Bangladesh

Date: 09 Sep 2011

Date: 09/09/2011

This work is dedicated to my dad and mom, Md Mostofa and Jahanara Begum; I know there is no need to say, I love you more than anything else.

"It would be an unsound fancy and self-contradictory to expect that things which have never yet been done can be done except by means which have never yet been tried."

-Francis Bacon (1561 – 1626

ACKNOWLEDGEMENT

I would like to distinguish the enduring and insightful support of my main supervisor for this study, Professor Dr. Bernard J. Pierson. Without his insightful motivation, I could not have finished this study. I am indebted to him for having continuous faith in my ability and for guiding me throughout the study. I thank A. P. Wan Ismail Wan Yusoff for being my co-supervisor.

This project was funded by a Shell grant to Universiti Teknologi PETRONAS. Without this gracious support, this project would not have been completed.

I would like to thank PETRONAS for giving permission to use the data. I am thankful to Sarawak Shell Berhad (SSB), for allowing me to study the cores, providing thin sections of excellent quality, and permission to access some confidential reports. Special thanks to Mr. Mohammad Yamin Ali from PETRONAS to share his publications on Central Luconia and Ting King King for sharing some data and information from SSB.

I deeply thank to Professor Dr. Rudy Swennen and Dr. Anneleen Foubert for their valuable suggestions and guidance while working at the Geology Section of the Earth and Environmental Sciences Department of the Katholieke Universiteit Leuven, Belgium. I am really grateful to Professor Rudy Swennen for his continuous guidance while using several microscopes and advising me throughout the study.

My family has stood by my side no matter what decision I made. I love them more deeply than words can express. Thank you mom and dad for all sacrifices you made along the way, thank you for instilling all your values and ethics into me. You are the greatest parents a kid could ask for. Thanks to my loving brother Sumon and caring sister Rozi for being so generous to me by sharing my responsibilities during my absence.

This project was mostly completed at SEACARL (South-East Asia Carbonate Research Laboratory) centre of UTP. I would like to express my gratitude to my friend Solomon Kassa for being such a generous companion during the tough days of the study. I would like to thank my colleagues at SEACARL: Aicha, Ani, Atilia, Dedeche, Haylay, Hissein, Jasmin, Rulli, Sara, and Syazwani.

ABSTRACT

The effects of microporosity on carbonates have been addressed in numerous publications; there is, however, almost no published literature on microporosity in the Miocene carbonates of Southeast Asia. This study aims at quantifying, and classifying microporosity in the Miocene carbonate reservoirs of Central Luconia, offshore Sarawak and at assessing its effects on reservoir properties.

Digital Image Analysis (DIA) of thin sections and scanning electron microscope (SEM) images are useful tools to quantify porosity in reservoir rocks. DIA technique uses thin section images taken under polarizing microscope, fluorescence microscope, and scanning electron microscope to estimate the amount of microporosity present in carbonate reservoirs.

The quantification of microporosity leads to determining its empirical relationships with permeability and sonic velocity. These relationships can be used for a better understanding of the reservoir system. This study on the Miocene carbonate reservoirs of Central Luconia, offshore Sarawak, Malaysia revealed an inverse relationship between microporosity and permeability. Permeability in the Miocene carbonate reservoir is reduced with an increase in microporosity at different depths in the same reservoir, characterized by the same amount of total porosity. The relationship between porosity and permeability in the Miocene carbonate reservoirs shows a better correlation when microporosity is considered and subtracted from the total porosity of the reservoir. Microporosity in the carbonate reservoirs of Central Luconia, offshore Sarawak, affects the elastic properties of the rock. Microporosity reduces the sonic velocity of the Miocene carbonate reservoirs. Microporosity can occur in grain, cement or matrix and it is related to the diagenetic history of the carbonate reservoirs. Depending on the crystallometry and morphometry of micrite particles, microporosity can vary both in amount and in nature (microporosity can reach up to 25% by volume of the rock or 80% of the total porosity of the reservoir).

Different kinds of micrite microtextures may produce different kinds of microporosity. This studyproposes a classification of micrite microtextures and microporosity. Four different types of micrite microtextures are classified in this study; these are rounded micrites, subrounded micrites, microrhombic and polyhedral micrites, and compact anhedral micrites. Four different types of micropores are classified based on their pore sizes, those are a) Very fine micropores (0.1 to 2 μm), b) Fine micropores (2 to 4 μm), c) Medium micropores (4 to 6 μm), and d) Coarse micropores (6 to 10 μm). The classification of microporosity allows its occurrence in carbonate reservoirs to be explained depending on micrite microtextures.

ABSTRAK

Kesan mikroporositi pada karbonat telah dikaji dalam banyak penerbitan, namun hampir tidak ada kajian yang diterbitkan tentang mikroporositi karbonat Miosen di Asia Tenggara. Kajian ini bertujuan untuk mengukur, dan mengklasifikasikan mikroporositi yang terdapat pada batuan takungan karbonat Miosen di Luconia Tengah, luar pesisir Sarawak serta kesan ke atas sifat-sifat batuan takungan.

Analisis Imej Digital (DIA) daripada keratan batuan nipis dan mikroskop imbasan elektron (SEM) adalah alat yang berguna untuk mengukur keliangan dalam batuan takungan. Teknik DIA menggunakan imej keratan batuan nipis yang diambil di bawah mikroskop polarisasi, mikroskop pendarfluor, dan mikroskop pengimbas elektron untuk menganggarkan jumlah mikroporositi yang hadir dalam batuan takungan karbonat.

Kuantifikasi daripada mikroporositi membawa kepada penentuan hubungan empirik antara mikroporositi dengan kebolehtelapan dan halaju sonik. Hubungan ini boleh digunakan untuk pemahaman yang lebih baik tentang sistem takungan. Kajian mengenai batuan takungan karbonat Miosen Luconia Tengah, luar pesisir Sarawak, Malaysia ini menunjukkan hubungan antara mikroporositi dan kebolehtelapan adalah saling bertentangan. Pada jumlan keliangan yang sama, kebolehtelapan dalam batuan karbonat takungan Miosen berkurangan dengan peningkatan mikroporositi pada kedalaman yang berbeza di dalam batuan takungan karbonat yang sama. Hubungan antara keliangan dan kebolehtelapan batuan takungan karbonat Miosen menunjukkan korelasi yang lebih baik apabila mikroporositi diambil kira dan ditolak daripada jumlah keliangan takungan itu. Mikroporositi dalam batuan takungan karbonat Luconia Tengah, luar pesisir Sarawak, mempengaruhi sifat kekenyalan batuan. Mikroporositi mengurangkan halaju sonik batuan takungan karbonat Miosen. Mikroporositi boleh terbentuk dalam simen, butiran atau matriks dan ia berkaitan dengan sejarah diagenetik batuan takungan karbonat. Bergantung kepada kristalometri

dan morfometri zarah mkrit, mikroporositi adalah berbagai dalam jumlah dan asal (mikroporositi boleh mencapai sehingga 25% isipadu batuan atau 80% jumlah porositi dalam batuan takungan). Pelbagai jenis mikrotekstur mikrit boleh menghasilkan pelbagai jenis mikroporositi. Kajian ini mencadangkan pengelasan mikrotekstur mikrit dan mikroporositi. Empat jenis mikrotekstur mikrit dapat dikelaskan dalam kajian ini; iaitu mikrit bulat, mikrit sub-bulat, mikrit mikrorhombik dan polihedral, dan mikrit anhedral padat. Empat jenis mikroporositi dikelaskan berdasarkan saiz liang, a) Sahgat halus (0.1 to 2 μm), b) Halus (2 to 4 μm), c) Sederhana (4 to 6 μm) dan d) Kasar (6 to 10 μm). Pengelasan mikroporositi membolehkan proses pembentukan batuan takungan karbonat dijelaskan berdasarkan kepada mikrotekstur mikrit.

TABLE OF CONTENTS

LIST OF TABLES

LIST OF FIGURES

CHAPTER 1

INTRODUCTION

1.1 Introduction

In contrast with siliciclastics, the generation and deposition of most carbonates is mostly controlled by biological activity (as much as 90%; Moore, 1989). Certain prerequisites are needed for carbonates to form (e.g., temperature, light, salinity, and the availability of nutrients), these parameters control their environment of deposition. As a result most carbonates are limited to shallow, tropical marine depositional settings. Carbonate sediments are composed of a small variety of minerals (compared to clastics) that are highly susceptible to chemical alteration, recrystallization, and dissolution; i.e. diagenesis. There is significant potential for diagenetic modification before and throughout burial, often with multiple diagenetic events superimposed, and a continual modification of reservoir quality.

The complexity in the pore systems of carbonates is mostly due to the biological origin of carbonate sediments and their chemical reactivity. The biological origin of carbonates is mostly responsible for primary porosity whereas chemical reactivity of carbonates will lead to the formation of secondary porosity through diagenetic processes. Since more than half of the earth's hydrocarbon reserves are contained within pore systems in carbonate reservoirs, studying these pore systems has always been an integral part of hydrocarbon exploration. Carbonate reservoir characterization needs the integration of quantitative physical parameters such as porosity and permeability. Heterogeneity in carbonate rocks is the principal reason for its improper characterization and this has become more apparent as attempts are made to characterize petrophysical properties at various scales (Sharma and Prasad, 2009).

Large uncertainties in the petrophysical properties of carbonates are due to wide variations in pore type, pore shape, and interconnectivity (Knackstedt et al., 2008). Many studies have demonstrated the importance of pore structures of carbonates on their petrophysical properties (e.g. Anselmetti and Eberli, 1993, 1999; Anselmetti et al.,1998; Wang, 1997; Baechle et al., 2004; Saleh and Castagna, 2004; Kumar and Han, 2005; Rossebø et al., 2005). A lack of correlation between porosity and other physical properties, particularly permeability and sonic velocity is often encountered while dealing with carbonate reservoirs (Hatfield and Garnham, 2001).

Porosity is the ratio of total pore space to the total volume of the rock, and is usually given as a percentage. The pore system in carbonates is not simple in type and distribution within a reservoir (Choquette and Pray, 1970). Carbonate reservoirs have a wide range of porosity both locally in a single reservoir zone and regionally between different reservoir zones. This study concentrates on the former type of variation for a producing reservoir zone in a carbonate platform of Central Luconia province of offshore Sarawak, Malaysia.

Porosity in carbonate rocks can be divided into two main pore systems: macropore, and micropore system. These pore systems are divided on the basis of the pore size and their relative contribution to fluid flow in the rock. Because of their smaller pore diameter, micropores contribute less (or not at all) to fluid flow in carbonates. Different definitions of microporosity have been proposed and applied in the literature (e.g. Choquette and Pray, 1970; Pittman, 1971; Anselmetti et al., 1998; Cantrell and Hagerty, 1999; Lønøy, 2006; and Weger et al., 2009). In this study micropores were defined as all pores that are less than 10 microns in diameter. Since micropores are very small in diameter (less than 10 microns) conventional transmitted light microscopy does not allow observing them in thin sections. Digital Image Analysis (DIA) can be a useful technique to quantify microporosity in carbonates. Microporosity (when present) in carbonate reservoirs affects the reservoir properties (e.g. porosity, permeability, saturation) and elastic properties (e.g. sonic velocity) of the reservoir. Microporosity can occur in the grains, matrix or cement of carbonate reservoirs. The presence and amount of microporosity varies in different carbonate reservoirs and even in different depth zones of a single reservoir. Traditional pore

type classifications of carbonates describe the pore structures but fail to quantify the pore system for correlation to the rock's physical properties (Knackstedt et al., 2008). The most widely used classifications of porosity in carbonates are those of Choquette and Pray (1970) and Lønøy (2006). Choquette and Pray (1970) classified pores according to the fabric selectivity of the sediments, whereas the classification by Lønøy (2006) is texturally derived mostly from Choquette and Pray (1970) and incorporates pore-size differentiation. A classification scheme for micropores that can relate the abundance, occurrence, and distribution of microporosity, could provide a framework for better understanding of the flow-related properties of microporous Miocene carbonate reservoirs of offshore Sarawak. The study of microtextures of micrites is a key factor for understanding the abundance, occurrence, and distribution of microporosity in carbonates.

1.2 Effects of Microporosity in Carbonate Reservoirs

Micropores are important in that they can provide a pathway connecting microporous grains to one another and to macropores (Cantrell and Hagerty, 1999). In order to develop an accurate reservoir performance model and volumetric assessment, a systematic effort to recognize and quantify microporosity should be an integral part of any reservoir study (Cantrell and Hagerty, 1999). When microporosity is present in a reservoir, the water held in micropores by capillary attraction tends to be immobile and is called bound water. These bound waters may not be producible. Zones with significant water-filled microporosity may contain and produce water-free hydrocarbon from micropores even though wireline logs may indicate the zone to be apparently water saturated (as high as 90%) (Keith and Pittman, 1983; Cantrell and Hagerty, 1999; Petricola et al., 1995). Numerous carbonate reservoirs in the Middle East are dominantly micritic or mud supported microporous facies (Wilson, 1975, 1980; Budd, 1989; Witt and Gokdag, 1994). Their microporous nature makes the hydrocarbon extraction difficult because of the heterogenous distribution of reservoir properties, and strong capillary forces which retain much of the oil in place (Kirkham et al., 1996).

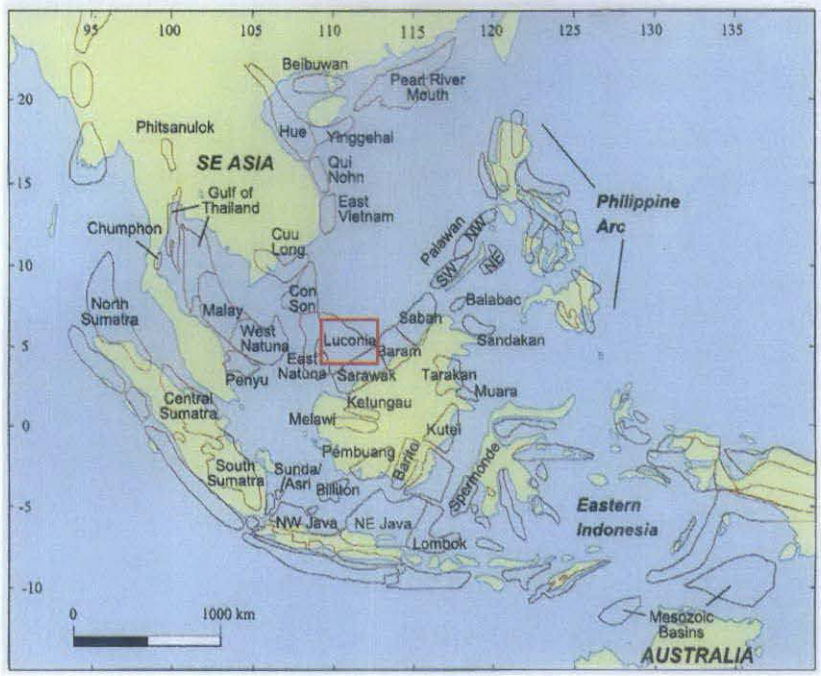

Figure 1.1: Location map of the Luconia Province, offshore of Sarawak (Doust and Sumner, 2007).

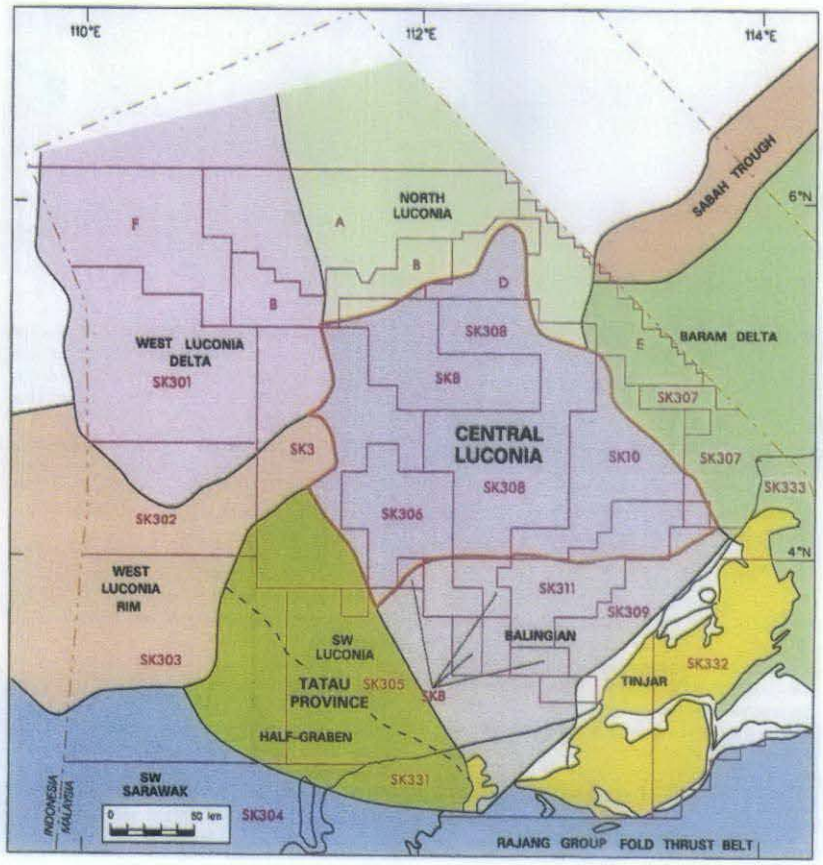

Figure 1.2: Location of Central Luconia province relatetive to other major Provinces of northern Borneo (PETRONAS, 1999).

Traditional pore type classifications (ignoring micropores as a pore system) sometimes describe pore structures successfully but fail to quantify the pore system for correlation to the rock's physical properties (Baechle et al., 2004; Knackstedt et al., 2008; Weger et al., 2009). Many studies have recognized that acoustic velocity in carbonates is dependent upon pore geometry (Anselmetti and Eberli, 1993, 1997, 1999; Kenter and Ivanov, 1995; Wang, 1997; Sun et al., 2001; Eberli et al., 2003; Baechle et al., 2004; Weger et al., 2004, 2009). Permeability and elastic properties are strongly related to pore structures. Empirical data show that microporosity affects the permeability and sonic velocity of carbonate reservoirs (Baechle et al., 2008, 2004; Weger et al., 2004). An estimation of the amount of microporosity from the basic acoustic properties has the potential to improve reservoir quality prediction in carbonate reservoirs with complex pore systems (Baechle et al., 2008). A rock physics model that captures the presence of both macro- and microporosity, as well as their respective stiffness, is needed to better estimate velocity and permeability (Baechle et al., 2008).

1.3 Study Area

The Central Luconia Province of offshore Sarawak is a major hydrocarbon producing province in Malaysia. More than 200 carbonate buildups have been seismically mapped in Central Luconia, of which some 65 have been drilled (Figures 1.1, 1.2). To date, 56 of the carbonate buildups are proven to contain commercial quantities of non-associated gas (Epting, 1980; PETRONAS, 1999; Sarawak Shell Bhd., pers. com.). This study concentrates on one of the Miocene carbonate platforms of Central Luconia that is proven to contain non-associated gas and is currently in production. The data and samples were collected from cored intervals of the reservoir zone in a well drilled in the platform.

1.4 Problem Statement

The effects of microporosity in carbonates have been addressed in numerous publications over the last few years. There are, however, a limited number of publications reporting rigorous studies of microporosity in carbonates. Most work on microporosity has been done on Palaeozoic and Mesozoic carbonates (particularly the Palaeozoic and Mesozoic carbonate reservoirs of the Middle-East). There are very limited data and information published so far on micropososity in Cenozoic carbonates. Microporosity in the Miocene carbonates of Southeast Asia has so far been virtually ignored, possibly because it has been assumed that it was insignificant. As a result, the scarcity of research work on microporosity in the Miocene carbonates of Central Luconia, offshore Sarawak left a few fundamental questions un-addressed, and/or un-answered:

1) Is there microporosity in the Miocene carbonate reservoirs of Central Luconia and how can it be quantified?
2) What are the effects of microporosity on the permeability and sonic velocity of the Miocene carbonate reservoirs of Central Luconia?
3) Can we explain and predict the occurrence of microporosity in Miocene carbonates and can we classify microporosity according to its occurrence?

This study will address these questions using some fundamental methods as well as a few new approaches.

1.5 Objectives

The primary objectives of this study are as follows:

1. To detect and quantify microporosity in the reservoirs of a Miocene carbonate platform of Central Luconia by applying a dual porosity system.
2. To establish the relationship between microporosity, macroporosity, permeability, and sonic velocity of carbonate reservoirs.

3. To propose a classification scheme for microporosity related to the microtextures of the Miocene carbonate reservoirs of Central Luconia that will help to predict the occurrence of microporosity.

1.6 Thesis Outline

This thesis contains five chapters. Chapter 1 is the introduction chapter containing the problem statement and objectives of the study. Chapter 2 presents the regional overview of the study area and the literature review of previously published research work. Chapter 3 deals with the methods of investigation used in this study. In this chapter the instruments and analysis methods are discussed. Chapter 4 presents the results and discussion of the study. This chapter consists of the results, their meaning, and implications. Chapter 5 presents the conclusion and a few recommendations for further studies.

CHAPTER 2

REGIONAL OVERVIEW AND PREVIOUS WORK

2.1. Geological Setting of Central Luconia Carbonate Platforms

The Central Luconia Province of the Sarawak Shelf, offshore Sarawak, Malaysia, is located between a compressive realm in the south and the extensional area of the South China Basin in the north. Central Luconia is bound to the north by the present shelf edge while in the south, west and east it is bordered by the geological provinces of Balingian, the western Sarawak clastic shelf and the Baram delta respectively. According to Epting (1980), seismic evidence indicates that contemporaneous crustal extension in the Central Luconia area resulted in the development of a horst-graben pattern. The formation of the deep South China basin allowed marine currents to supply large amounts of nutrient-rich water to the Sarawak shelf and enabled the prolific growth of Middle to Late Miocene carbonate build-ups (Mohammad Yamin Ali, 1996). The size and distribution of these buildups were mainly structurally controlled (Epting, 1980). Over 200 carbonate build-ups, ranging in size from a few km^2 to more than 200 km^2, have been seismically mapped in Central Luconia (Figure 2.1). Fifty six of the carbonate build-ups are proven to contain commercial quantities of non-associated gas. With a total volume of more than 40 TSCF of recoverable gas, the central Luconia province contains about 40% of the total non-associated gas reserve in Malaysia (Noad, 2001; PETRONAS, 1999; Sarawak Shell Bhd., pers. com.). The tectonics and sedimentation in offshore Sarawak are largely controlled by the continuous opening of the South China Sea Basin from the Middle Oligocene to the Middle Miocene. The Luconia Shoal (Platform) is a micro-continental block bounded by transform faults, which separates it from the Baram delta province to the east and the Rajang (West Luconia) delta province to the west. The area remained stable throughout the Tertiary, resulting in carbonate deposition and reef

growth, contemporaneous with clastic deposition in the Baram and Rajang deltas. The basin fill consists of several kilometres of sediments of Oligocene to Recent age, ranging from coastal plain to deeper marine sequences, representing 8 regressive depositional cycles (PETRONAS, 1999) (Figure 2.2).

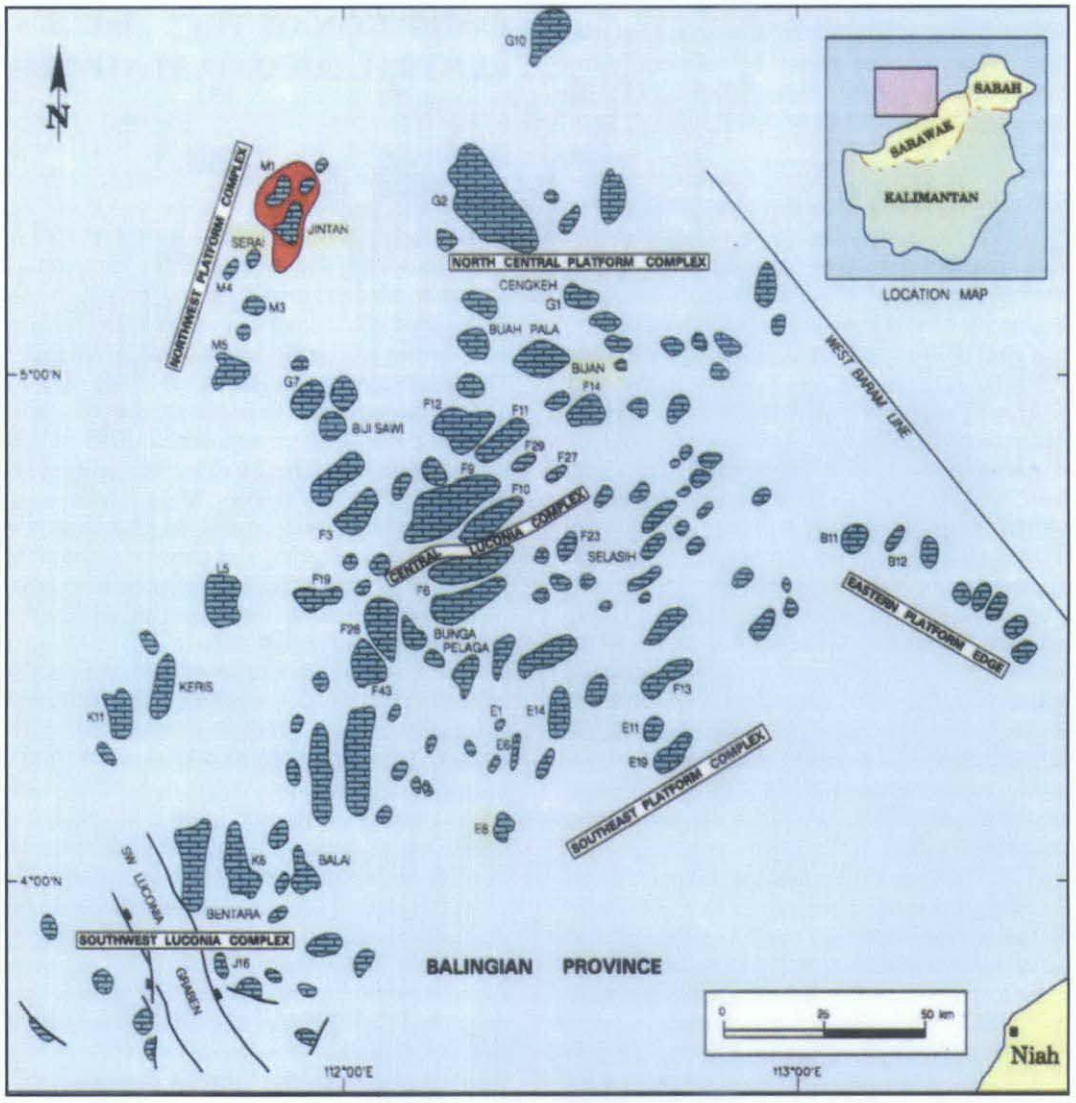

Figure 2.1: The areal distributions of major carbonate platforms of Central Luconia (PETRONAS, 1999).

The carbonate production in Central Luconia was primarily controlled by the growth of corals and coralline algae. This community of organisms forms a wave-resistant framework generally occupying a well-defined zone often termed as 'reef complex' (Figure 2.3). As shown in Figure 2.3 each environmental unit may comprise several physiographic zones. Furthermore, the recognition of the various

environments is often made difficult by a strong diagenetic overprint on the carbonates (Epting, 1980).

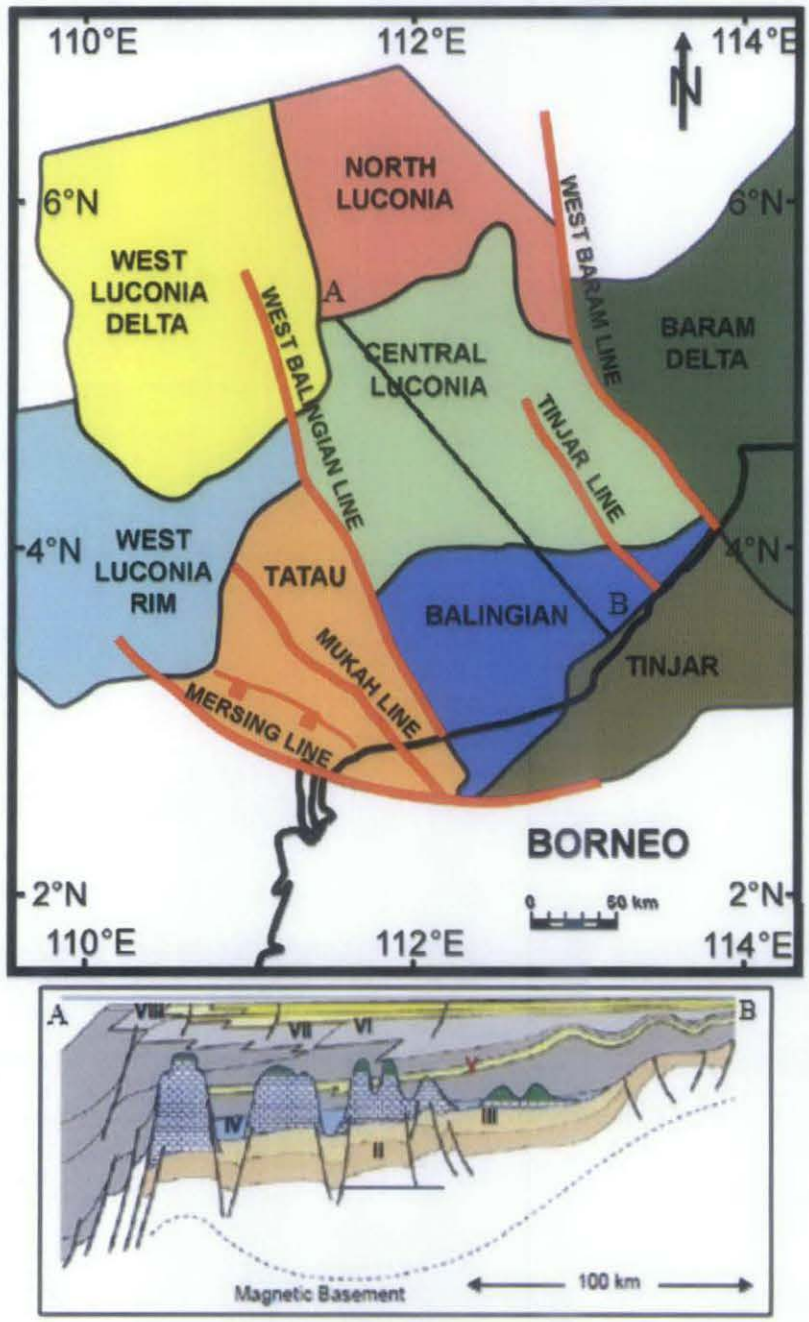

Figure 2.2: Location map of Central Luconia province (Modified from Hutchison, 2005) with a schematic cross section along NNW-SSE direction (Modified from Epting 1980).

The geometry and internal organisation of the Central Luconia carbonates are similar to those encountered in any other shallow water carbonate body in that they are determined by the net result of two major processes: the rate of (predominantly

skeletal) carbonate production and the rate of relative sea level changes (a combination of eustatic sea level fluctuations and subsidence of the sub-stratum) (Epting, 1980; Noad, 2001). Epting (1980) summarized the four cases of development of the carbonate build-ups of Central Luconia (Figure 2.4).

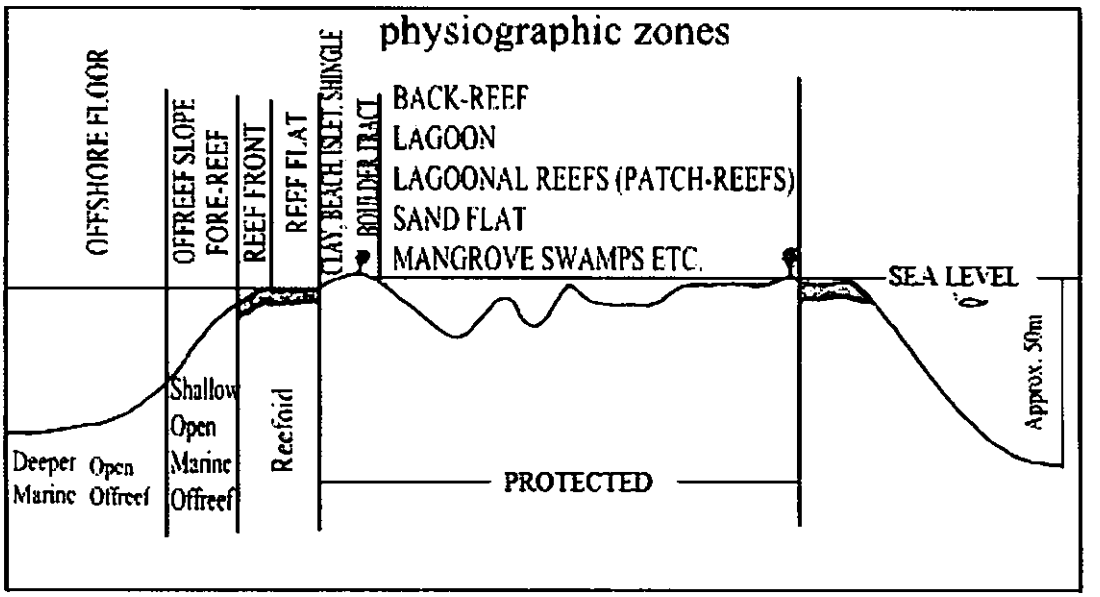

Figure 2.3: Areal distribution of environments of deposition and physiographic zones in a Central Luconia build-up (Epting, 1980).

1. *The rate of carbonate production is of the same magnitude as rising sea level:* As long as the growth of rock-forming organisms keeps pace with the rising sea level, generation of the reef debris will be maintained and carbonate sedimentation in the lagoon will continue in a shallow marine environment. Under this circumstance the carbonate complex actively grows upwards. This is a classic buildup situation characterized by a steep organic reef flank (Figure 2.4 A).

2. *The rate of carbonate production exceeds the rate of sea level rise:* In this case, depending on the availability of accommodation space, a build-out system develops. The reef flat and the fore-reef slope migrate seaward and the lagoon becomes enlarged (Figure 2.4 B). In this situation the protected part of the carbonate complex may undergo a further differentiation into distinct physiographic zones characterized by different sedimentary environments (e.g. intertidal and supratidal flats).

3. *The rate of carbonate production cannot keep pace with rising sea level (but the rise is not fast enough to drown the whole carbonate complex):* In this system a build-in system will develop. The actively growing fringing reef complex will move inwards to topographically elevated (e.g. previously supratidal or emergent) areas (Figure 2.4 C1). In the absence of the latter, the carbonate complex will become submerged and a shallow marine bank will be established (Figure 2.4 C2). Although a coral/algal community may persist in a subdued form, a different and diverse fauna and flora is likely to colonise the bank.

4. *The rate of carbonate production is greatly reduced or stopped due to a sea level fall:* In this case the reef is likely to become inactive. Growth of coral/algal communities will be halted or restricted to marginal rims. Some dissolution may occur, giving rise to clay on the reef complex as insoluble residue. Simultaneously the lagoon may also become infilled by intertidal and supratidal sediments which, depending on whether the climate was humid or arid, will be lignitic or evaporitic respectively.

2.1.1 Sedimentation in Central Luconia Carbonates

The Central Luconia province has undergone several episodes of sedimentation. A number of individual structural elements had a long-lived effect on sedimentation on the platforms, and have directly affected the geometry of the pre-carbonate siliciclastics, the carbonate build-ups, and the overlying siliciclastics. During cycle I times, deepwater argillaceous and shallow marine siliciclastic successions were deposited by an early synrift graben filling sedimentation process. This was followed by a late phase of synrift sedimentation throughout cycles II and III times during the opening of the South China sea. Continuous subsidence and formation of half-grabens resulted in widespread Middle to Upper Miocene carbonate deposition during cycles IV and V times. This was eventually terminated by the influx of siliciclastic sediments

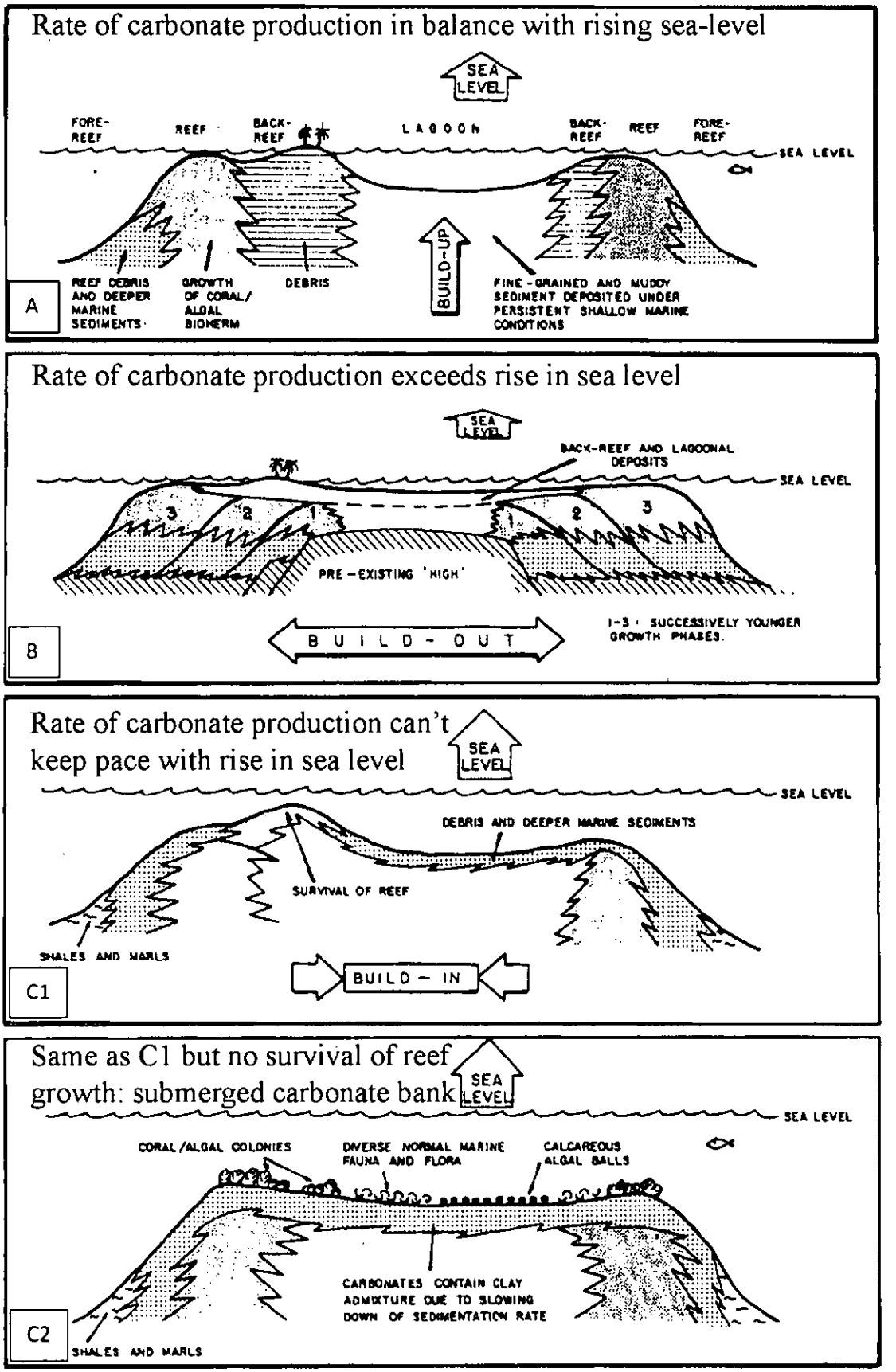

Figure 2.4: Main development stages of carbonate buildup systems in Central Luconia (Epting, 1980).

derived from the uplifted Rajang Fold-Thrust Belt during cycles V and VIII times (Figure 2.5) (PETRONAS, 1999).

According to Epting (1980), all four situations mentioned above occurred in a specific pattern in space and time in the Miocene carbonate platforms of Central Luconia (Figure 2.6).

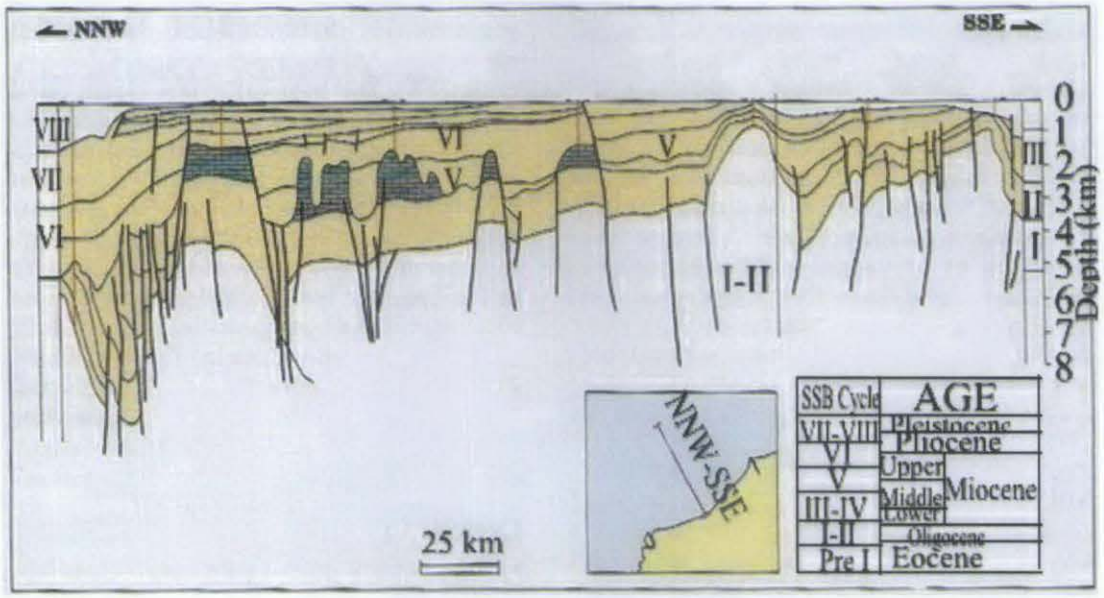

Figure 2.5: A schematic cross section along NNW-SSE direction across the continental shelf of offshore northwest Sarawak (Modified from PETRONAS, 1999).

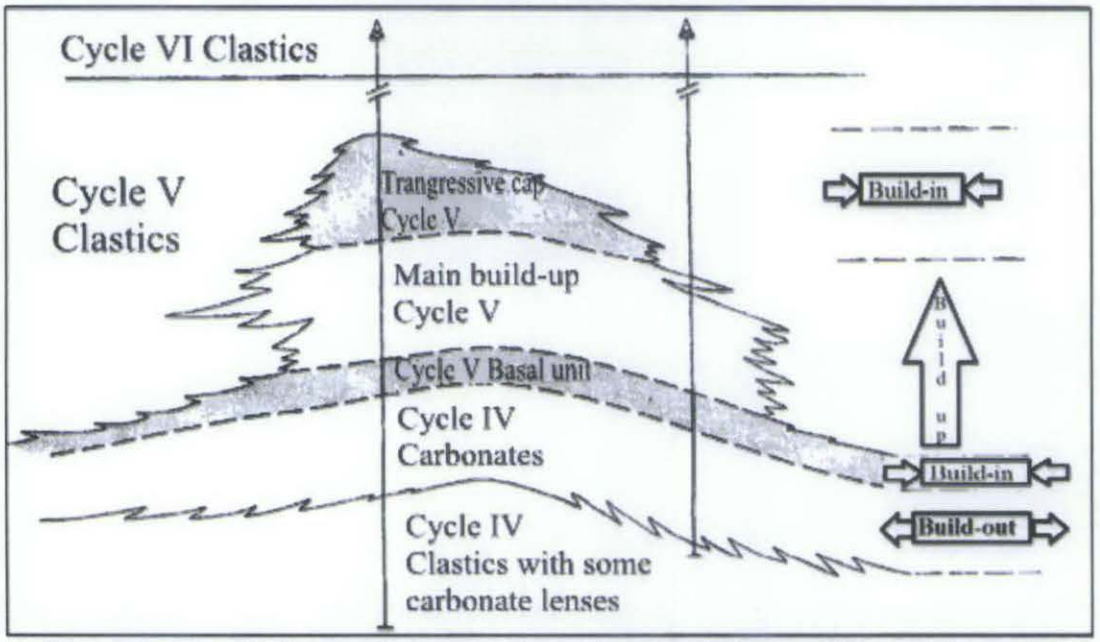

Figure 2.6: Typical growth pattern of a carbonate platform of Central Luconia (Modified from Epting, 1980).

2.1.2 Carbonate Reservoirs in Field X

Field X is one of the main carbonate gas fields in the Central Luconia Province, offshore Sarawak. This field, located in the centre of the Province, is a platform-type Miocene carbonate build-up. Diagenetic studies were done on the carbonates of Field X in studies of cores from two wells, A, and B by Sarawak Shell Bhd. (SSB) in 1991. Nine types of lithofacies were defined in these studies. Five of these lithofacies are good quality reservoir lithofacies, they are distinct but they form a gradational spectrum and in descending order of reservoir quality they are defined as: Chalky limestone (LC), Mouldic Dolomite (DM), Chalky Mouldic Limestone (LCM), Mouldic Dolomitic Limestone (LDM), and Mouldic Limestone (LM). In terms of total percentage of core, the order from most common to least is: LCM, LM, all poor-quality lithofacies (T), LC, LDM, DM. The poorer-quality lithofacies are Argillaceous Limestone (ALT), Tight Limestone (LT), Tight Dolomitic Limestone (LDT), and Tight Dolomite (DT) (Shell Sarawak Bhd., pers. com.). These lithofacies classes were defined in a confidential report by Shell Sarawak Bhd., using macroscopic observations of the core as well as the analysis of thin sections.

2.2 Quantification of Microporosity

2.2.1 Microporosity

Microporosity has been defined by many researchers in both a quantitative and a qualititative manner. Depending on the definitions, the quantification approaches differ in terms of maximum pore diameter of micropores.

2.2.1.1 Quantitative Definition of Microporosity

Microporosity can occur in the grains, cement or matrix of a carbonate reservoir. It occurs in ancient rocks and modern sediments. Different definitions of microporosity are proposed and applied in the literature. Various geoscientists, and petrophysicists

used their own criteria to define microporosity in carbonates (Figure 2.7). The earliest workers like Choquette and Pray (1970) defined micropores as the pores with a diameter smaller than 1/16 mm (62.5 μm). Pittman (1971) defined micropores as the pores with a diameter of 1 μm or less. Anselmetti et al. (1998) and Weger et al. (2009) suggested 20 microns and 30 microns, respectively, as the maximum average pore diameter for microporosity. Lønøy (2006) proposed a more detailed pore type classification in which he categorizes micropores with varying diameter from maximum 50 microns to less than 10 microns depending on the pore types. Coalson et al. (1985) used 5 microns as the upper size limit for micropores. Whilst many petrophysically visible pores are less than 62.5 microns in diameter, pores in the 1 micron diameter range are not optically resolvable with a standard petrographic microscope (Cantrell and Hagerty, 1999). Lambert et al. (2006) and Cantrell and Hagerty (1999) used 10 μm as the maximum pore diameter for micropores in their study. Their microporosity definition is based on the idea that microporosity is the difference between total measured porosity and porosity measured using thin section images.

2.2.1.2 Qualitative Definition of Microporosity

Ehrlich et al. (1991) stated that image porosity is associated with the effective porosity and the difference between total porosity and image porosity generally represents porosity associated with immobile fluids i.e. microporosity. Baechle et al. (2004, 2008) defined microporosity as the image macroporosity subtracted from the total plug porosity. Lambert et al. (2006) quantified microporosity by subtracting image porosity from the total porosity.

Considering the microporosity definitions used in literature so far, microporosity in carbonate reservoirs was defined in this study as the pores that are less than 10 microns in diameter and was quantified by subtracting the thin section image porosity from total plug porosity.

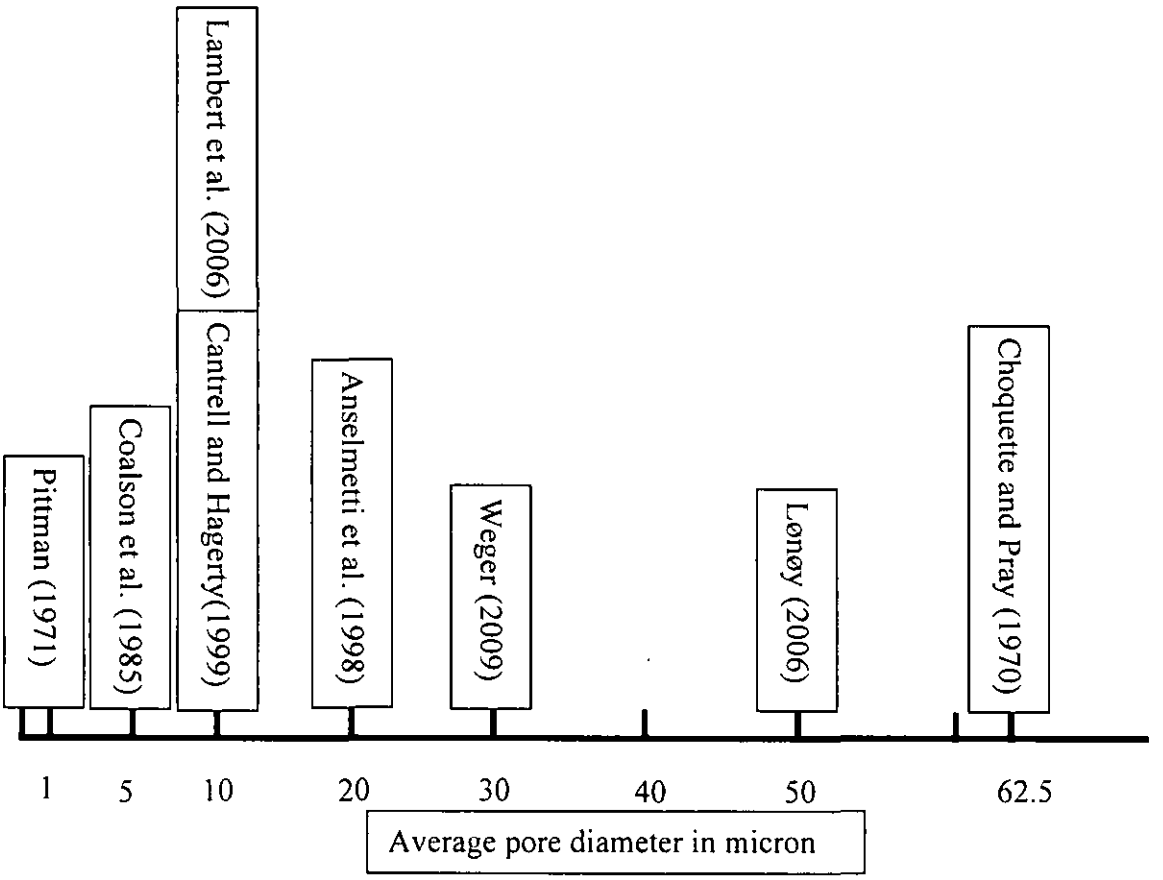

Figure 2.7: The quantitative definition of microporosity used in literature.

2.2.2 Microporosity Quantification using DIA

Digital Image Analysis (DIA) is a fast growing technique to quantify several physical parameters (e.g. pore size, pore shape, pore area, pore volume, grain percentage, grain area, cement etc.) from digital photomicrographs (Ehrlich et al., 1984, Fortey, 1995; Lindqvist and Akesson, 2001). There are several programs or software that can be used for DIA to do the measurements.

Several researchers used images from petrographic microscope to quantify porosity in carbonates. (Ehrlich et al., 1984; Fortey, 1995; Mowers and Budd, 1996; Cantrell and Hagerty, 1999; Lindqvist and Åkesson, 2001; Lambert et al., 2006). The quantification of microporosity includes the quantification of macroporosity (thin section image porosity) and core plug measurement of total porosity. The quantification of macroporosity includes 2 main processes, image acquisition and image segmentation or analysis. Thin section photographs can be captured using

digital camera. For image analysis several software have been used by different researchers. Weger et al. (2004) summarized the DIA technique with four basic steps, thin section preparation, image acquisition, image segmentation, and quantification of feature characteristics in their workflow. After image acquisition they segmented their images into pore space and rock space using digital photomicrographs from either plane polarized light, or a combination of plain- and cross-polarized light.

Depending on the size of the micropores different researchers used their own methods to quantify microporosity in carbonate reservoirs. However most of the researchers used the basic concept of quantifying microporosity by estimating the difference between the observed porosity on thin section images and the total porosity (e.g. Ehrlich et al., 1991, Cantrell and Hagerty, 1999; Baechle et al., 2004, Lambert et al., 2006). Photomicrographs captured using optical microscope as well as conventional digital cameras have been used by many researchers in the investigation of sandstone and carbonate reservoirs (Etris et al., 1988; Ferm et al., 1993; Mowers and Budd, 1996; Anselmetti et al., 1998; Cerepi et al., 2002; Van den Berg, 2002; Keehm et al., 2003). Al-Bazzaz and Al-Mehanna (2007) used digital image analysis to estimate visible pores in thin sections using the following simple formula,

$$\text{Porosity, } \Phi = \frac{\sum \text{Pore Area}}{\sum \text{Pore Area} + \sum \text{Grain Area}}$$

They subtracted the area covered by the grains from the total area of the image to obtain an estimate of the area of the pores. Then comparing the area of the pore spaces with the total area of the image they documented the percentage of visible porosity (macroporosity) on the thin section images.

Cantrell and Hagerty (1999) used petrographic thin sections point counting method to determine optically visible porosity; this visible porosity included all pores greater than about 10 μm in size (in other words macropores only). Cantrell and Hagerty (1999) deducted the visible porosity from the total porosity measured on the corresponding core plug (the thin sections were cut from the clipped end of the core plugs) using a porosimeter to derive the amount of microporosity.

Baechle et al. (2004) estimated microporosity by comparing thin section image porosity with the core plug porosity measured using helium gas. Lambert et al. (2006) defined micropores as pores that are less than 10 μm in diameter. They estimated microporosity by subtracting the visible porosity in thin section images observed under polarizing microscope from the total porosity measured using core plugs. Ehrlich et al. (1991) mentioned that image porosity is associated with the effective porosity and the difference between total porosity and image porosity generally represents porosity associated with essential immobile fluids, i.e. microporosity. Here image porosity means the porosity that is estimated from thin section images under transmitted light (in most cases). It is explicitly assumed by several researchers working on porosity estimation using optical petrography that the two-dimensional depiction of porosity is representative of the three-dimensional porosity distribution in reservoirs (e.g. Ehrlich et al., 1984, 1991; Mowers and Budd, 1996).

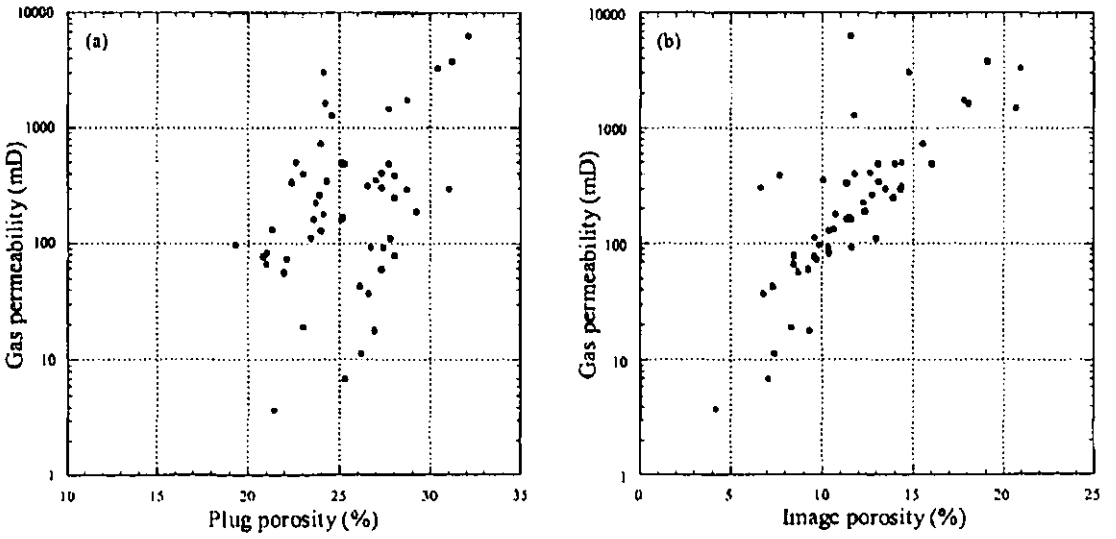

Figure 2.8: Image porosity gives a better correlation with permeability (Correlation coefficient, $r^2 = 0.84$) than the plug porosity (Correlation coefficient, $r^2 = 0.41$) (Hatfield and Garnham, 2001).

2.3 Effects of Microporosity on Permeability and Sonic Velocity

Various authors addressed the porosity permeability correlation in carbonate reservoirs. Some of the studies showed that pores that are very small in diameter

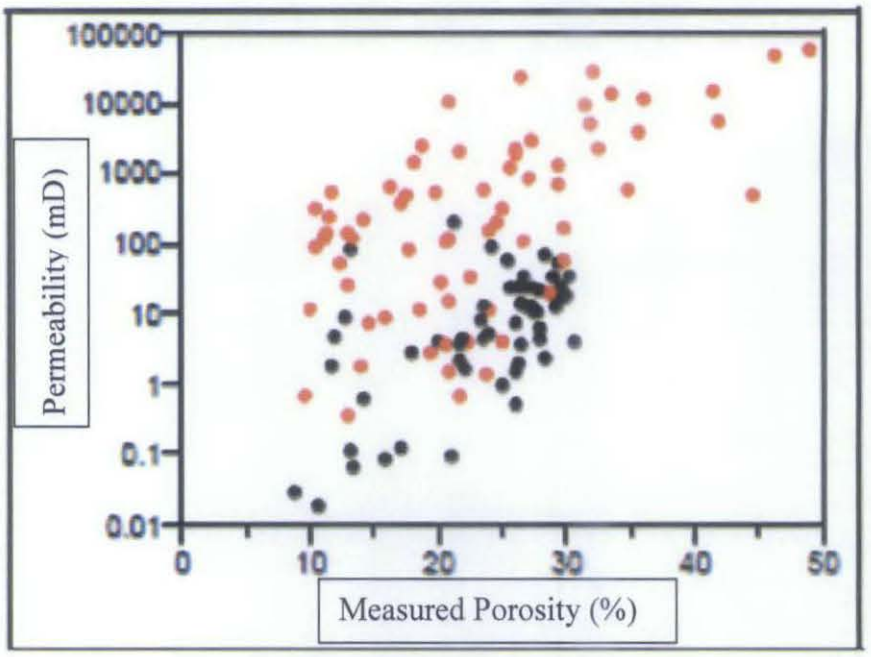

Figure 2.9: The crossplot between total porosity and permeability (Baechle et al., 2004).

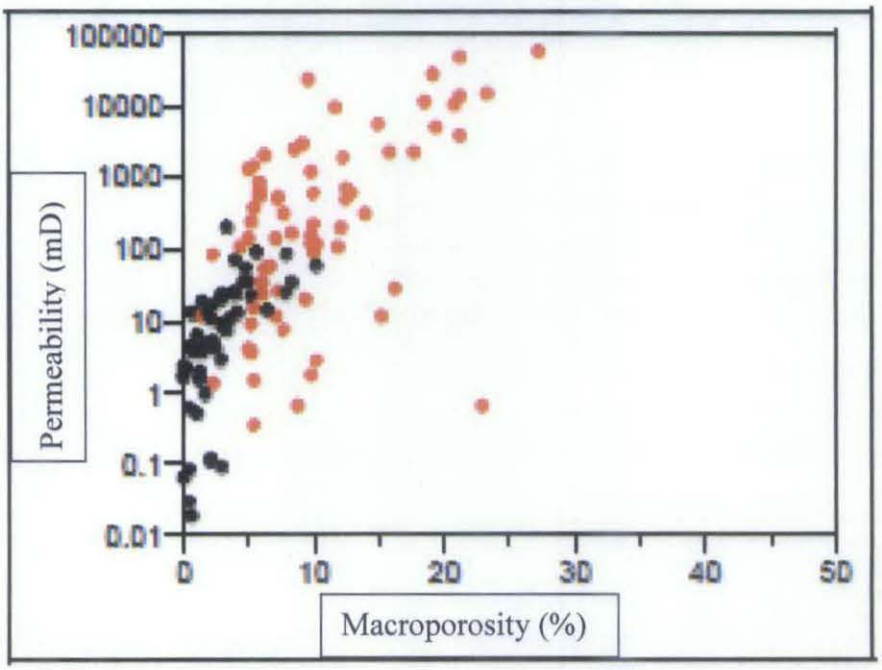

Figure 2.10: The crossplot between macroporosity (image porosity) and permeability. The figure shows that samples with pore structure associated with small dominant pore size (black dots) are restricted to permeabilities below 100 mD. The overall permeability uncertainty in a poro-perm cross plot is reduced to two and a half orders of magnitude while comparing macroporosity with permeability (Baechle et al., 2004).

contribute little to the fluid flow in the reservoir. Flügel (2004) mentioned that fluid flow rates in carbonates decrease with an increasing proportion of fine-grained matrix, pure micrites exhibiting the lowest permeability. Hatfield and Garnham (2001) studied the porosity-permeability relationship of a sandstone reservoir formation using 54 sandstone plugs collected from eight wells. They showed that for that sandstone reservoir formation, deducting micropores (pores with an area of 13 μm^2) from the total porosity allowed a far better correlation between porosity and permeability, thus allowing a more effective predicton of permeability (Figure 2.8).

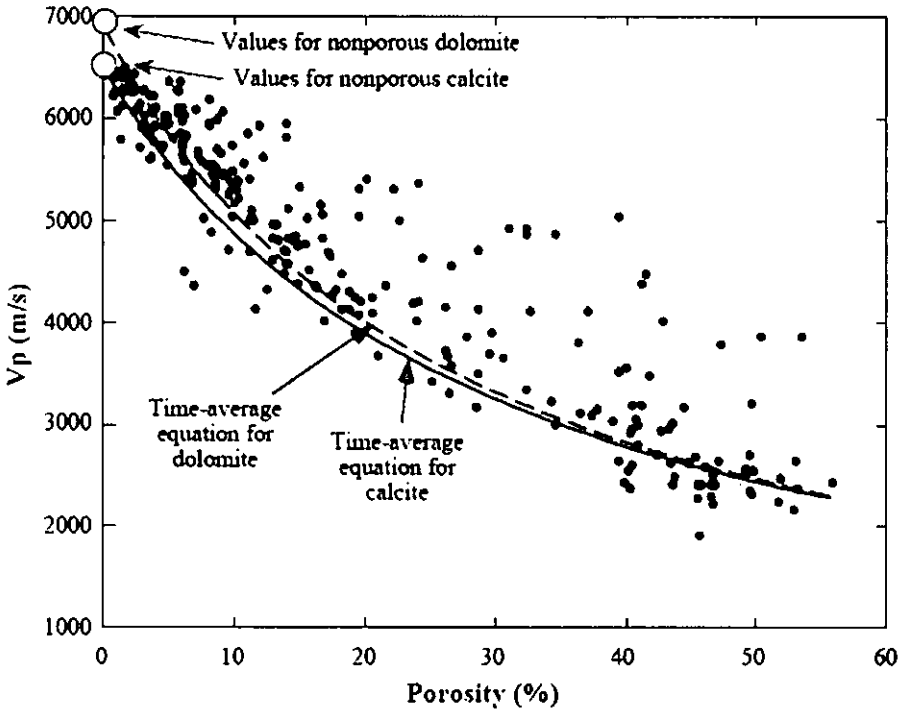

Figure 2.11: Crossplot of p-wave velocity and porosity compared with the time average equation (Wyllie et al., 1956) for calcite as well as dolomite (Anselmetti and Eberli, 1999).

Baechle et al (2004) demonstrated that using image analysis leads to a reduction of uncertainties in permeability scatter. They stated that the image macroporosity (the difference between measured total porosity and microporosity) gives a better prediction of permeability in carbonates. They showed that using the image macroporosity versus permeability trend reduces the uncertainty in permeability prediction by more than one order of magnitude (Figures 2.9, 2.10).

Pore geometry is proved to be a crucial factor in controlling acoustic properties in carbonates (Brie et al., 1985; Anselmetti and Eberli, 1993, 1997, 1999; Kenter and Ivanov, 1995, Baechle et al., 2004; Weger et al., 2009). Anselmetti and Eberli (1993, 1997, 1999) showed how variations of pore space geometry in carbonates influence

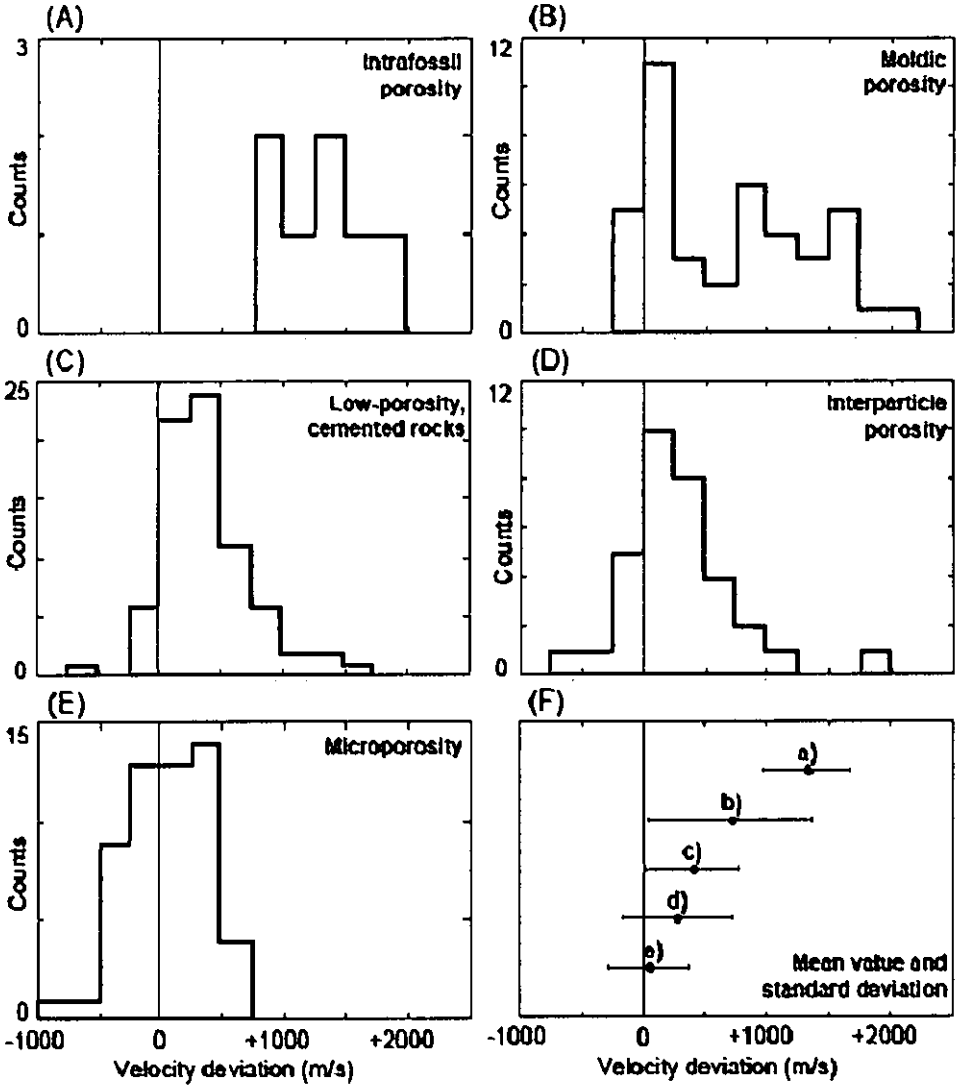

Figure 2.12: (A-E) Velocity deviations of different pore type categories. Porosity-velocity values of samples with zero deviation (marked by a vertical line) are exactly described by the empirical time-average equation for calcite. (F) Mean values and standard deviation of all five pore type.

acoustic velocities. Anselmetti and Eberli (1999) demonstrated the strong dependence of sonic velocities to the combined factors of porosity and pore structure in carbonates (Figure 2.11). They defined "velocity deviation" as the difference between measured velocities and velocities estimated using Wyllie's time average equation (Wyllie et al., 1956). Using the classification scheme of Choquette and Pray (1970) and Lucia

(1983), Anselmetti and Eberli (1999) distinguished five categories of pore types in thin sections (Figure 2.12). They showed that each of the pore types has a specific effect on the acoustic properties of the reservoir due to its geometric properties with the solid rock phase. They demonstrated that rock samples with microporosity or interparticle porosity show little deviation from Wyllie's time average equation (Figure 2.12). In rocks with these kinds of pore types sonic velocitities are generally low for their given porosity.

Baechle et al. (2004) demonstrated that microporosity leads to a better correlation with acoustic velocity than the total porosity. They showed that the crossplot of compressional velocity and porosity (Figures 2.13, 2.14) of carbonate samples show a large scatter of (Between the lowest and highest porosity values) up to 2500 m/s at 26% porosity. Most of the samples fall slightly above the Wyllie time-average velocity trend. They mentioned that samples dominated by microporosity are identified in the vicinity of the time-average velocity trend. Using quantitatively calculated microporosity from digital image of thin sections, Baechle et al. (2004) showed that the correlation coefficient between porosity and velocity significantly improves from 0.52 to 0.82 (Figures 2.13, 2.14) when using microporosity instead of total porosity.

Weger et al. (2009) studied the effect of pore structure on sonic velocity and permeability in carbonates. They showed that the velocity-porosity data of all core-plug samples show a characteristic first-order trend of increasing acoustic velocity with decreasing porosity. They demonstrated that carbonates with large pores generally show high velocity whereas carbonates with small pores mostly show low velocity (Figure 2.15).

Weger et al. (2009) defined perimeter over area (PoA) as the ratio between the total pore-space area on a thin section and the total perimeter that encloses the pore space and dominant pore size (DomSize) as the upper boundary of pore sizes of which 50% of the porosity on a thin section is composed. These parameters were quantified using DIA to observe the effects of pore shape on sonic velocity of

carbonates. The result also showed that the pores with smaller DomSize have lower velocity than those pores with larger DomSize values.

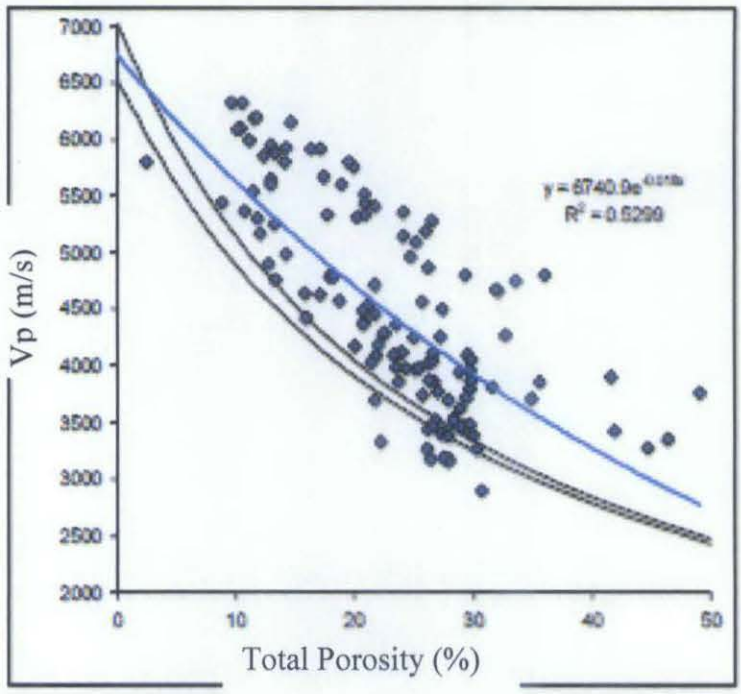

Figure 2.13: Crossplot of P wave velocity and total porosity. The two time-average velocity trendlines represent calcite and dolomite trends (Baechle et al., 2004).

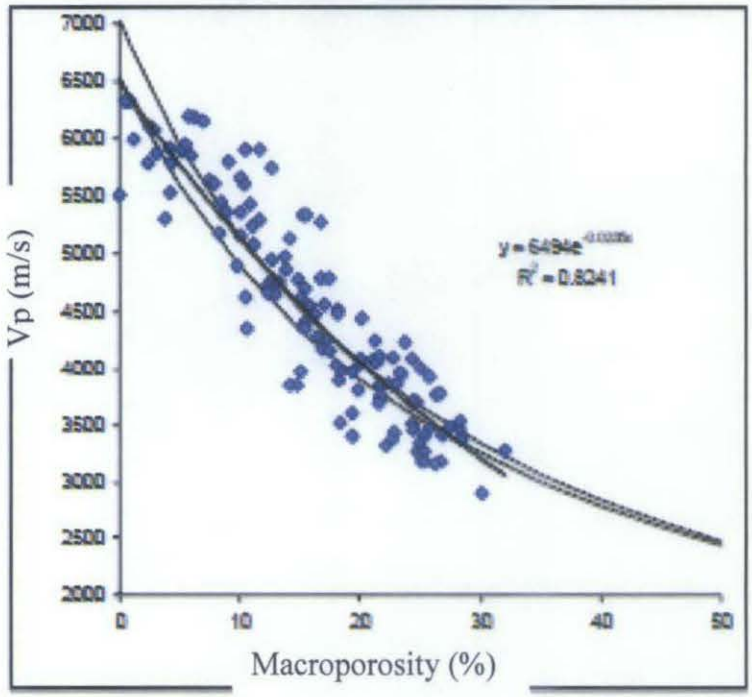

Figure 2.14: Crossplot of P wave velocity and macroporosity. The two time-average velocity trendlines represent calcite and dolomite trends (Baechle et al., 2004).

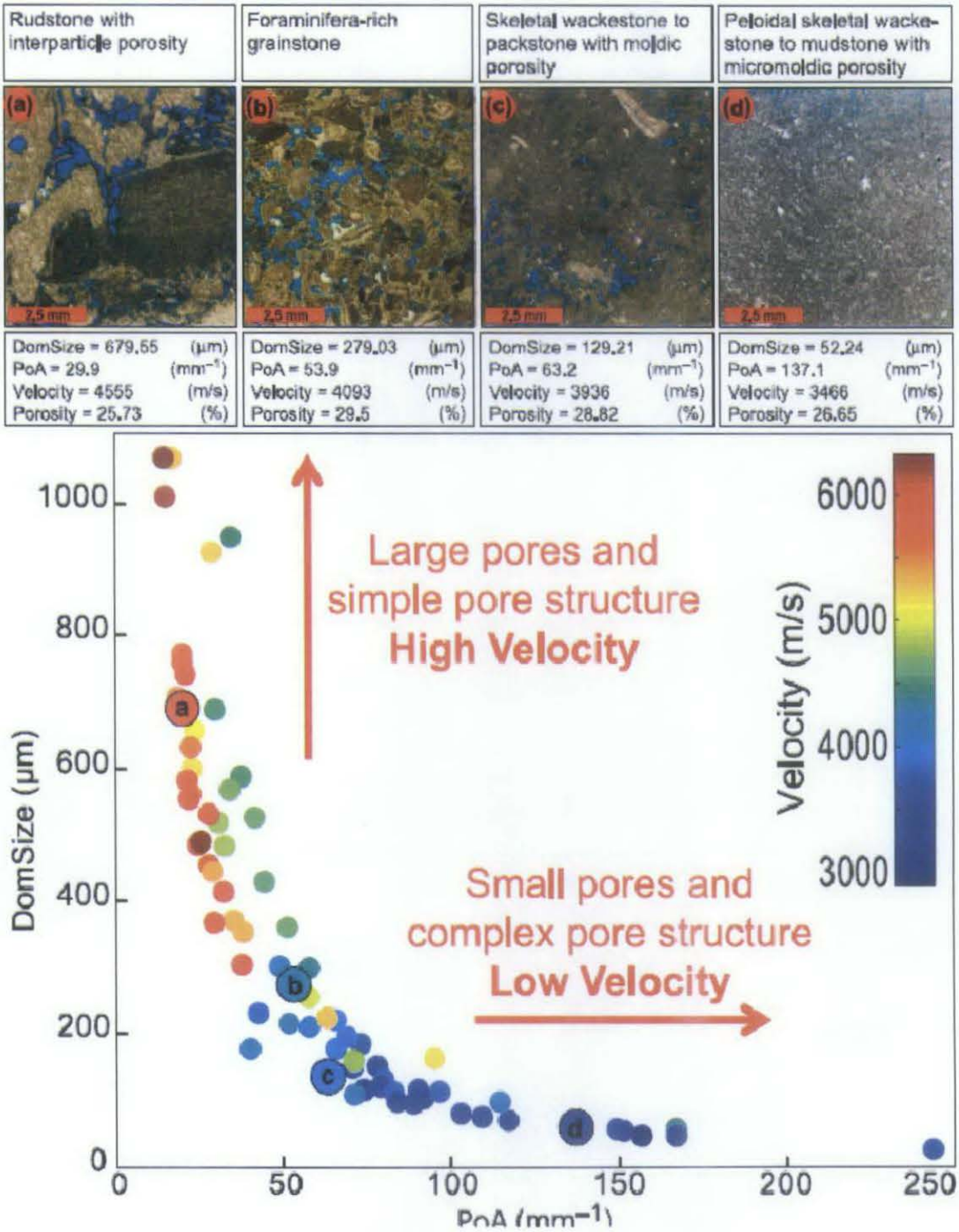

Figure 2.15: Crossplot of perimeter over area (PoA) versus dominant pore size (DomSize), where the measured acoustic velocity is superimposed in colour. (a-d) Thin section images are shown to illustrate carbonate pore types corresponding to certain combination of digital image analysis (DIA) parameters and velocity (Weger et al., 2009).

2.4 Classification of Microporosity

2.4.1 Micrites

The term 'micrite' in general refers to microcrystalline calcite. Originally micrite was proposed as a genetic term referring to lithified mechanically deposited lime mud (Folk, 1959). Most authors, however, now use the term in a non-genetic descriptive sense for a rock composed of fine grained calcite crystals and particles formed in place or by the accumulation of fine-grained pre-existing carbonate material. His broad definition even includes microcrystalline cement and micrite cement, precipitated as micron sized calcite in reefs, beachrocks, hardgrounds and caliche, and occurring in primary mud-free, grain supported sediments of carbonate slopes (Wilber and Neuman 1993). In general, micrite is understood to be the fine-grained matrix of carbonate rocks and the fine-grained constituents of carbonate grains. The original micrite definition relies strongly on crystal size limits which can only be recognized in petrographical thin section or through the use of SEM (Flügel, 2004).

Few topics in carbonate sedimentology have been debated as controversially as the origin and classification of fine-grained carbonate rocks. Today fine-grained carbonate muds originate in non-marine environments (e.g. pedogenic and lacustrine settings), and marine environments including shallow marine intertidal and subtidal settings (e.g. tidal channels, algal mats, lagoons, platforms), reefs, and deep-marine ocean floors (Flügel, 2004).

Sorby (1879) explained the origin of microcrystalline calcite in limestone as:

1) In-place formation of fine-grained carbonates triggered by biochemical and physicochemical factors.
2) Post mortem disintegration of calcareous algae.
3) Physical or biological abrasion of skeletal materials.
4) Accumulation of pelagic calcareous planktons and
5) A result of diagenetic processes including cementation and recrystallisation (Table 2.1).

Table 2.1: Terminology and genetic modes of origin of carbonate muds and limestones composed of microcrystalline calcite (micrite) (Modified from Flügel, 2004).

		Process
Automicrite (autochthonous micrite) Formed in place at the seabottom or within the sediment	Abiogenic ('inorganic')	Physicochemical precipitation triggered by salinity and water temperature fluctuations
	Biologically induced	Carbonate precipitation mediated by organic matrices (Ca-binding organic macromolecules), causing organomineralization and formation of *organomicrite*
	Biologically controlled	Metabolic processes of heterotroph and chemolithotroph bacteria and other microbes causing microenvironmental changes which induce carbonate precipitation
		Metabolic processes of phototrophic cyanobacteria and algae causing carbonate precipitation
Allomicrite (Allochthonous micrite), Deposition of disintegrated skeletal material and of fine erosional detritus	Disintegration of predominantly benthic biota	Disintegration of benthic calcareous algae into sub-microscopic fragments (Halimeda model)
		Disintegration of epibionts living on seagrass and macro-algae
		Disintegration of invertebrate skeletons
		Bioerosion causing detrital abrasion and microborings causing 'micritization'
	Disintegration of pelagic biota	Accumulation of calcareous planktons (foraminifera: coccolithophorids and other nannofossils causing *'nannomicrites'*
	Erosion and abrasion	Mechanical erosion of limestones, e.g. at coasts

Honjo (1969) differentiated micrites formed by growth of carbonate in place or resulting from the destruction, accumulation and deposition of pre-existing carbonate particles characterized by subhedral polygonal calcite grains meeting at interfaces (orthomicrites), and micrites composed of calcareous pelagic biota (nannoagorite). These primary micrites are often contrasted with the secondary micrites and pseudomicrites resulting from diagenetic processes (Wolf, 1965).

Several genetically defined terms are used to designate the major modes of micrite genesis; these are:

a) Automicrite (Wolf, 1965) refers to 'autochthonous' micrites which is interpreted to be a product of in-place formation of fine-grained calcite or aragonite on the sea-floor or within the sediment as an authigenic product triggered by physico-chemical, microbial, photosynthetic and biochemical processes (Flügel, 2004). The term was coined in the context of studies of mud mounds and biocalcification (Reitner and Neuweiler, 1995, Neuweiler et al., 1997). Automicrite exhibits specific fabrics and has a uniform mineralogical and chemical composition.

b) Allomicrite (Wolf, 1965) refers to 'allochthonous' micrite and is interpreted as the sedimentary microcrystalline matrix derived from the breakdown of various carbonate grains and the deposition of fine-grained materials. Allomicrites may contain mineralogically and chemically different constituents.

c) The term 'orthomicrite' (Honjo, 1969) designates micrites made of subhedral polygonal clay-sized calcite grains meeting at interfaces.

2.4.2 Modes of Formation of Micrites

The discrimination of micrites generated by different processes is of great importance for paleoenvironmental interpretation, basin analysis and understanding of the

properties of fine-grained carbonate rocks (Flügel, 2004). Table 2.1 summarises the different modes of formation of micrites.

Initially, the microcrystalline matrix of limestone was considered as a chemical rock, precipitated directly from sea water. This view was based on the interpretation of carbonate muds in the hypersaline lagoons of the Bahamas as an exclusively physicochemical precipitation of Mg-calcite and aragonite in conjunction with high salinity and extreme temperature (Cloud, 1962; De Groot, 1965; Loreau, 1982; Dix, 2001), but was also contested by geochemical data (Husseini and Matthews, 1972).

2.4.2.1 Automicrites

Automicrites are the primary products of in-place mineralization. Automicrites are fundamentally different from allomicrites which are a microcrystalline sedimentary matrix formed by the deposition of disintegrated skeletal material and fine erosional detritus. Automicrites include biologically induced, biologically controlled as well as inorganic carbonates. There are several processes that trigger the formation of autochthonous micrites, such as,

1. **Carbonate precipitation mediated by organic matrices:** Organic matrices (Ca-binding organic macromolecules) by mediating organomineralization (Reitner, 1993; Reitner et al., 1995) may cause the formation of 'organomicrites'. Carbonate mineralization concepts based on the interaction with 'Acidic Organic Macromolecules (AOM)' were first used to explain the skeletal structures of the organisms (Degens 1979; Addadi and Weiner 1989; Lowenstam and Weiner, 1983; Simkiss and Wilbur, 1989), and were further developed in the context of automicrite formation (Reitner et al., 2000).

2. **Metabolic processes of heterotroph and chemolithotroph bacteria and other microbes:** Metabolic processes of heterotroph and chemolithotroph bacteria and other microbes causing changes in the microenvironment surrounding the bacterium and including calcium carbonate precipitation. Bacterial controls on carbonate precipitation were at one time controversially

discussed but have now been confirmed by several experimental studies as well as field observations (Flügel, 2004).

3. **Metabolic processes of phototrophic cyanobacteria and algae:** Metabolic processes of phototroph cyanobacteria and algae that reduce CO_2 to organic carbon compounds, and thus shift the solubility equilibrium toward the precipitation of carbonate (Flügel, 2004).

Flügel (2004) described the characteristic criteria of automicrites as biolaminated structures, clotted peloidal microfabrics or extremely fine-grained cryptocrystalline textures. A common automicrite microfacies formed in slope settings are boundstones composed of small peloids that are associated with cement layers (Keim and Schlager 1999). Modern automicrites as well as peloidal and microcrystalline carbonate cements consist of Mg-calcite and aragonite. The same mineralogies have been inferred for ancient automicrites but a low-Mg calcite composition might be a possibility, too (Flügel, 2004).

2.4.2.2 Allomicrites

Allomicrites (allochthonous micrites) originate from the destruction of calcareous algae and invertebrate skeletons, bioerosion, accumulation of calcareous plankton as well as from the erosion and abrasion of lithified carbonates (Table 2.1). In shallow waters, tropical storms and ebb-tidal currents may cause a mixing of bank and ocean waters which can lead to a redistribution of genetically different carbonate muds. Carbonate muds produced on shallow marine platforms are also a major source for periplatform sediments deposited on slopes or in basins (Flügel, 2004). As mentioned in Table 2.1, there are several modes of origin of allomicrites.

1. **Disintegration of benthic calcareous algae into sub-microscopic fragments (Halimeda model):** The disintegration of modern calcareous green algae causes the formation of sand- to clay-sized particles. Processes involved in the disintegration, deposition and redeposition of algal particles are exemplified with the udoteacean alga Halimeda (Figure 2.16). The ultra-structural

elements of the calcareous skeleton of this kind and other green algae are aragonite needles. These needles are set free after the decomposition of organic matter (Flügel, 2004). Morphologically similar needles are abundant in carbonate muds of Great Bahama Bank and Florida Bay as well as in Pacific lagoons (Lowenstam and Epstein, 1957; Stockman et al., 1967; Neumann and Land, 1975; Nelsen and Ginsburg, 1986). Green algae, closely comparable with modern Halimeda have been known since the Late Permian (Poncet, 1989), were more common in Late Triassic (Flügel, 1988) and became rock-building constituents of warm-water platform carbonates during the Cretaceous and in the Tertiary (Hillis, 2001).

2. **Disintegration of epibionts living on seagrass and macro-algae:** The disintegration of epibionts living on seagrass and micro-algae causes the formation of allomicrites. Seagrass (Thalassia, Posidonia, Zostera and others) is abundant in shallow subtidal and intertidal settings. Seagrass can tolerate a wide range of salinities and, occurs most prolifically in water depths between 2 and 15m (Flügel, 2004). The mud banks of southern Florida, sometimes regarded as an analogue of ancient mud mounds (Bosence, 1985), four important controls of seagrass on carbonate mud production and energy baffling is documented in the mud banks of southern Florida: a) The long and dense root systems (rhizomes), extending a few tens of centimetres below the sea bed, stabilize and bind the sediment. b) The long blades have a baffling effect, can trap passing suspension-transported particles and reduce current speeds (Ginsburg, 1957; Scoffin, 1970; Almasi et al., 1987). Depending on the density of the meadows, large amounts of muddy sediment (packstones and wackestones) will accumulate. c) Seagrass stabilizes the substrate permitting colonization by stable-bottom sediment-producing and sediment-reworking communities, and d) Very importantly, seagrass blades provide a constantly renewable substrate onto which benthic organisms can attach and grow (Ginsburg and Lowenstam, 1958). Seagrass is known as far back as the Late Cretaceous and floating macro-algae at least since the Jurassic, but perhaps from the Devonian (Flügel, 2004).

3. **Disintegration of invertebrate skeletons:** Sorby (1879) recognized that invertebrate skeletons disintegrate after death by 'maceration' processes into microscopic elements forming calcareous muds and silt- to sand-sized particles. Destructive processes include:

   a) Destructive diagenesis (physicochemical dissolution due to carbonate undersaturation), common in colder sea water at higher latitudes and characterized by dissolution and breakdown of solid carbonates on the sea floor and in contact with sea water.

   b) Microbial degradation of skeletal-binding organic matter under aerobic conditions at the sediment/water interface or just below it (Henrich and Wefer, 1986; Freiwald, 1995). The susceptibility to dissolution of carbonate grains depends on the amount of skeletal binding organic matter, as well as on the size, shape and roughness of the crystallites (Walter, 1985).

   c) Degradation by microbores.

   d) Mechanical erosion and abrasion in high energy environments (Folk and Robles, 1964; Swinchatt, 1965; Matthews, 1966; Stieglitz, 1972). Tidal currents and wave actions in lagoons may be effective in grinding grains. The formation of allomicrites by the disintegration of invertebrate skeletons appears to be a common mode both in shallow-marine and deep-marine settings (Flügel, 2004).

4. **Bioerosion causing detrital abrasion and microborings causing 'micritization':** Bioerosion by marine and non-marine boring and grazing organisms is a major process in the production of clay- and silt-sized carbonate particles contributing greatly to the formation of micrite and calcisiltite. Biological erosion destroys organic skeletons, grains and carbonate substrates, and creates cavities. Processes involved in bioerosion are corrosion by endolithic organisms and loosening of hard substrates by dissolution. Organisms which are able to disintegrate hard carbonate substrates and skeletons include microbes, algae, foraminifera, sponges, near-shore bryozoans, worms (sipunculids, polychaetes), molluscs, arthropods

(cirripedians) and echinoderms (regular echinoids) (Flügel, 2004). Chemical-mechanical borings by clionid siliceous sponges in skeletons or rocks, produce large quantities of fine-grained carbonate sediment (up to 30% of the total sediment) in deeper

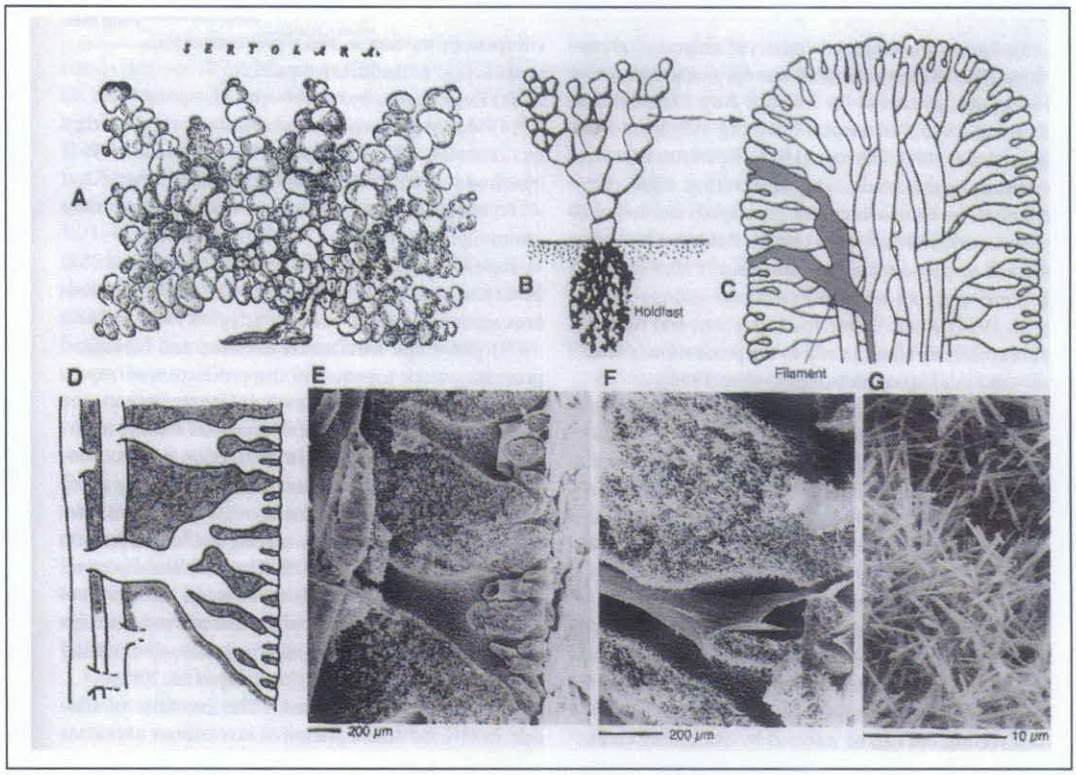

Figure 2.16: The Halimeda model showing the disintegration of calcareous algae. A) The first species of Halimeda as documented in 1599 by the Italian naturalist Imperato. B) The basic holdfasts of the sand growing species act as anchors in times of storms. C) Internal structure of a segment. D) Differentiation of cortical filaments. Calcification (gray pattern) takes place around and between the filaments. E) Calcification on and between medullar (left) and cortical filaments. F) Close-up of the cortex exhibiting remains of organic membranes. G) Aragonitic nodules. (A, B and C modified from Hillis-Colinvaux, 1980; D modified from Hillis, 1959).

intertidal and subtidal zones; most boring chips are silt-sized (Futterer, 1974; Moore and Shedd, 1977). Bioerosion is responsible for significant carbonate production in reefs (Van Treek et al., 1996). Abrasion and bioerosion of totally micritized skeletal grains provide the dominant source of Mg-calcite lime mud in some modern lagoonal environments (Reid et al., 1992). Carbonate mud production triggered by bioerosion is equally effective in tropical and nontropical

environments (Farrow and Fyfe, 1988; Gaillard et al., 1994). Grazing and rasping organisms (e.g. molluscs, echinoderms, fishes) produce large amounts of fine-grained carbonate sediment in intertidal and subtidal environments. A combination of bioerosion caused by microbores, predominantly cyanobacteria, and subsequent grazing by gastropods and sea-urchins on endolithic microflora within the intertidal and supratidal zone is one of the main causes of the erosion of limestone coasts (Torunski,1979).

5. **Accumulation of calcareous planktons (foraminifera: coccolithophorids and other nannofossils causing 'nannomicrites':** The accumulation of calcareous plankton on the deep shelf and in basin may produce allomicrite. Modern pelagic carbonate mud deposited largely in water depths of several hundred to several thousand meters are dominated by:

   a) accumulations of calcitic planktonic foraminifera associated with tests of nannoplankton (foraminiferal mud),

   b) accumulations of calcitic nannoplankton consisting predominantly of planktonic algae, and

   c) deposition of pelagic gastropods (aragonitic pteropods and heteropods; pteropod mud).

   Planktonic foraminifera evolved at the beginning of the Mesozoic and diversified through the Cretaceous and Cenozoic (Flügel, 2004). Although a small part of the original live planktonic assemblages become incorporated in the sediment, tests of planktonic foraminifera contribute significantly to the particle flux from shallow to deep waters and to the composition of pelagic carbonate muds (Berger, 1971, 1975). The transition from death assemblage to sediment assemblage is strongly controlled by dissolution of calcite on the sea floor which in turn is a function of the overlying waters and the aggressiveness of the bottom waters. Both factors depend on oceanic circulation patterns (Flügel, 2004). Some planktonic foraminifera disarticulate into individual chambers and the chamber walls may dissociate into crystallites (Lowenstam

and Weiner 1983). However most constituents of foraminiferal carbonate muds range from silt to sand size.

6. **Mechanical erosion of limestones, e.g. at coasts:** In high energy environments limestone coasts may undergo thorough mechanical erosion causing abrasion of clay and silt-sized carbonate particles. Examples have been described from the Adriatic coast (Schneider, 1977) and from the coast of the Persian Gulf and Puerto Rico (Pilkey and Noble, 1966; Kukal and Saadallah, 1973). Abrasion can be facilitated by bio-erosional loosening of rock surfaces. Bioerosion describes the erosion of ocean substrates and less often in terrestrial substrates by living organisms. Indications for micrites formed by abrasion are poor sorting and the association of fine-grained carbonates and non-carbonates particles (Lindholm, 1969), a very small crystal size (<2.4 μm), as well as rounding and good sorting (Peszat, 1991). Because of the lack of calcareous plankton in the Paleozoic, some authors have argued that Paleozoic micrites formed in deeper ramp, slope and basinal environments, may represent fine-grained carbonate eroded and winnowed from shallower platforms or carbonate coasts (Flügel, 2004).

Flügel (2004) addressed the importance of nannofossils for the formation of allomicrites both in Late Jurassic deep water and shallow water setting using the Solnhofen-Oberalm model (Figure 2.17).

2.4.3 Texture of Limestone

The texture of limestone has been studied by several researchers for decades to classify the rocks. Folk (1959, 1962) made the earliest attempts at classifying limestone according to its various textures. Folk (1962) documented 3 major families of limestone including 8 groups forming a complete spectrum of textural types. The bases for the Folk (1962) classification are,

1) The relative proportion of allochems and carbonate mud,
2) The sorting of allochems, and

3) The rounding of allochems.

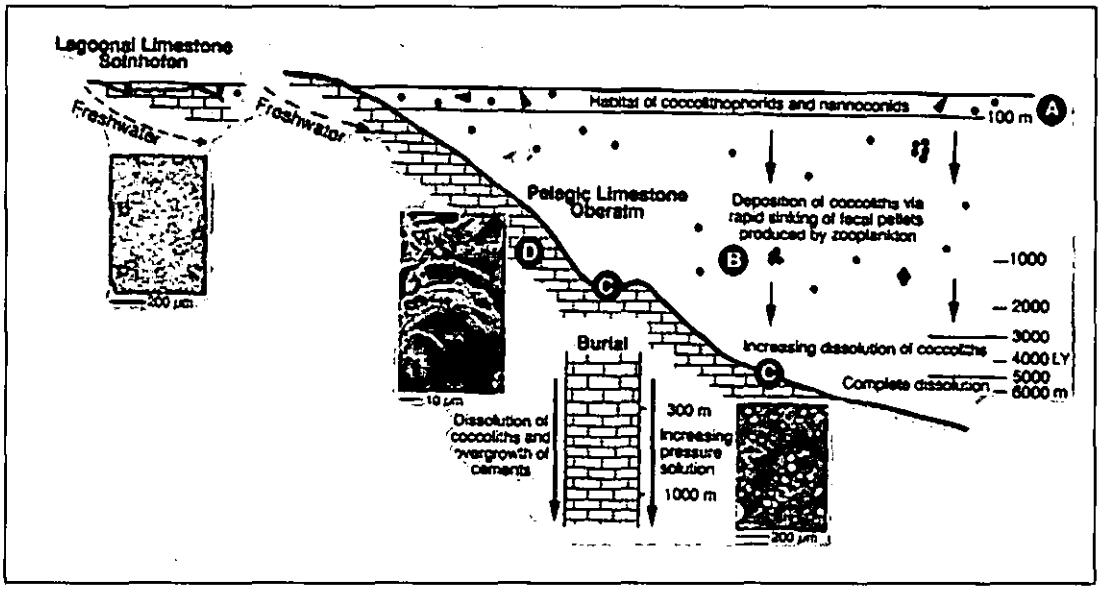

Figure 2.17: The Solnhofen-Oberalm model, showing micrite formation in different depositional setting and diagenetic environments of coccoliths and other calcareous nanno-organisms. A) Most coccolithophorids flourish in water depths down to about 100m, B) most coccoliths are transported to the sea bottom enclosed in fecal pellets produced by zooplankton and fish, C) Increasing dissolution at the water sea/bottom interface occurs at depth below 3000m, D) Grain-to-grain pressure solution related to increasing burial causes further dissolution at burial depths >300m, and provides a source for the carbonate needed for the growth of porefilling calcite. Another source is the dissolution of aragonitic shells (Flügel, 2004).

Folk (1959) proposed the term 'allochem' and defined it as 'allo' meaning 'out of the ordinary' and 'chem' being short of chemical precipitate; to indicate that these are not ordinary chemical precipitates as the chemists think of them, but are complexes, that have achieved a higher order of organization, and in nearly all cases have also undergone transportation. He mentioned four allochem types that are volumetrically important in limestone. These are a) intraclasts, b) oolites, c) fossils, and d) pellets. He suggested that limestone can be divided in 3 major families by determining the relative proportions of three end members,

1) Allochems.
2) Microcrystalline ooze.
3) Sparry calcite cement.

In Folk (1962) classification, allochems represent the framework of the rock and include the shells, oolites, carbonate pebbles, or pellets that made up the bulk of most limestones. Microcrystalline ooze represents a clay-size matrix whose presence signifies a lack of vigorous currents. Sparry calcite cement simply fills up pore spaces in the rock where microcrystalline ooze has been washed out or was not available. Thus he showed that the relative proportions of microcrystalline ooze and sparry calcite cement are an important feature of the rock. Folk (1962) classified limestones into eleven main types representing 3 of the major limestone families mentioned above (Figure 2.18).

Folk (1962) also proposed a classification scheme to represent the textural maturity of the limestone types he classified (Figure 2.19). He mentioned that the classification scheme for textural maturity is purely descriptive, although certain genetic implications were inherent. He interpreted the first mentioned limestone type in the sequence (micrite and dismicrite) as representing the lower energy environments, whereas the last mentioned types (biosparites) represent the higher energy environments. Consequently the sequence could represent the change from a deep marine basin up into a shallow shelf, and then to the surf and beach zone, or it could represent a passage from a protected and very shallow lagoon out to a barrier bar. Folk (1962) also mentioned the fact that one can conceive of many exceptions, a micrite could form in a high-energy zone if lime mud were trapped by slimy algae and held firmly from removal by waves, and a sparite might form in a calm lagoon if fossil fragments accumulated and the chemistry was such that there was no lime mud forming by precipitation or by abrasion in the environment. He called those examples as unusual exceptions to the general rule.

Dunham (1962) classified carbonate rocks according to the depositional textures. This is the most widely used and perhaps the most referred classification of carbonate rocks after Folk (1962). Dunham (1962) emphasized three textural features particularly useful in classifying those carbonate rocks that retain their depositional texture. These are,

1) Presence or absence of carbonate mud, which differentiate muddy carbonate from grainstone.

2) Abundance of grains, which allows muddy carbonates to be subdivided into mudstone, wackestone, and packstone.
3) Presence of signs of binding during deposition, which characterizes boundstones.

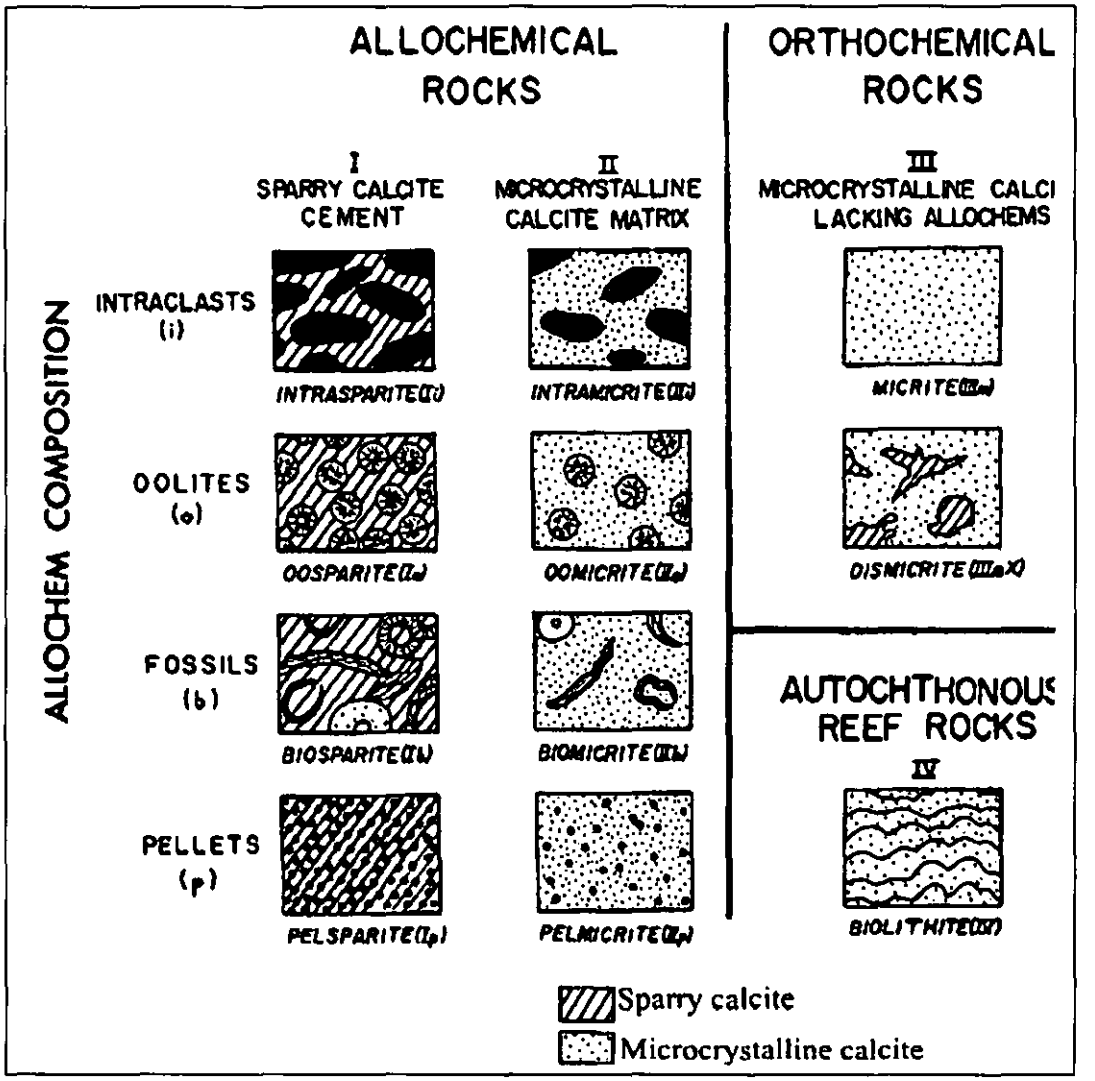

Figure 2.18: Graphical representation of the classification of limestone (Folk, 1962).

Dunham (1962) mentioned that the distinction between grain-support and mud-support differentiates packstone from wackestone (Table 2.2). Packstone is full of its particular mixture of grains, wackestone is not. He mentioned rocks retaining too little to their depositional texture to be classified as crystalline carbonates.

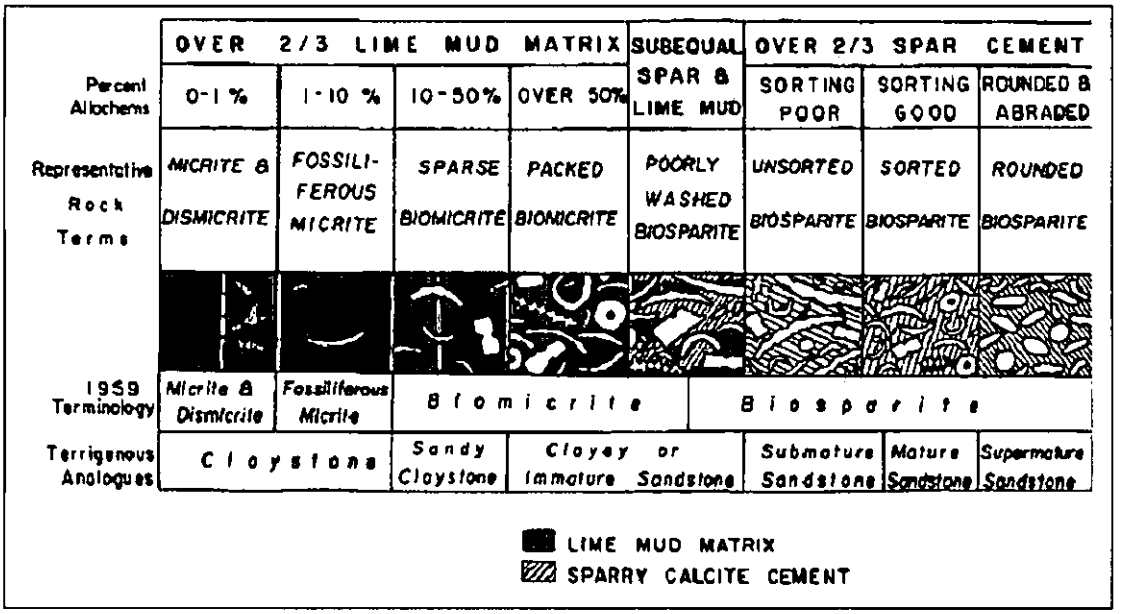

Figure 2.19: A textural spectrum for carbonate sediments showing eight sequential stages. In general low energy sediments occur to the left, with successively higher energy sediments to the right (Folk, 1962).

Some researchers expanded and revised the Dunham classification introducing several textural terms as well as grain sizes. Embry and Klovan (1971) introduced a classification scheme for limestone explaining the depositional textures. This classification is based on the Dunham classification scheme; they introduced the grain-size aspect by distinguishing grains smaller or larger than 2 mm. They also introduced new categories, floatstone and rudstone corresponding to wackestone and grainstone, and packstone respectively. Embry and Klovan (1971) added subdivisions to the boundstone category (Table 2.3).

Table 2.2: Classification of carbonate rocks according to depositional texture (Dunham, 1962).

<table>
<tr><td colspan="5">DEPOSITIONAL TEXTURE RECOGNIZABLE</td><td rowspan="3">DEPOSITIONAL TEXTURE NOT RECOGNIZABLE

Crystalline Carbonate

(Subdivide according to classifications designed to bear on physical texture or diagenesis.)</td></tr>
<tr><td colspan="4">Original components not bound together during deposition</td><td rowspan="2">Original componenets were bound together during deposition as shown by intergrown skeletal matter, lamination contrary to gravity, on sediment-floored cavities that are roofed over by organic or questionably organic matter and are too large to be interstices.</td></tr>
<tr><td colspan="3">Contains mud
(Particles of clay and fine silt size)</td><td rowspan="2">Lacks mud and is grain supported</td></tr>
<tr><td colspan="2">Mud-supported</td><td rowspan="2">Grain-supported</td><td></td></tr>
<tr><td>Less than 10 % grains</td><td>More than 10 % grains</td><td></td><td></td><td></td></tr>
<tr><td>Mudstone</td><td>Wackestone</td><td>Packstone</td><td>Grainstone</td><td>Boundstone</td><td></td></tr>
</table>

Wright (1992) suggested a few terms describing diagenetic changes of depositional fabrics (Table 2.4). He emphasized that the fine-grained matrix commonly called mud is not necessarily identical with micrite, but corresponds to a matrix consisting of clay-sized and silt-sized constituents. This classification replaced

Table 2.3: Classification of limestone (Embry and Klovan, 1971).

<table>
<tr><td colspan="6">ALLOCHTHONOUS LIMESTONE
Original components not organically original
Bound during deposition</td><td colspan="3">AUTOCHTHONOUS LIMESTONE
Components organically bound during deposition</td></tr>
<tr><td colspan="2">Less than 10% > 2mm components contain lime mud (< 0.03mm)</td><td colspan="2">No lime mud</td><td colspan="2">Encrust and bind</td><td rowspan="3">Build a rigid framework</td><td rowspan="3">Encrust and bind</td><td rowspan="3">Act as bafflers</td></tr>
<tr><td colspan="2">Mud supported</td><td colspan="2" rowspan="3">Grain supported
Boundstone
Bindstone</td><td rowspan="3">Bafflestone</td><td rowspan="3"></td></tr>
<tr><td>Less than 10% grains (>0.03mm and < 2mm)</td><td>Greater than 10% grains</td></tr>
<tr><td colspan="6"></td><td colspan="3">Boundstone</td></tr>
<tr><td>Mudstone</td><td>Wackestone</td><td>Packstone</td><td>Grainstone</td><td>Floatstone</td><td>Rudstone</td><td>Framestone</td><td>Bindstone</td><td>Bafflestone</td></tr>
</table>

Table 2.4: Classification of limestone (Wright, 1992).

DEPOSITIONAL				BIOLOGICAL			DIAGENETIC			
Mixed suppored (clay and silt grains)		Grain-supported		In situ organisms			Non-obliterative			Obliterative
< 10% Grains	> 10% Grains	With matrix	No matrix	Rigid organisms dominant	Encrusting binding organisms	Organisms acted to baffle	Main component in cement	Many grains contacts micro-stylolites Condensed	Most grain as contacts are micro-stylolites Fittedd	Crystals > 10mm
Calci-mudstone	Wackestone	Packstone	Grainstone	Framestone	Boundstone	Bafflestone	Cementstone	Grainstone		Sparstone
	Floatstone	Rudstone								Crystals < 10mm Micro-sparstone
	Grains > 2mm									

a few terms used in the classification by Embry and Klovan (1971). Wright (1992) replaced the term 'mudstone' by 'calcimudstone', and 'bindstone' by 'boundstone'.

2.4.4 Porosity Classification in Carbonates

Carbonate rocks often show a lack of correlation between porosity and other physical properties, in particular permeability and velocity. Studies on porosity in carbonate rocks are crucial in understanding diagenetic processes and are highly significant in evaluating reservoir rocks (Wardlaw, 1979; Ehrlich et al., 1991; Chilingarian et al., 1992; Moore, 2001). Permeability and elastic properties are strongly related to the pore structure. As a result, rock samples of equal porosity can exhibit a wide variation in permeability and velocity (Baechle et al., 2004). Many studies have demonstrated the importance of the pore structure in carbonates on petrophysical properties (e.g., Anselmetti and Eberli, 1993; Wang, 1997; Saleh and Castagna, 2004; Kumar and Han, 2005; Rossebø et al., 2005; Knackstedt et al., 2008). Several geoscientists and petrophysicists have emphasized the use of a dual porosity system for the classification of carbonate pores (Pittman, 1971; Cantrell 1999, Lønøy, 2006; Baechle et al., 2007; Baechle et al., 2008; Knackstedt et al., 2008). Archie (1952) made the first attempt at relating rock fabrics with the petrophysical properties of carbonate rocks; he was one of the earliest researchers who emphasized the importance of pore structure in carbonate pore type classification. Archie's classification scheme (1952) consists of two parts, the texture of the matrix (Table 2.5), and the character of the visible pore structure (Table 2.6).

The most widely used porosity classification scheme is the one developed by Choquette and Pray (1970). The classification was one of the earliest attempts to interpret the pore system in carbonate rocks by recognising 15 basic porosity types, among those, 7 are abundant types (interparticle, intraparticle, intercrystal, moldic, fenestral, fracture, and vug), and 8 are specialized types (Table 2.7). In the Choquette and Pray (1970) classification scheme, modifying terms are used to characterize genesis, size and shape, and abundance of porosity. The genetic modifiers involve a) process of modification (solution, cementation, and internal sedimentation), b)

direction or stage of modification (enlarged, reduced, or filled), and c) time of porosity formation (primary, secondary, predepositional, depositional, and post depositional). With the basic porosity types, these genetic modifiers permit designation of porosity origin and evolution.

Table 2.5: The classification of matrix texture of carbonate rocks (Archie, 1952).

Texture of Matrix	*Appearance of Hand Sample*	*Appearance under Microscope 10X to 15X*
Type I Compact Crystalline	Crystalline, hard, dense, sharp edges and smooth faces on breaking. Resinous	Matrix made up of crystals tightly interlocking, allowing no visible pore space between crystals, commonly producing "feather edge" on breaking due to fracturing of clusters of crystals in thin flakes
Type II Chalky	Dull, earthy or "chalky." Crystalline appearance absent because small crystals are less tightly interlocked, thus reflecting light in different directions, or made up of extremely fine granules or sea organisms. May be siliceous or argillaceous	Crystals, less effectively interlocking than the foregoing, joining at different angles. Extremely fine texture may still appear "chalky" under this power, but others may begin to appear crystalline Grain size for this type is less than about 0.05 mm. Coarser textures classed as Type III
Type III Granular or Saccharoidal	Sandy or sugary appearing (Sucrose). Size of crystals or granules classed as: Very fine=0.05 mm. Fine =0.1 mm. Medium =0.2 mm. Coarse =0.4 mm.	Crystals interlocking at different angles, generally allowing space for considerable porosity between crystals. Oölitic and other granular textures fall in this class

Table 2.6: The classification of visible pore size of carbonate rocks (Archie, 1952).

Class A	No visible porosity under about 10^x resolution microscope or where pore size is less than about 0.01 mm in diameter.
Class B	Visible porosity, greater than 0.01 but less than 0.1 mm.
Class C	Visible porosity, greater than 0.1 mm but but less than size of cuttings
Class D	Visible porosity, as evidenced by secondary crystal growth on faces of cuttings or "weathered-appearing" faces showing evidence of fracturing or solution channels; where pore size is greater than size of cutting

Table 2.7: Geologic classification of pores and pore systems in carbonate rocks (Choquette and Pray 1970).

BASIC POROSITY TYPES	
Fabric Selective	Not Fabric Selective
Interparticle	Fracture
Intra particle	Channel[1]
Intercrystal	Vug[1]
Moldic	Cavern[1]
Fenestral	[1]Cavern applies to man-sized or larger pores of channel or vug shapes
Shelter	
Growth Framework	

Fabric Selective or Not			
Breccia	Boring	Burrow	Shrinkage

Size Modifiers		
Classes		mm
Megapore	Large	256
	Small	32
Mesopore	Large	4
	Small	1/2
Micropore		1/16

The most widely used pore type classification systems for carbonate reservoirs are limited by the fact that the relation between porosity and permeability is poorly defined. This classification is very useful for porosity evaluation studies of macropores. However this classification scheme shows its limitation by ignoring the

micropore system in carbonates, whereas in some instances microporosity can exceed the amount of macropores and affect the reservoir properties to a great extent. Existing classification for porosity-permeability data do not, in many cases, optimally integrate sedimentology, diagenesis, and flow-related properties. A major challenge in the evaluation of carbonate reservoir is to understand the relationship between pore type, porosity, and permeability (Lønøy, 2006). .

Lucia (1983, 1995, 1999) defines the important geological parameters that can be described and mapped to allow accurate petrophysical quantification of carbonate geological models. Lucia (1995) divided carbonate pore spaces into 2 main divisions; interparticle (intergrain and intercrystal) and vuggy pores. Lucia (1995) mentioned that although the Archie classification (1952) is still useful for estimating physical properties, relating these descriptions to geologic models is difficult because the descriptions cannot be defined in depositional or diagenetic terms. The petrophysical classification of carbonate porosity presented by Lucia (1983) emphasized the petrophysical aspects of carbonate pore space, as does the Archie classification. By comparing rock-fabric descriptions with laboratory measurements of porosity, permeability, capillarity, Lucia (1983) showed that the most useful division of pore types for petrophysical purposes was of pore space between grains or crystals, called interparticle porosity, and all other pore space, called vuggy porosity. Vuggy pore space is further subdivided by Lucia (1983) into two groups depending on how the vugs are interconnected:

1) Vugs interconnected only through the interparticle pore network are separated vugs.
2) Vugs that form an interconnected pore system are touching vugs.

Lucia (1983) demonstrated that pore space located both between grains (intergrain porosity) and between crystals (intercrystal porosity) are petrophysically similar. He used one term 'interparticle' that identifies these petrophysically similar pore types (Table 2.8). Lucia (1983) defined vuggy porosity as pore space that is within grains or crystals, or that is significantly larger than grains or crystals; that is pore space that is not interparticle. Vugs are commonly present as leached grains, fossil chambers, fractures, and large, irregular cavities (Table 2.9).

Table 2.8: Geological and petrophysical classification of carbonate interparticle pore space based on size and sorting of grains and crystals (Lucia 1995).

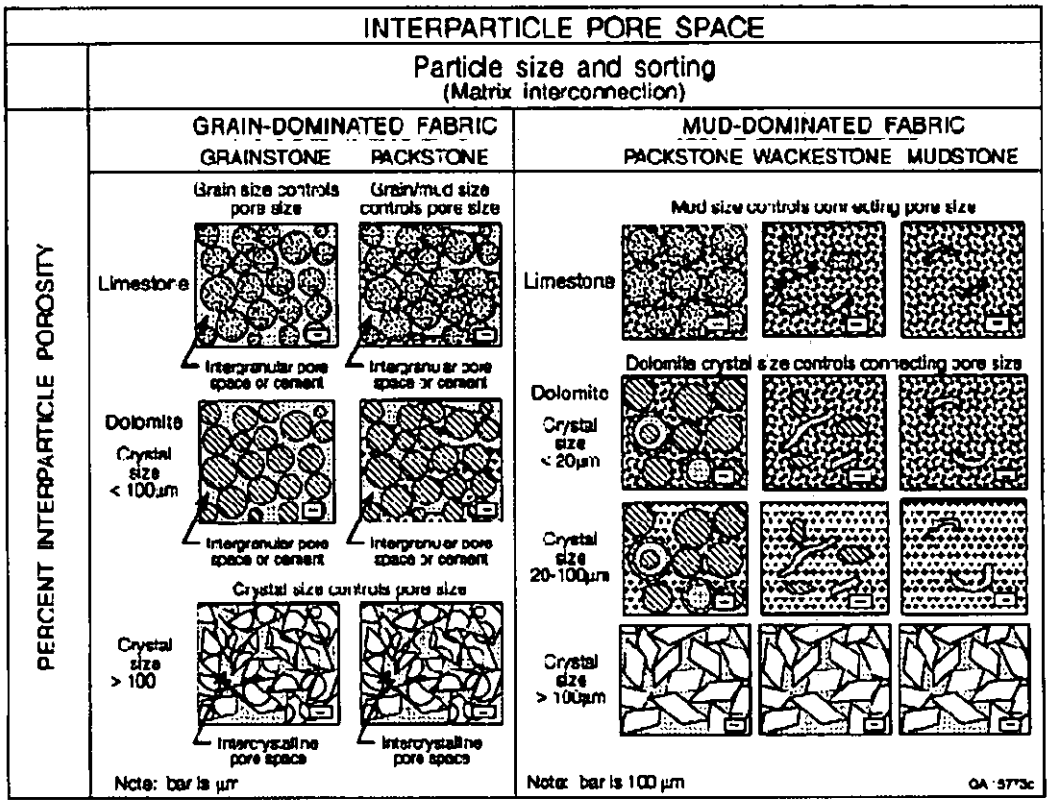

Table 2.10 summarize the comparison between the terminologies used in different pore type classifications. The semi quantitative classification of Lucia (1995) and the descriptive terminology of Choquette and Pray (1970) were used to propose a new pore-type classification scheme by Lønøy (2006) that includes 20 pore type classes (Table 2.11). Lønøy (2006) classification scheme represents a rigorous approach to combine sedimentological and diagenetic features with flow-related properties. Lønøy (2006) classification supports the observation of Lucia (1983) that pore size is a primary factor in understanding porosity-permeability relationship. Lønøy (2006) raised the point that Lucia (1983, 1995, 1999) classification scheme uses grain size (of particle or crystal) instead of pore size as the primary means of pore class division, whereas in the Lønøy (2006) classification scheme direct description of pore size was used instead of grain or crystal size.

Table 2.9: Gological and petrophysical classification of vuggy pore space based on vug interconnection (Lucia 1995).

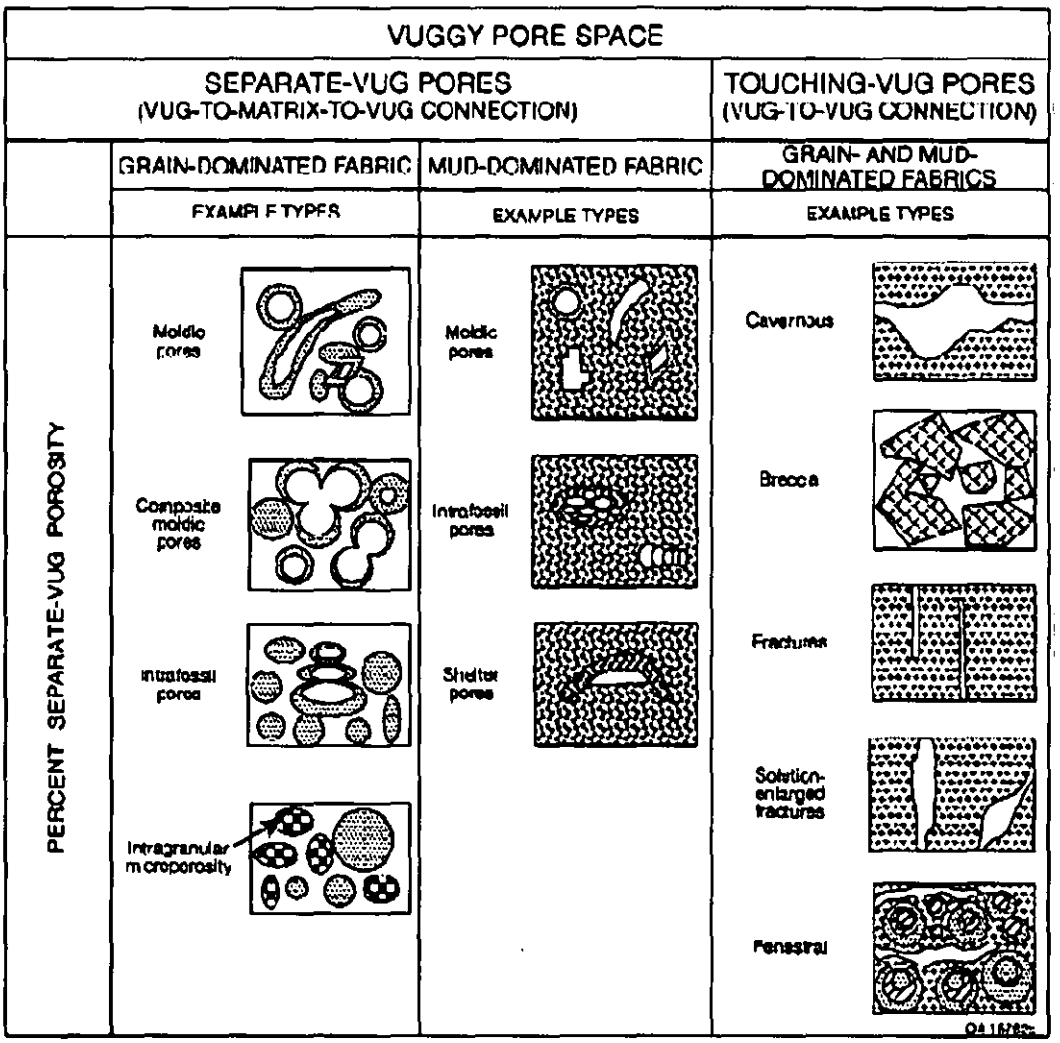

Table 2.10: A comparison between different carbonate pore type classifications (Modified from Lucia, 1995).

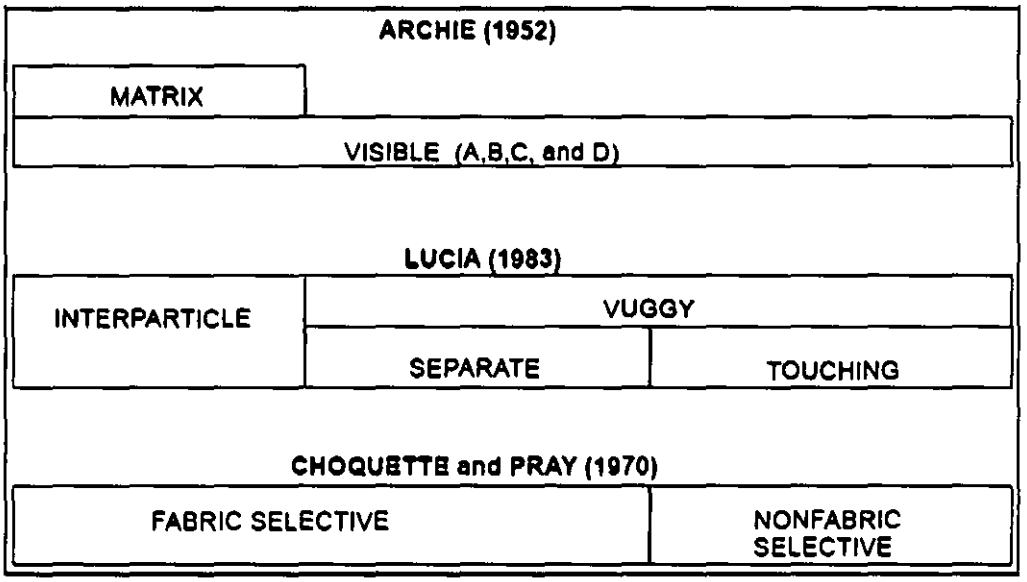

Table 2.11: Porosity classification system for carbonate rocks (Lønøy, 2006).

Pore Type	Pore Size	Pore Distribution	Pore Fabric
Interparticle	Micropores (10–50 μm)	Uniform	Interparticle, uniform micropores
		Patchy	Interparticle, patchy micropores
	Mesopores (50–100 μm)	Uniform	Interparticle, uniform mesopores
		Patchy	Interparticle, patchy mesopores
	Macropores (>100 μm)	Uniform	Interparticle, uniform macropores
		Patchy	Interparticle, patchy macropores
Intercrystalline	Micropores (10–20 μm)	Uniform	Intercrystalline, uniform micropores
		Patchy	Intercrystalline, patchy micropores
	Mesopores (20–60 μm)	Uniform	Intercrystalline, uniform mesopores
		Patchy	Intercrystalline, patchy mesopores
	Macropores (>60 μm)	Uniform	Intercrystalline, uniform macropores
		Patchy	Intercrystalline, patchy macropores
Intraparticle			Intraparticle
Moldic	Micropores (<10–20 μm)		Moldic micropores
	Macropores (>20–30 μm)		Moldic macropores
Vuggy			Vuggy
Mudstone microporosity	Micropores (<10 μm)		Tertiary chalk
			Cretaceous chalk
		Uniform	Chalky micropores, uniform
		Patchy	Chalky micropores, patchy

CHAPTER 3

METHOD OF INVESTIGATION

3.1 Introduction

This chapter discusses the data set, software, and research methodologies that were used in this study. The main part of the research was carried out at the South-East Asia Carbonate Research Laboratory (SEACARL), Department of Geoscience and Petroleum Engineering, Universiti Teknologi PETRONAS (UTP), Malaysia and partly at the Geology Section of the Department of Earth and Environmental Sciences, Katholieke Universiteit Leuven (KU Leuven), Belgium. For this research project, 2 months, from August 15 to October 15, 2010, were spent at the Katholieke Universiteit Leuven, Belgium. Several measurements and analysis such as Scanning Electron Microscopy (SEM), fluorescence microscopy and cathodoluminescence were carried out at the KU Leuven. Most of these facilities particularly fluorescence microscopy and cathodoluminescence were not available at UTP at the time this study was conducted. Ten samples were prepared using a micro-drill at the KU Leuven and sent to the Friedrich-Alexander-Universität, Nürnberg, Germany for carbon and oxygen isotope analysis.

In this study, micropores were defined as all pores that are less than 10 μm in maximum diameter i.e. the minimum size of pores resolvable with a petrographic microscope. The difference between the measured porosity from core plugs (X) and the porosity observed under the microscope (Y) (measured using DIA) was considered to represent microporosity.

Microporosity = X - Y

Porosity measurement of the core plug samples provided the percentage of total porosity present in the reservoirs at different depths. Digital Image Analysis (DIA),using optical petrography was used to estimate the amount of macroporosity (pores that are 10 microns or larger in diameter). Subtracting macroporosity from total porosity values, the amount of microporosity was determined for the available samples, taken at different depths.

Tables 3.1 and 3.2 show the flow charts of the methodologies that were followed during the study.

3.2 Data Set

In this study 33 core plug samples each in 1 inch diameter, were collected from rock cores taken in well A of field X in Central Luconia, offshore Sarawak, Malaysia. The samples were collected at a depth between 4000ft (1219m) and 4740ft (1444m) (Appendix A). All of these core plug samples represent carbonate reservoir with varying textures from wackstone to packstone according to the Dunham (1962) classification of carbonate rock textures. A total of 33 thin sections (impregnated with blue dyed epoxy) representing each of the core plugs were initially prepared. More than 300 thin section images taken with a polarizing microscope were acquired and analyzed using a Digital Image Analysis (DIA) software called 'Analysis' developed by Olympus. More than 250 photomicrographs were captured using the Scanning Electron Microscopy (SEM). Around 150 images were captured under ultraviolet light and analyzed using DIA.

3.3 Fluorescence Microscopy

Twenty thin sections were specially prepared for analysis under ultraviolet light with a fluorescence microscope. Rock samples were impregnated twice with yellow ultra low viscous fluorescent resin. The viscosity of the resin was as low as 20 cps at 25°C. This low viscosity of the resin allows rapid and complete infiltration within a minimum time. Final infiltration of the specimens was accomplished in 10 minutes

Table 3.1: Flow chart (1) showing the methodology of the study.

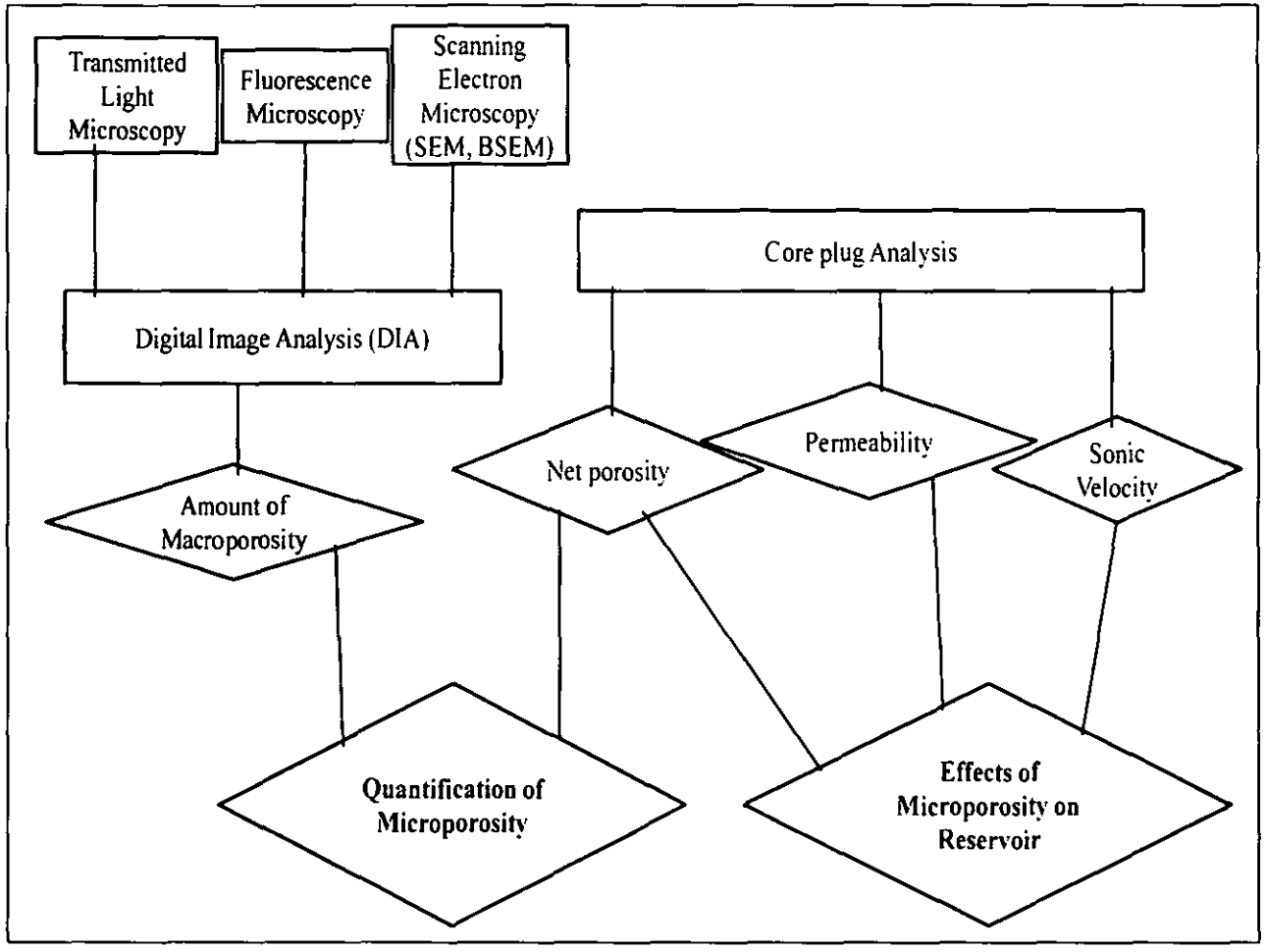

Table 3.2: Flow chart (2) showing the methodology of the research project

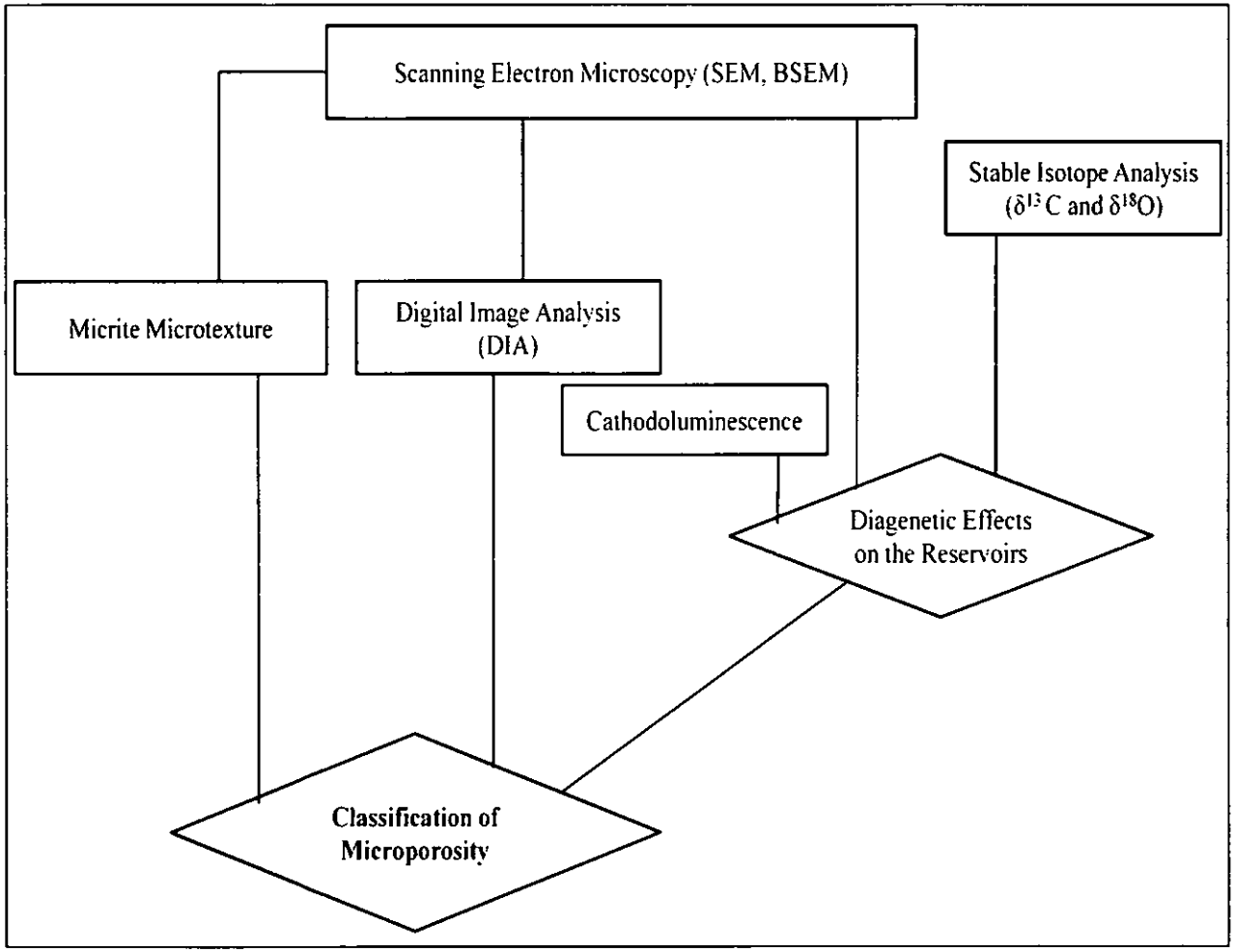

and the resin was polymerised at 60°C for 24 hours for each impregnation (Figure 3.1). Thin sections were then prepared from the samples impregnated with the resin. These thin sections were observed under ultraviolet light using fluorescence microscopy (Figure 3.2).

Figure 3.1: Impregnated core plug samples ready for thin section preparation

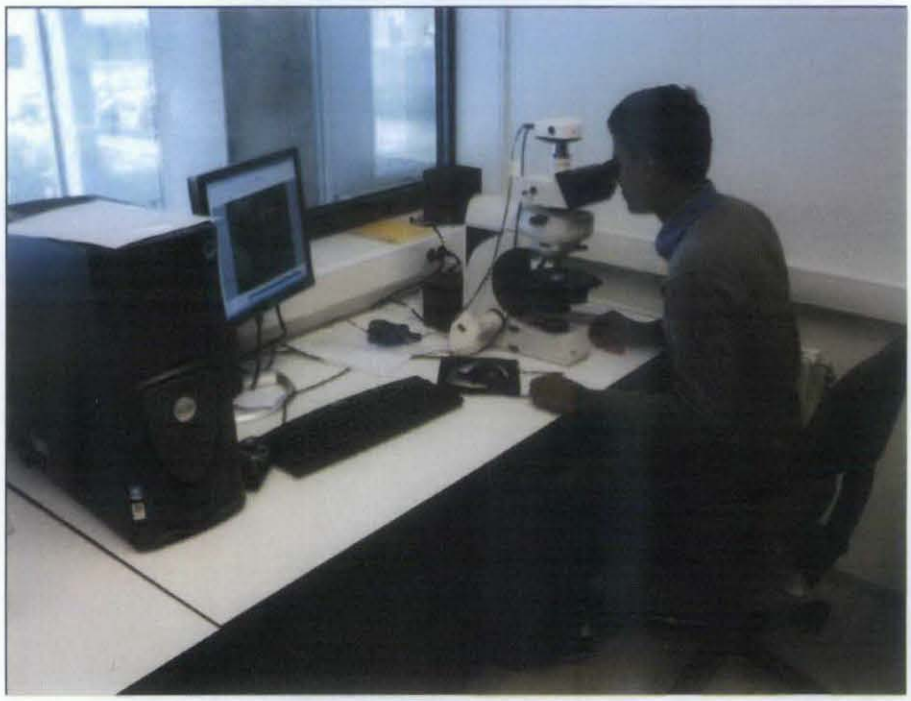

Figure 3.2: Fluorescence Microscope used in KU Leuven, Belgium.

The observation of twice impregnated thin sections with fluorescent resin under ultraviolet light has two important benefits as compared to the observation using a petrographic microscope under transmitted light. Firstly the double impregnation with fluorescent resin allows observation of areas where microporosity is not visible with conventional blue dyed impregnation. Secondly the observation under ultraviolet light uses reflected light, whereas petrographic microscope uses transmitted light. Thus observation under u-v light provides images from the surface of the thin sections allowing the observation of pores of a wide range of sizes (depending on the resolution of microscope) regardless of the thickness of the thin section. Accordingly, the amount of microporosity was quantified as the difference between total plug porosity and porosity from petrographic image analysis.

3.4 Scanning Electron Microscopy (SEM)

Scanning electron microscopy (SEM) allows examining surfaces at a magnification range from X10 to X300,000. Since this study was all about microporosity, the use of SEM was important. A Scanning Electron Microscopy (SEM) instrument, model JSM-6400, produced by JEOL Ltd. was used at the Geology Section of the Katholieke Universiteit Leuven. To prepare the stub-rock sample for SEM, a standard procedure was followed. Very small parts of the core plugs were taken and glued on metallic stubs using carbon glue (Figure 3.3). These stub samples were coated 3 times with gold, the first two times for 90 ms, and the third time for 60 ms. Gold coatings were done using SEM coating system SC 502. SEM was used to capture images from both polished thin sections and unpolished rock-stub samples (Figure 3.4).

3.5 Software

Digital Image Analysis of thin section images (under transmitted light) was done using a commercial DIA software called 'Analysis' developed by Olympus (Figure 3.5). SEM images were analyzed using a freeware software called 'J MicroVision' developed by Nicolas Roduit (University of Geneva, Switzerland).

Figure 3.3: Stub-rock samples preparation for gold coating.

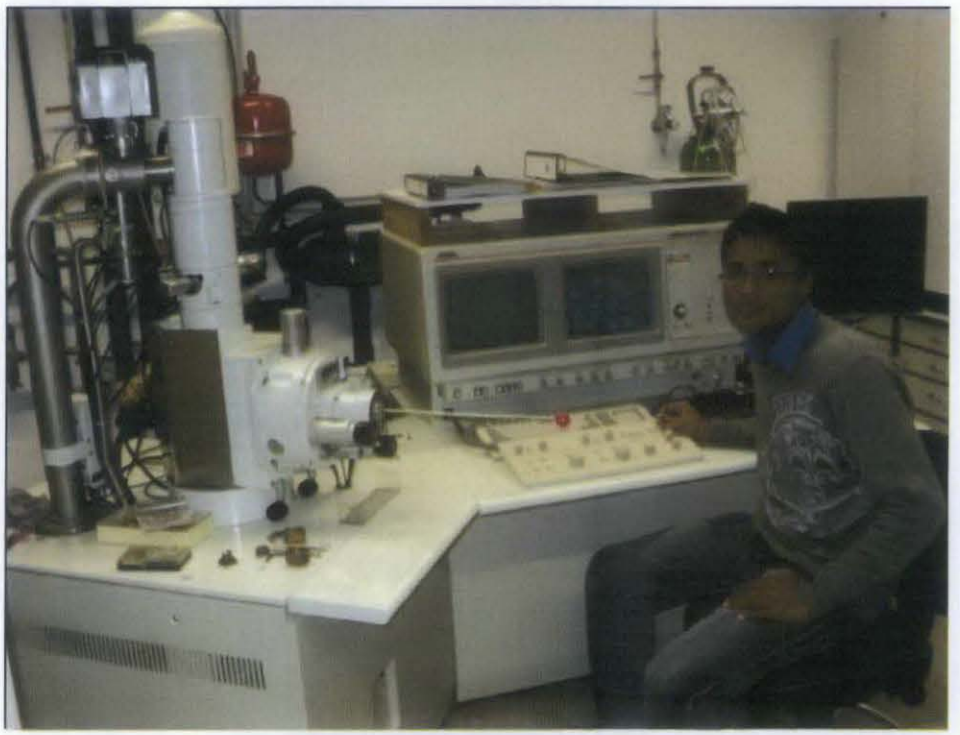

Figure 3.4: JSM-6400 Scanning electron microscope used in KU Leuven, Belgium. This SEM was used to visualize and quantify micropores in the rock samples.

3.6 Digital Image Analysis (DIA)

Digital Image Analysis (DIA) was performed on thin section images captured under transmitted light, ultraviolet light and SEM images.

3.6.1 DIA for Thin Section Images

3.6.1.1 Image Acquisition

Thin sections impregnated with blue dyed epoxy were prepared from each of the core plugs that were taken at different depths in the core. These 33 thin sections have been observed using an Olympus BX 51 microscope (Figure 3.5). On an average 10 images from each of the thin sections were captured under cross-polarized light using a high resolution Olympus DP 72 digital camera. These representative images were then analyzed for porosity measurement using a DIA technique. Three hundred thin section images were captured using a petrographic microscope under transmitted light (Figure 3.6).

Figure 3.5: Transmitted light microscope connected with DIA software 'Analysis'. The software analyzes the images captured using the microscope.

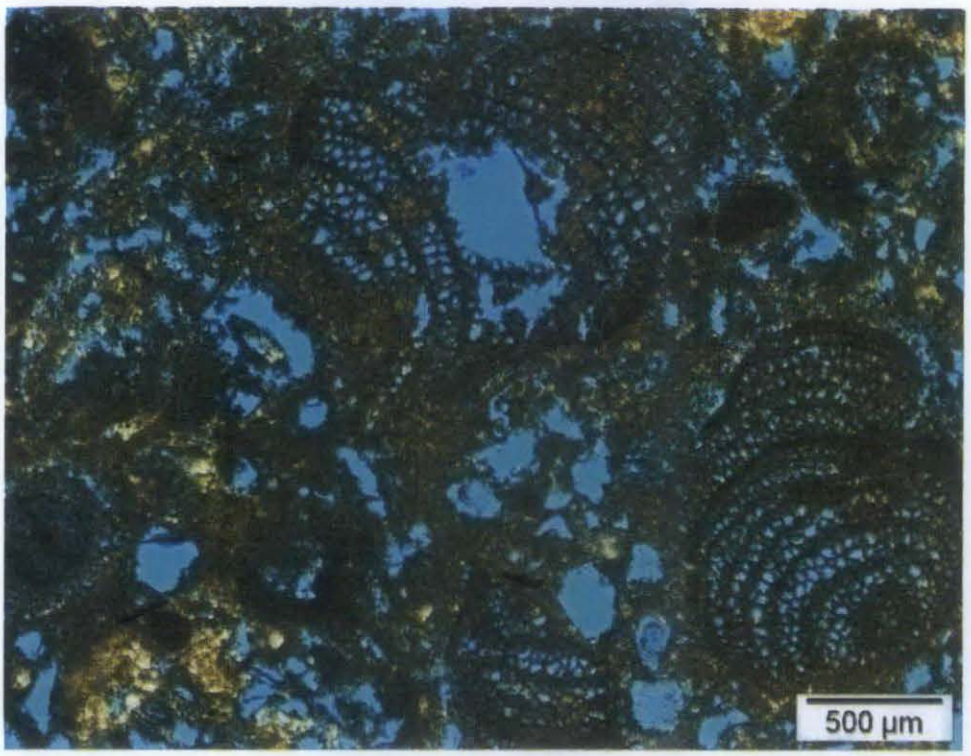

Figure 3.6: Thin section image captured using petrographic microscope under transmitted light. Impregnated blue dye shows the position of the macropores in thin section.

In a second phase, 20 thin sections were prepared with double impregnation. Around 150 images were captured from these thin sections using a fluorescence microscope under ultraviolet light (Figure 3.7). All images were captured in 'Tagged Image File' (TIF) format.

3.6.1.2 Image Analysis

The images were analyzed under cross polarized light using DIA technique to quantify the volume of pore spaces 10 microns or larger in diameter (macropores). Approximately 300 thin section images were analyzed to produce quantitative estimates of the proportion of macropores. In this analysis a particular threshold value of the impregnation resin was used for each image to identify the phase that represents the macropores as indicated by the blue-dyed epoxy. Phase analysis of the image was then used to determine the percentage of macroporosity (by area) (Figures 3.8, 3.9).

Figure 3.7: Thin section image captured using a fluorescence microscope under ultraviolet light. The macropores are luminescing (MaP) while the dark parts of the image represent the grain, cement, or matrix (Gr).

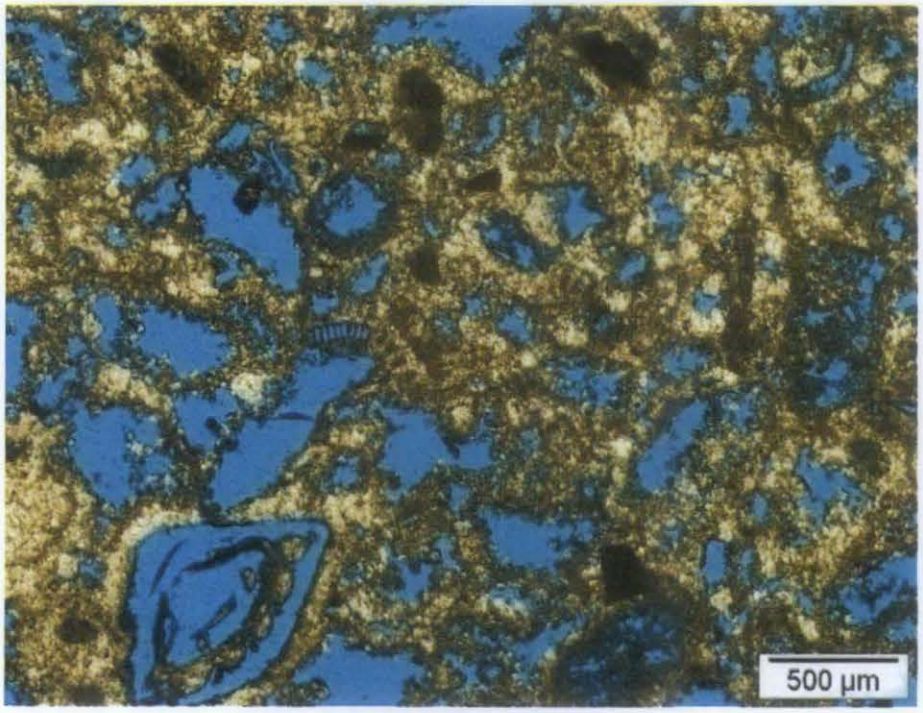

Figure 3.8: Macroporosity estimated to be 20.92% in the image of a core plug taken at a depth of 4130.7ft.

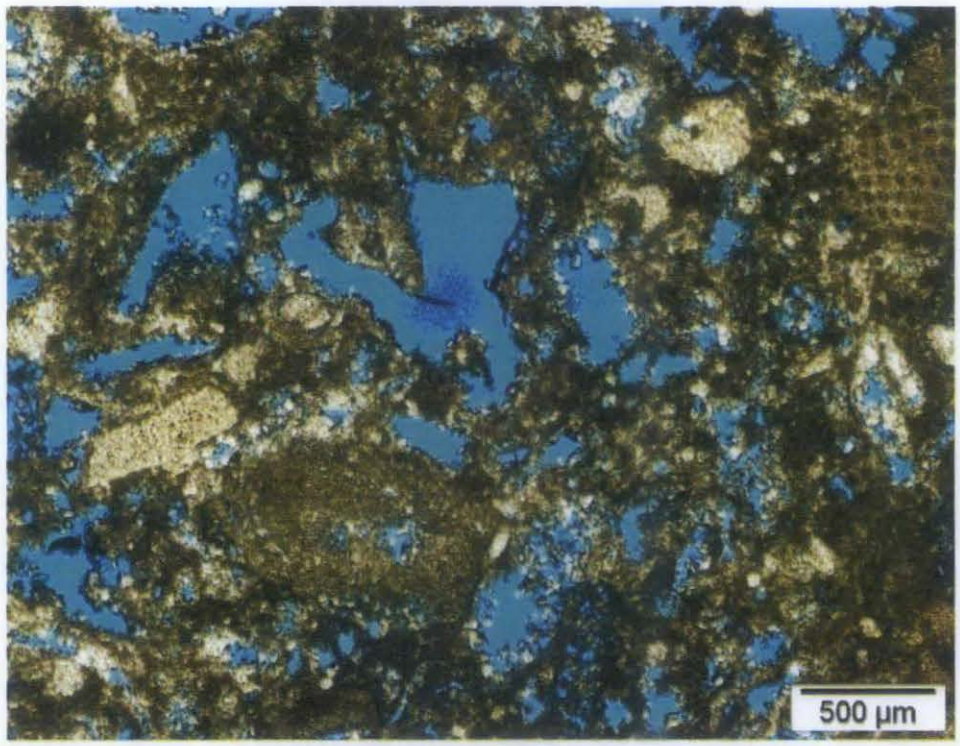

Figure 3.9: Macroporosity estimated to be 18.04% in the image of a core plug taken at a depth of 4688.6ft.

On average, 10 images were analyzed from each of the thin sections with some areas of overlap on the images. The arithmetic mean of the amount of macroporosity estimated from each of the images was taken as the representative macroporosity values for the corresponding core plug. More images from each thin section produce more steady and accurate results irrespective of the image position on the thin section. This factor was considered important because the selection of the location of images on thin sections is always subjective and depends on the observer. It is therefore important to obtain a result that represents the true amount of macroporosity present in a thin section, irrespective of the choice of image position and that can be considered as the representative macroporosity value for the corresponding core plug. However, processing too many images from a single thin section makes the image processing work more time-consuming and produces a huge data set that adds little precision in porosity quantification. Keeping these factors in mind, about 10 images were captured from each thin section, providing an optimum arithmetic mean of the macroporosity of a thin section (Appendix F). This mean value of macroporosity does not vary more than 1% with double the number of images.Since thin sections are about 30 µm in thickness, pores that are between 10 and 30 µm in diameter may not

be visible under transmitted light. To reconfirm the amount of estimated porosity obtained with thin section images (under transmitted light), quantification of macroporosity was also performed with fluorescence microscopy images taken under incident ultraviolet light in some selected samples.

3.6.1.3 Artificial Colour Coding

After quantification of macroporosity, thin section images were coded with false colour using the threshold values that represent the macropore phases on the image. Thus replicas of the thin section images were produced where the macropores were highlighted with artificial colours.

These artificial colour-coded images can be useful to study the macropore network in thin section, and also help to show the connectivity of macropores in two dimensions. Moreover these colour-coded images were also used to match with the original images after macroporosity quantification (Figure 3.10 - 3.15).

3.6.2 DIA for SEM Images

A Scanning Electron Microscope was used to capture photomicrographs from polished thin sections and unpolished rock-stub samples. More than 200 photomicrographs were captured from rock-stub samples and more than 50 photomicrographs were captured from polished thin sections. The representative photomicrographs of core plugs collected at different depths in the reservoirs were analyzed using a freeware software called 'J MicroVision' developed by Nicolas Roduit (University of Geneva, Switzerland). The analysis includes measurement of the crystal size of micrites as well as the diameter of micropores. In this DIA technique, images were first calibrated with the μm scale of the program. Then straight lines were drawn on each of the crystals to measure the maximum diameter (or maximum length of a side) of the crystals (Figures 3.16, 3.17). The same procedure was followed to measure the maximum diameter of the micropores as well.

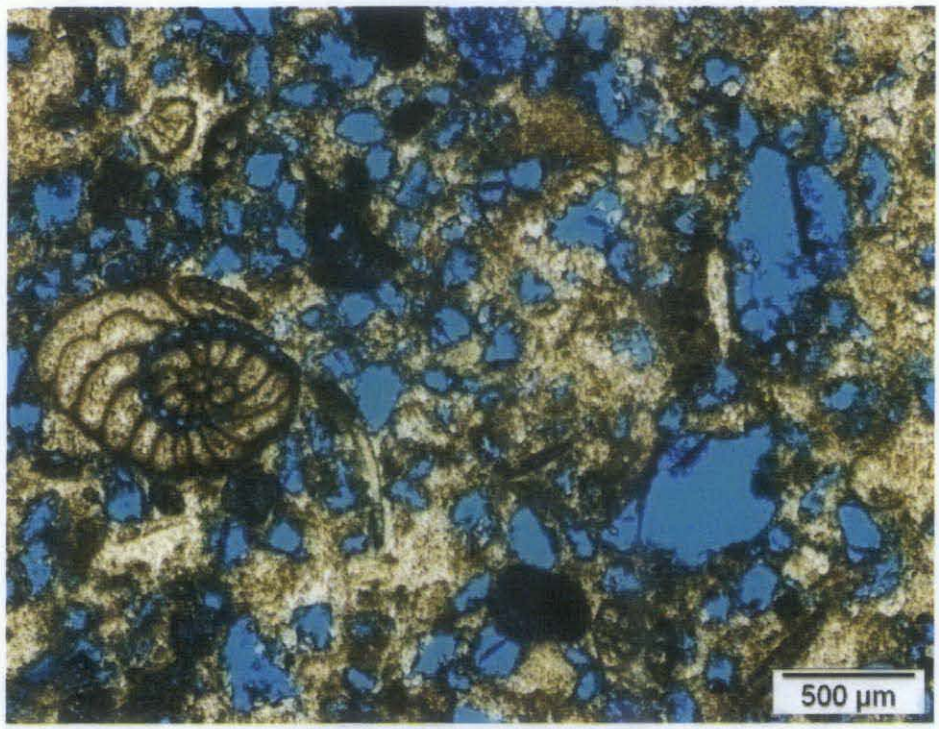

Figure 3.10: Pore spaces (visible with blue dyed epoxy) in the reservoir at a depth of 4334.8 ft. with 25.67% calculated macroporosity.

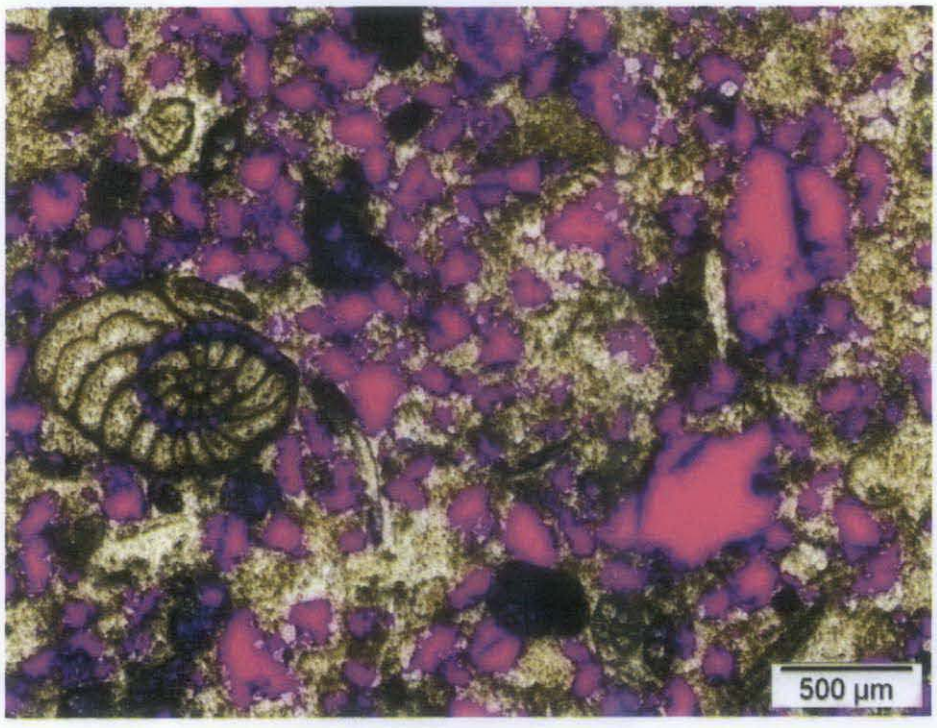

Figure 3.11: The false colour image using the threshold value as determined from Figure 3.10 highlights the macropores.

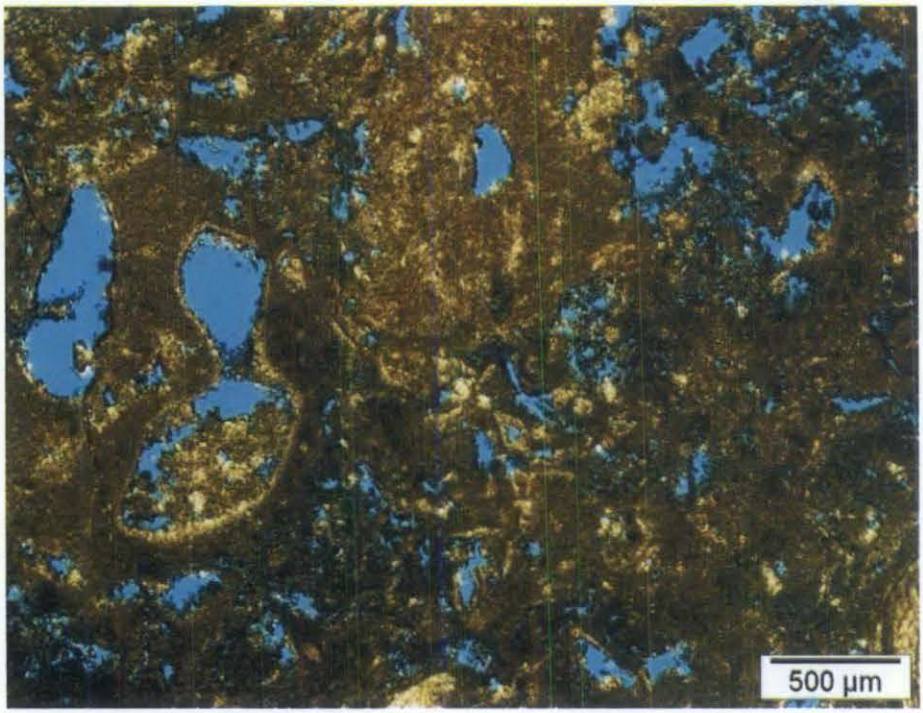

Figure 3.12: Pore spaces (visible with blue dyed epoxy) in the reservoir at a depth of 4100.9 ft. with 11.15% calculated macroporosity.

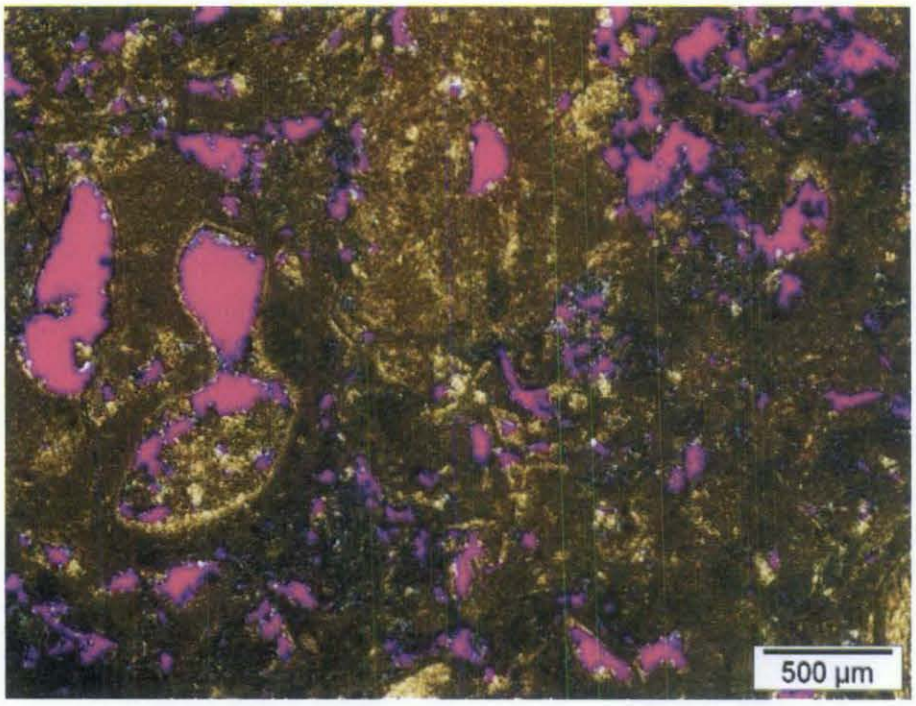

Figure 3.13: The false colour image using the threshold value as determined from Figure 3.12 highlights the macropores.

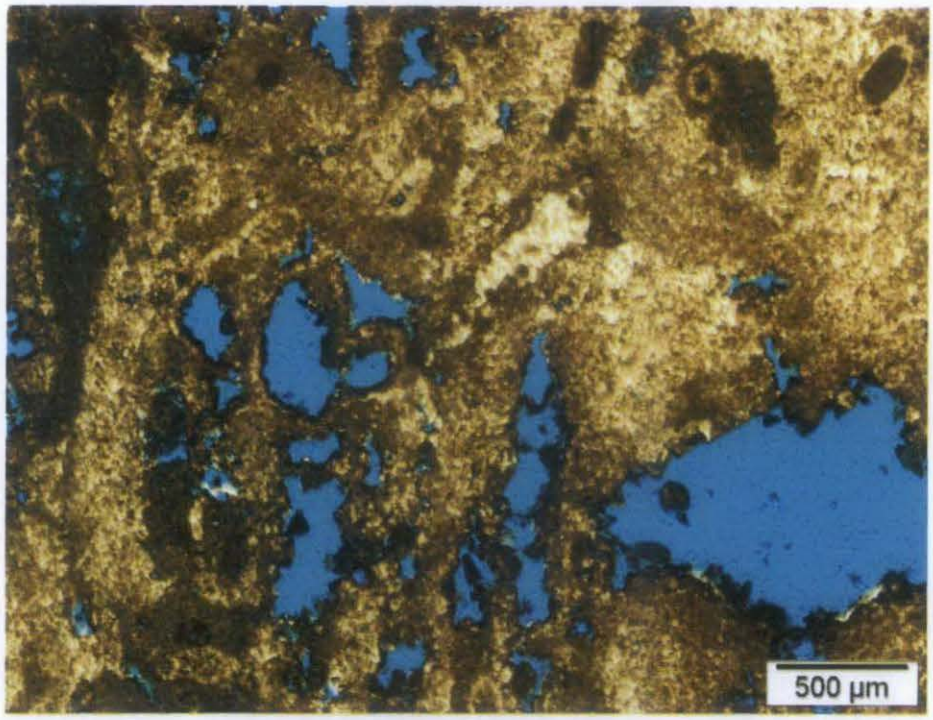

Figure 3.14: Pore spaces (visible with blue dyed epoxy) in the reservoir at a depth of 4080.1 ft. with 13.98% calculated macroporosity.

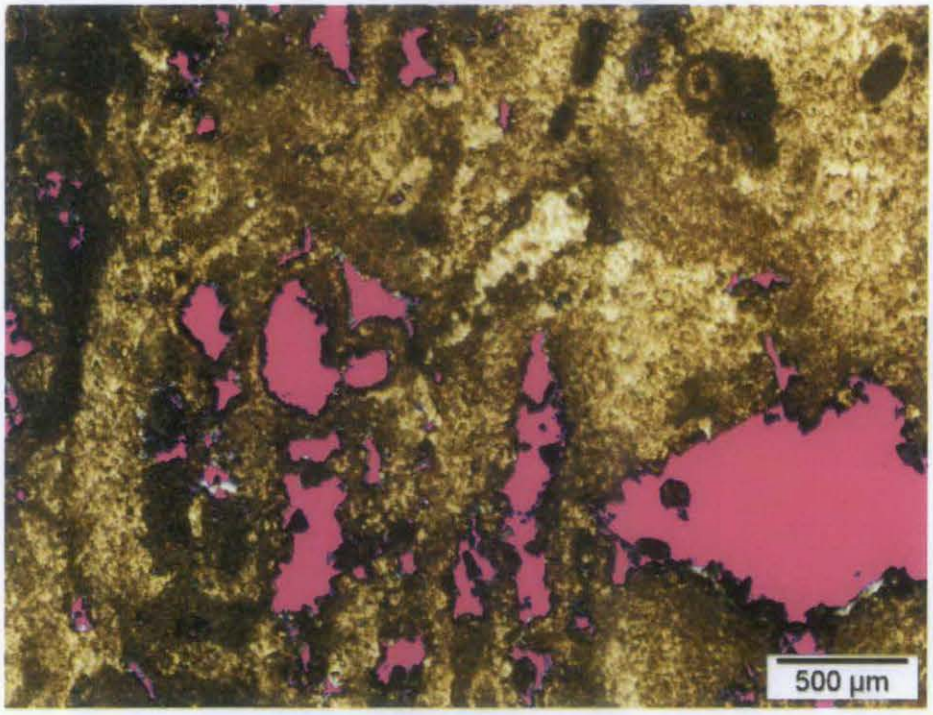

Figure 3.15: The false colour image using the threshold value as determined from Figure 3.14 highlights the macropores.

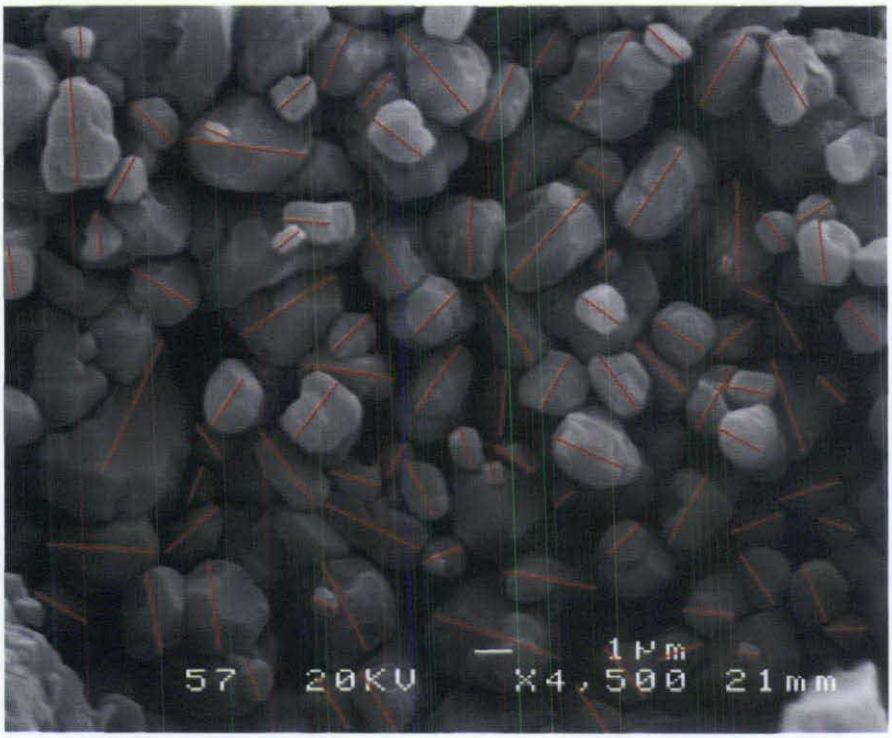

Figure 3.16: Measurement of the crystal size of micrite particles from photomicrographs of samples taken at a depth of 4334 ft in the reservoir.

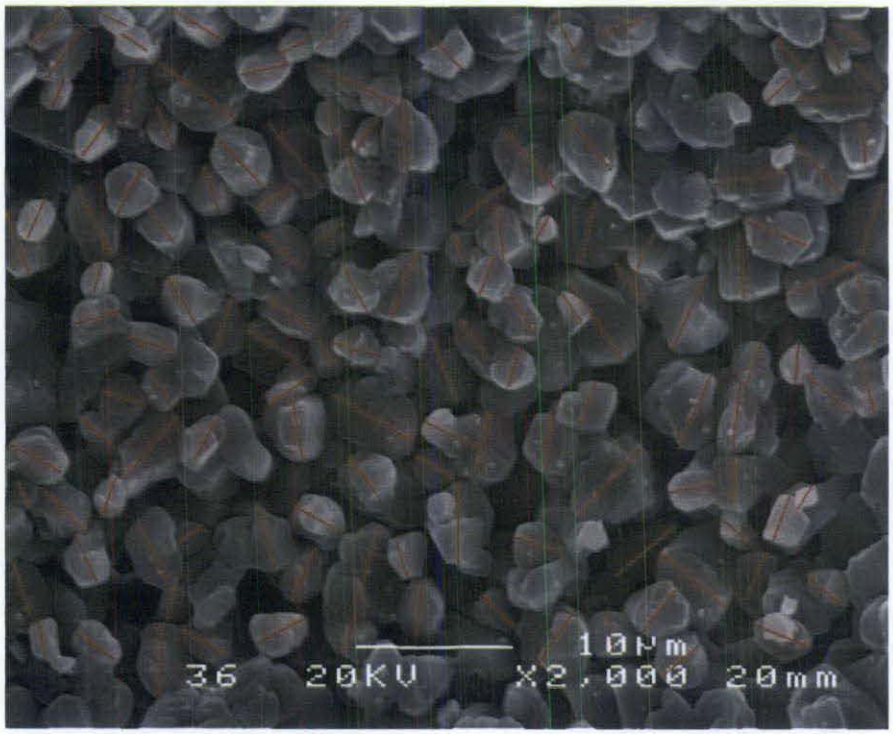

Figure 3.17: Measurement of the crystal size of micrite particles from photomicrographs of samples from a depth of 4139 ft in the reservoir.

3.7 Lithofacies

The various types of lithofacies were studied by describing the cores. This part of the study was done at Sarawak Shell Bhd, Miri. The total cored interval covering a depth range from 4018ft to 4740ft was studied (Figure 3.18). Cores were described in terms of their texture, grains, and lithologies (particularly the presence or absence of clay or mud) (Figure 3.19). The core description and observation of thin sections under petrographic microscope allowed the identification of different lithofacies as well as the exposure surfaces in the cored intervals of the reservoirs.

Figure 3.18: Cored intervals of the reservoirs were studied at the Sarawak Shell Bhd, Miri.

3.8 Core plug Analysis

Core plug analysis includes measurement of net porosity, permeability, and sonic velocity using 1 inch core plug samples.

3.8.1 Porosity, Permeability Measurement

To determine the total porosity and permeability of the core plug samples, an instrument called PoroPerm developed by Vinci Technologies was used (Figure 3.20). It uses helium (He) gas to derive porosity and permeability. Porosity and permeability of the core plugs were measured using gas (Klinkenberg corrected measurement for permeability) to protect the samples from dissolution (as happens in the case of water with carbonates).

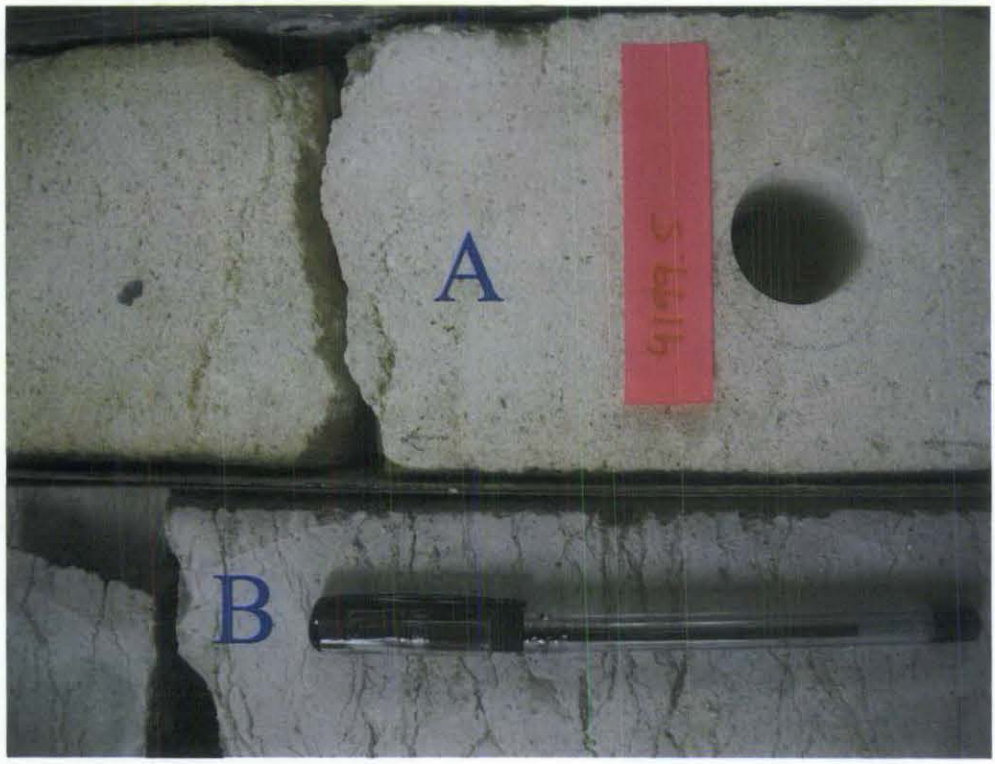

Figure 3.19: Two different lithofacies (marked as A and B) on the top and bottom of the image as observed during core study.

3.8.2 Sonic Velocity Measurement

Sonic velocities of the core plug samples were determined using a Sonic Viewer SX instrument developed by OYO. Both P-wave and S-wave velocities in the longitudinal direction of the core plug samples were determined for each of the 33 core plug samples.

Figure 3.20: Gas derived porosity and permeability measurement instrument called PoroPerm.

3.9 Cathodoluminescence

The cathodoluminescence (CL) operation utilizes the visible light emitted when electrons strike the specimen in a vacuum chamber. The earliest geological use of CL was made by Long and Agrell (1965) and Sippel (1968). CL is now a standard technique in the petrographical study of rock samples. Materials vary greatly in their luminescent properties and minor traces of impurities in minerals can affect the luminescent properties. Cathodoluminescence study was done in KU Leuven with an in-house developed software and a digital camera to capture the images (Figure 3.21). The CL analysis was carried out using a Technosyn Cold Cathodoluminescence Model 8200 Mark II. The operating conditions were 16-20 kV gun potential, 350-600 μA beam current, 0.05 Torr vacuum and 5 mm band width.

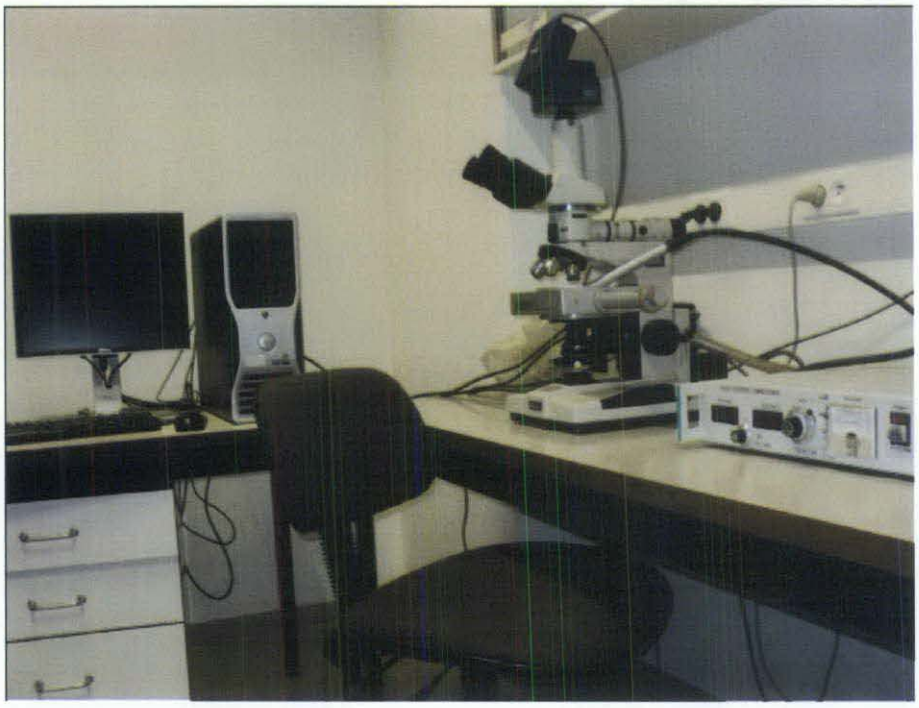

Figure 3.21: Cathodoluminescence microscope used in KU Leuven. The images were captured using a digital camera attached to the microscope.

3.10 Stable Isotope Analysis

Isotopes are atoms whose nuclei contain the same number of protons but a different number of neutrons. Most of the 1500 or so naturally occurring isotopes are unstable and undergo radioactive decay to other isotopes. A subset of isotopes, however, is not radioactive, at least within our ability to measure decay times. These are called stable isotopes (Emery and Robinson, 1993). The analysis of these isotopes can provide not only information on the source of an element of a mineral or fluid, but also the temperature and water composition under which a mineral precipitated. Ten samples were selected and powder samples were collected using a microdrill (Figure 3.22). The powder samples were sent to Friedrich-Alexander-Universitat, Germany for carbon and oxygen stable isotope analysis. Powder samples were digested with 100% phosphoric acid at 70°C using a Gasbench connected to a ThermoFinnigan Five Plus masspectrometer. The ^{13}C and ^{18}O isotope composition of the samples were analyzed and all values were reported in per mil relative to V-PDB. PDB is the acronym for the Pee Dee Belemnite, a reference standard material which has long been exhausted. All

other standards are ultimately calibrated back to this material (Emery and Robinson, 1993).

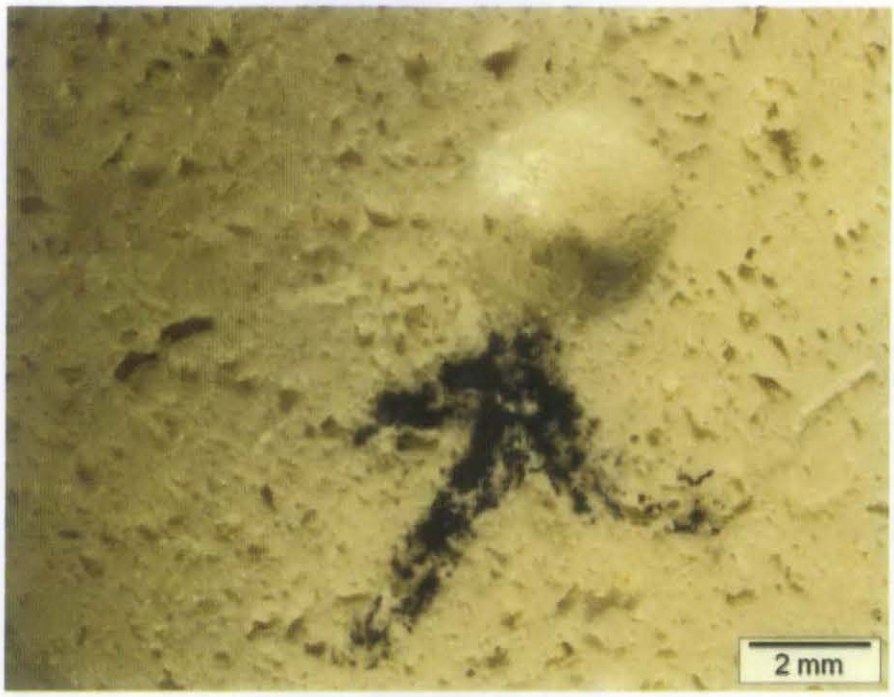

Figure 3.22: Sample taken for ^{13}C and ^{18}O isotope analysis from the core plugs using mini hand driller.

CHAPTER 4

RESULTS AND DISCUSSION

4.1 Introduction

This chapter presents the results of the core study, microscopic study and petrophysical measurements performed on the core plug samples and thin sections. The initial concern of this study was to establish a method to quantify microporosity present in reservoirs of a Miocene carbonate platform of Central Luconia. After quantifying microporosity, the study aimed to demonstrate the effects of microporosity on reservoir properties. The study also focused on explaining the occurrence and distribution of microporosity. Finally, efforts were made to propose a classification scheme for micrite microtextures and microporosity in the Miocene carbonates of Central Luconia.

Microporosity has important effects on the macroporosity, permeability, and sonic velocity of the reservoir. The quantification of microporosity can reduce the uncertainty in permeability prediction by providing a better correlation between porosity and permeability. Digital Image Analysis can be a key technique to quantify microporosity in carbonate reservoirs. The crystallometry and morphometry of micrite particles were studied under a Scanning Electron Microscope (SEM) to determine the occurrence of different micrite microtextures in Miocene carbonates. This study revealed four different classes of micrite microtextures. Depending on micrite microtexture classes, a classification scheme for microporosity is proposed that describes four classes of micropores. The crossplot of macroporosity and permeability reveals different clusters of datapoints. These clusters can be explained in light of the microporosity classes that are proposed during the study.

4.2 Quantification of Microporosity

The first objective of this project was to establish a method to quantify microporosity in Miocene Carbonates. In this study, micropores were defined as all pores that are less than 10 μm in maximum diameter. As discussed in Chapter 3 (Method of Investigation), the difference between observed porosity in DIA and the measured porosity from core plug is considered to represent microporosity. The first step towards the quantification of microporosity is the estimation of macroporosity using DIA followed by the estimation of microporosity.

4.2.1 Estimation and Representation of Macroporosity

Digital Image Analysis was used to quantify the macropores (pores which are 10 microns or larger in diameter) (Appendix F). The DIA methodology has been discussed in detail in the method of investigation Chapter of this thesis. After quantifying the macropores using thin section images under petrographic images, DIA was used to produce false coloured images that represent the macropore distribution with different colours (Figures 4.1 – 4.4). These false coloured images provide a quick look and a better understanding of macropore distribution in the thin sections.

4.2.2 Estimation of Microporosity

In this study, micropores were defined as all pores that are less than 10 microns in maximum diameter. The difference between the measured total porosity from core plugs and the observed porosity in 'Digital Image Analysis' (DIA) is considered to represent microporosity. DIA, using optical petrography, is applied to estimate the amount of macroporosity (pores that are 10 microns or larger in diameter). Porosity measurement of the core plug samples provides the total amount of porosity present in the reservoirs at different depths. Subtracting macroporosity from total porosity values, the amount of microporosity in carbonate reservoirs is determined at different depths. The amount varies between 4 and 25% (Figure 4.5 – 4.7). Table 4.1 represents the data set showing the corresponding amounts of macroporosity and microporosity amount quantified at different depths of the reservoirs.

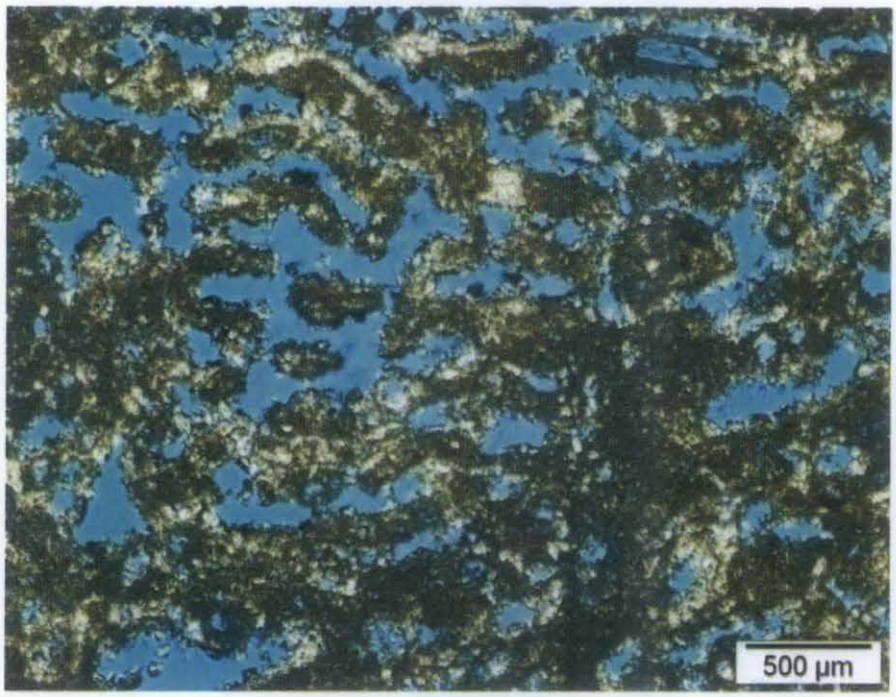

Figure 4.1: Photomicrograph of mouldic porosity developed in coral Porites observed at a depth of 4740.1ft.

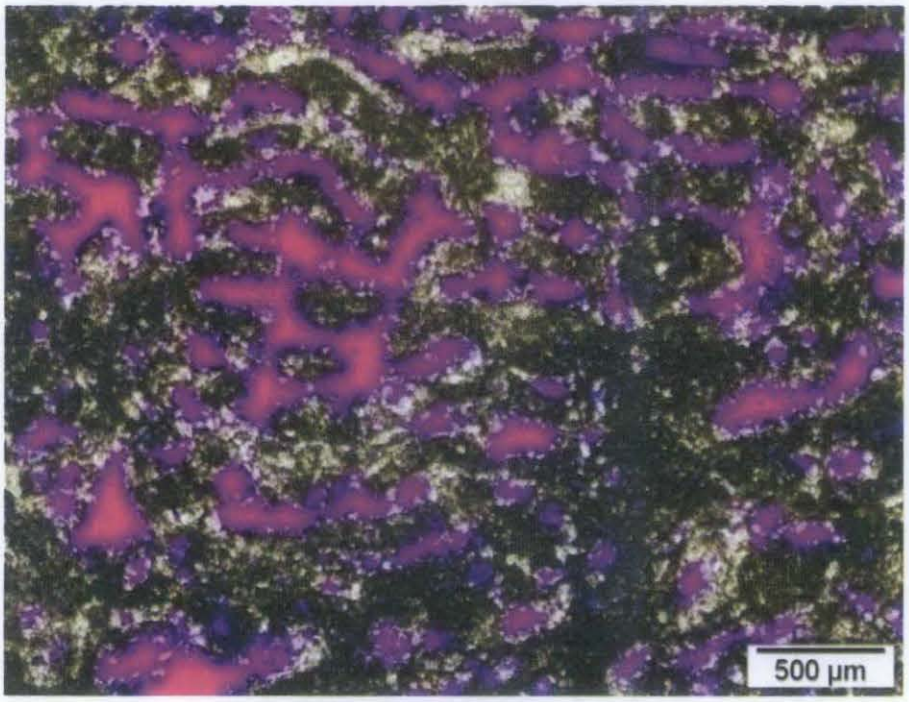

Figure 4.2: False coloured image produced from figure 4.1 using DIA that provides a better visualization of the macropore distribution.

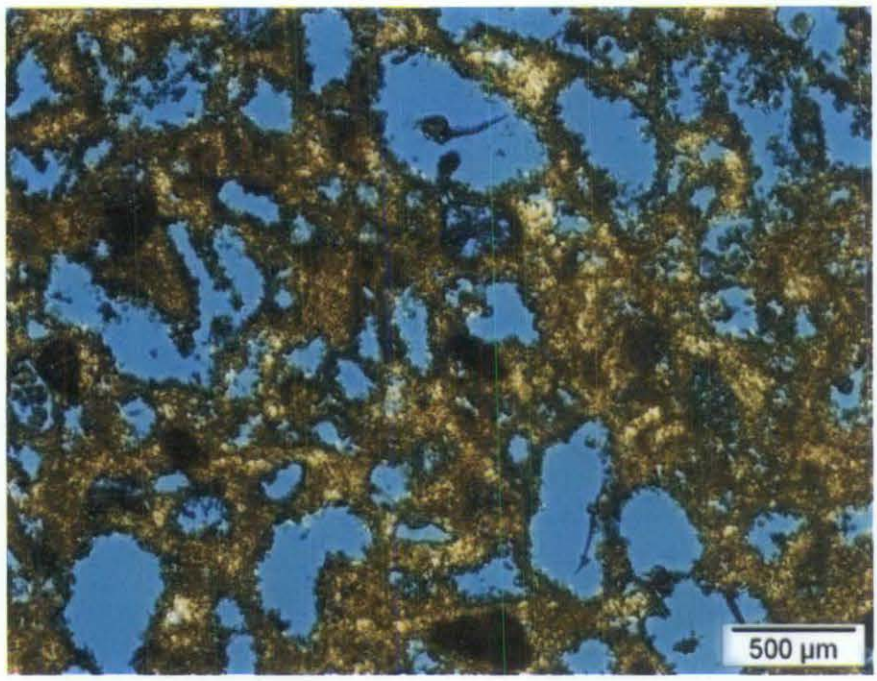

Figure 4.3: Moldic pores observed at a depth of 4130.7ft.

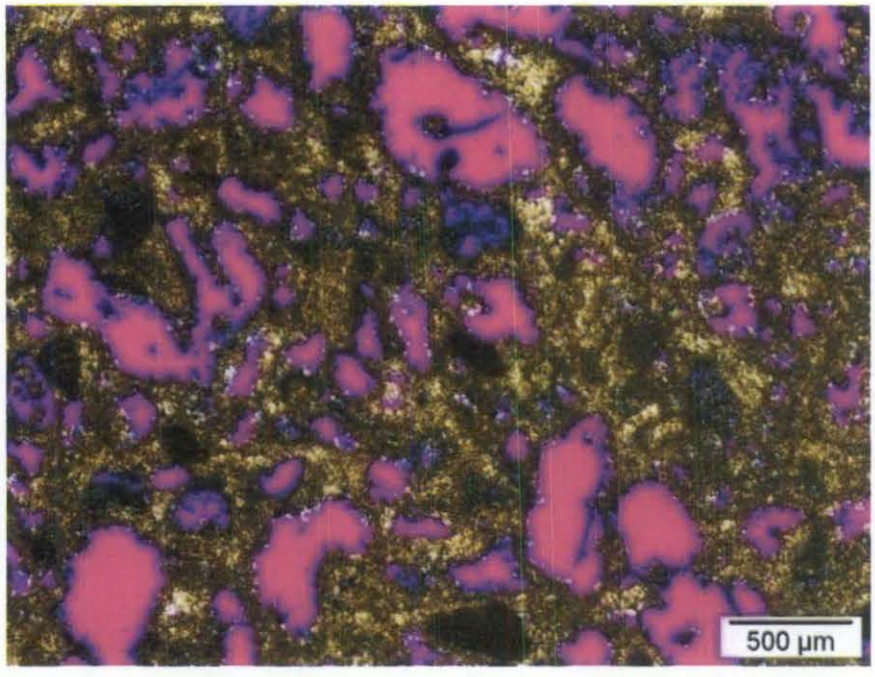

Figure 4.4: False coloured image produced from figure 4.3 using DIA that represents a better visualization of the macropore distribution.

Micropores are not visible under transmitted light microscope as observed in Figure 4.5. Therefore the transmitted light thin section images do not show the variation in microporosity present in the reservoir, whereas microspores are visible under Scanning Electron Microscope (SEM).

Table 4.1: Quantification of microporosity at different depths of the reservoirs

Plug No.	Depth (Feet)	Plug Porosity (%)	DIA Porosity (%)	Microporosity (%)
1	4740.1	36.99	18.46	18.53
2	4688.6	24.416	18.19	6.23
3	4647.9	Broken Plug	21.07	N/A
4	4606.4	36.649	21.65	15.00
5	4592.4	33.256	22.27	10.99
6	4568	16.091	7.16	8.93
7	4534.1	29.228	19.28	9.95
8	4516.4	23.706	5.86	17.85
9	4459.3	Broken Plug	24.87	
10	4440.2	21.346	12.18	9.17
11	4382.2	34.993	21.93	13.06
12	4354.1	29.742	24.92	4.82
13	4334.8	31.641	19.08	12.56
14	4303.9	33.955	24.55	9.41
15	4294	Broken Plug	6.97	N/A
16	4277.6	21.555	6.86	14.70
17	4238.9	32.311	12.04	20.27
18	4229.5	28.128	20.49	7.64
19	4215.9	30.007	19.08	10.93
20	4212.2	21.682	16.32	5.36
21	4199.5	19.818	9.712	10.11
22	4169.7	33.074	23.81	9.26
23	4161.6	36.122	24.04	12.08
24	4139.6	35.823	24.03	11.79
25	4130.7	32.963	20.60	12.36
26	4120.7	Broken Plug	11.05	N/A
27	4111.3	25.806	16.47	9.34
28	4100.9	Broken Plug	13.81	N/A
29	4080.1	Broken Plug	12.94	N/A
30	4070.9	15.693	1.83	13.86
31	4052.7	34.839	21.14	13.70
32	4047.5	35.004	9.99	25.01
33	4018.2	21.743	16.80	4.94

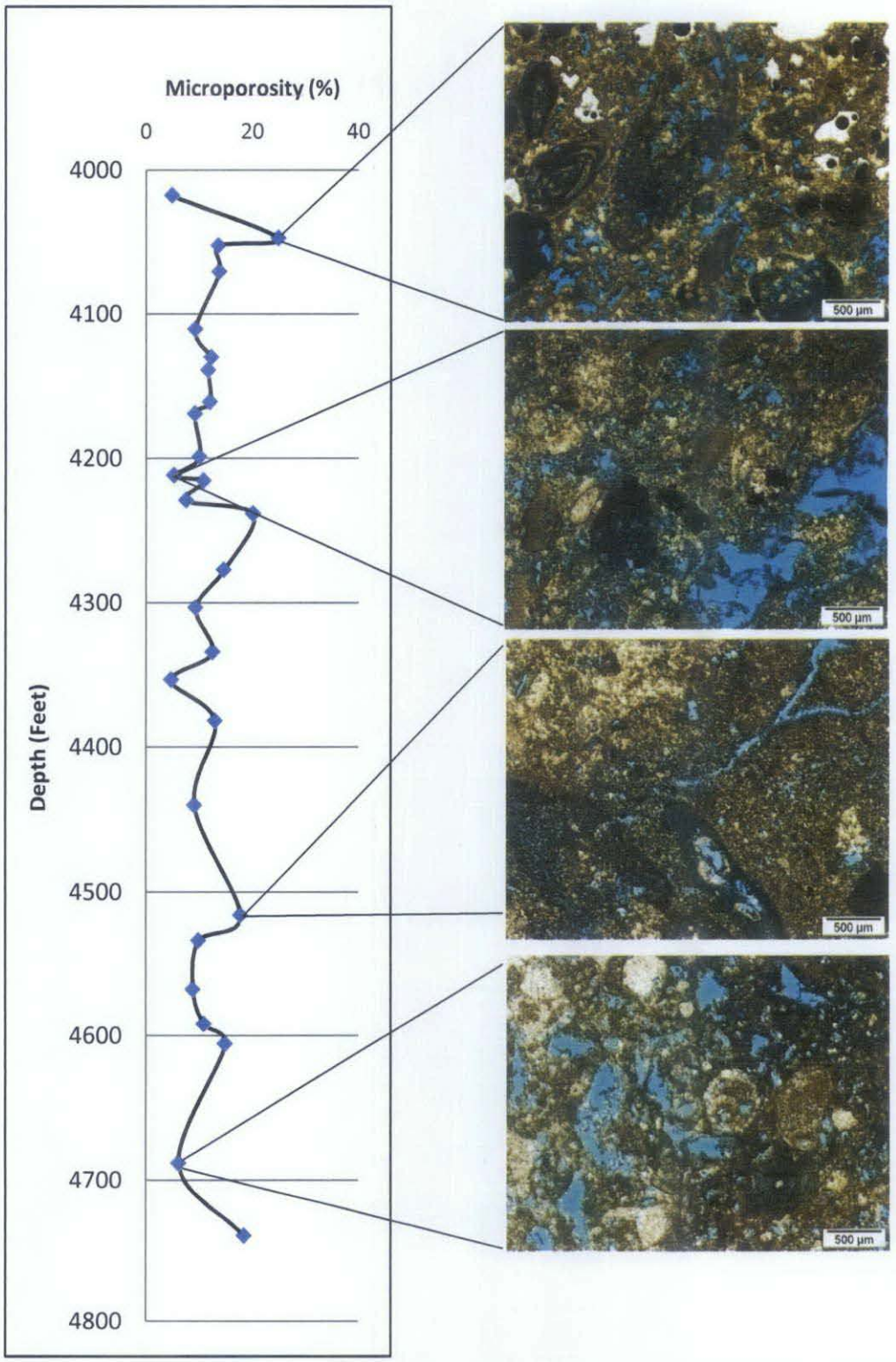

Figure 4.5: The distribution of micropores observed under transmitted light at different depths of the reservoirs.

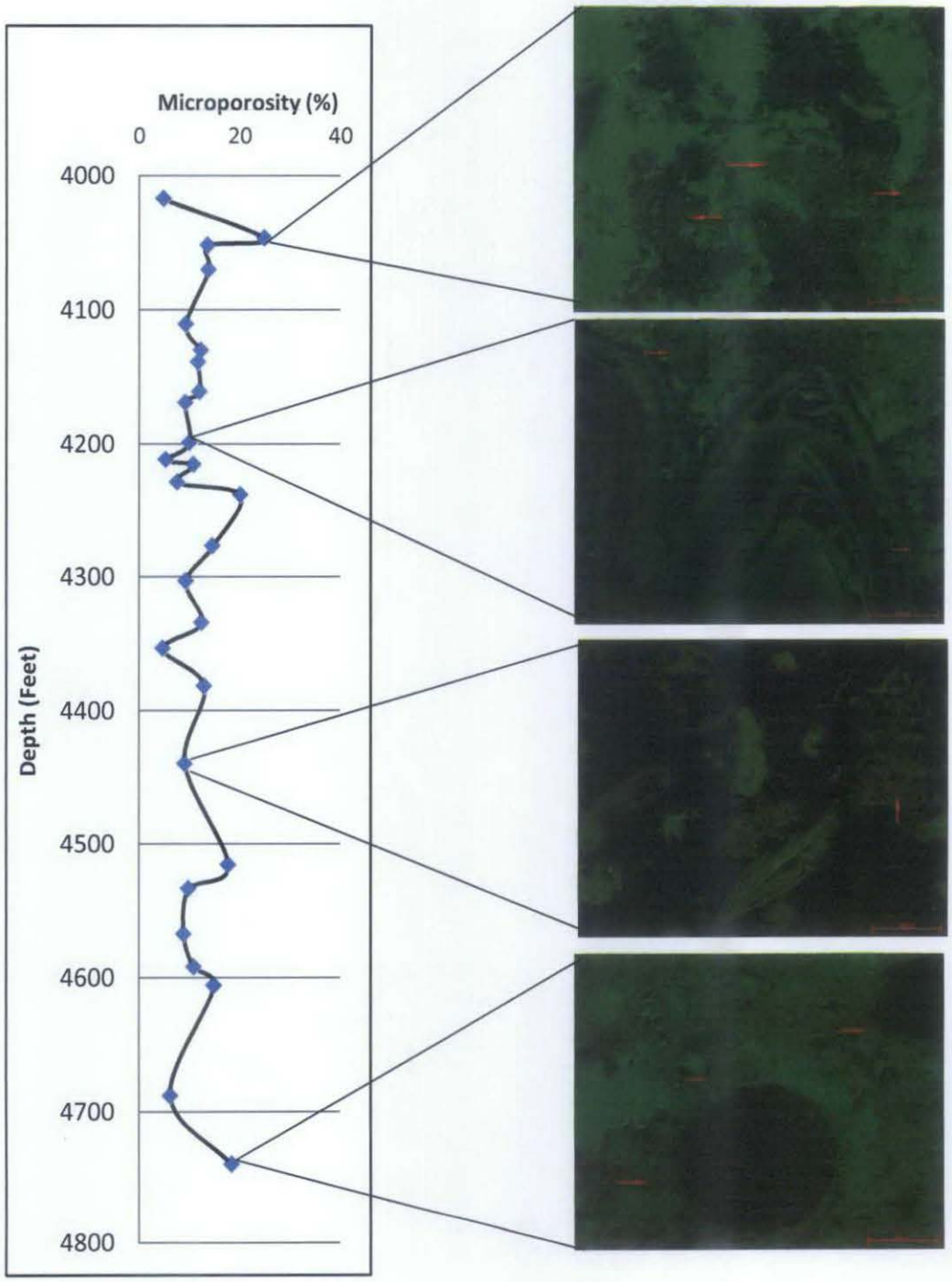

Figure 4.7: Thin sections impregnated with ultra low viscous fluorescent resin were observed under fluorescence microscope. The arrows indicate the areas with microporosity.

Different microtextures show different characteristics under SEM and the amount of microporosity present in the reservoir also varies with the type of micrite microtexture (Figure 4.6). The microporous areas in the reservoirs can be identified

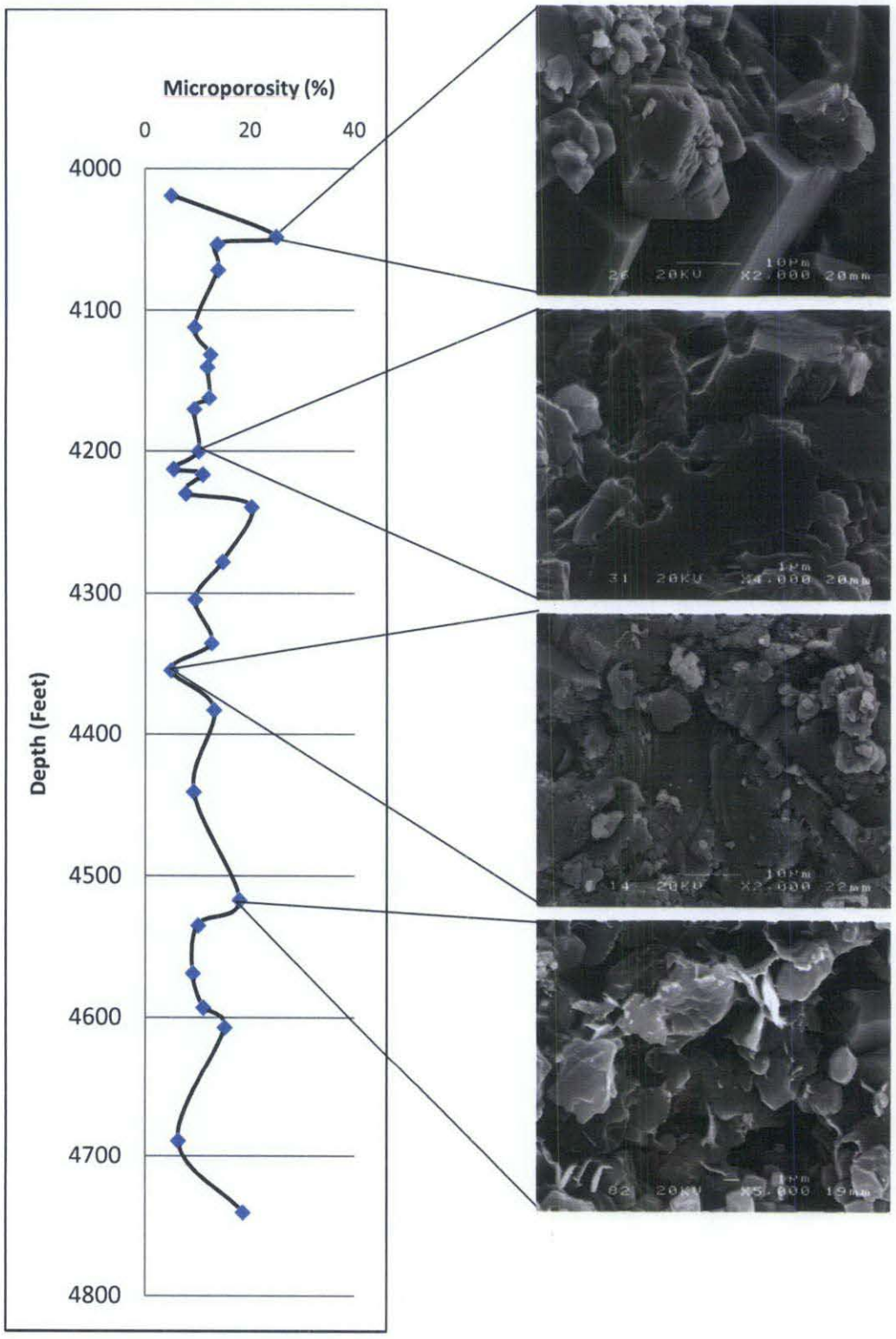

Figure 4.6: The occurrence of microporosity with different microtextures observed under SEM.

using thin section photomicrographs captured under ultraviolet light using thin sections double impregnated with ultra low viscous fluorescent resin (Figure 4.7).

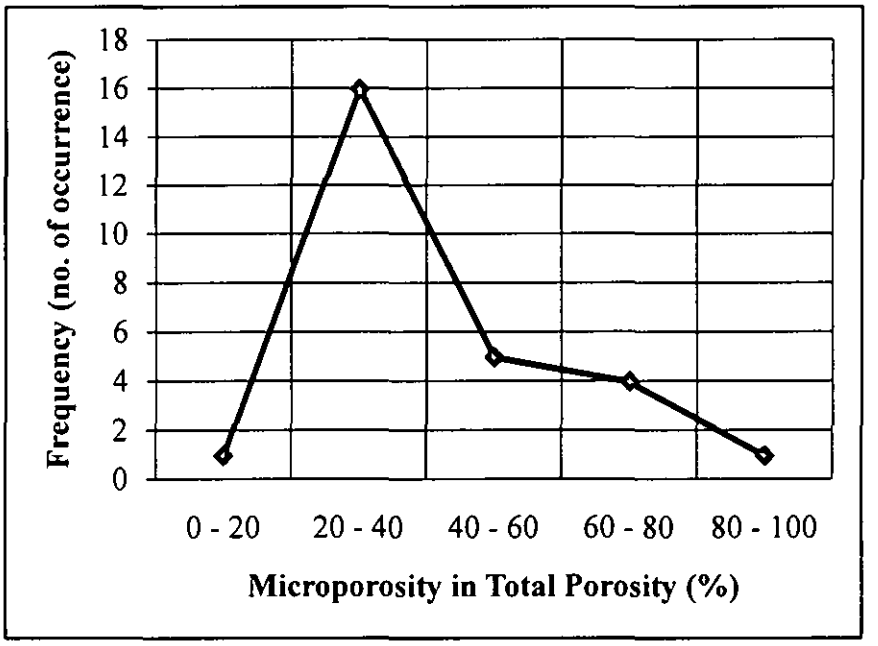

Figure 4.8: The frequency distribution of microporosity contribution to total porosity. The most number of samples give 20-40% of microporosity in terms of total porosity.

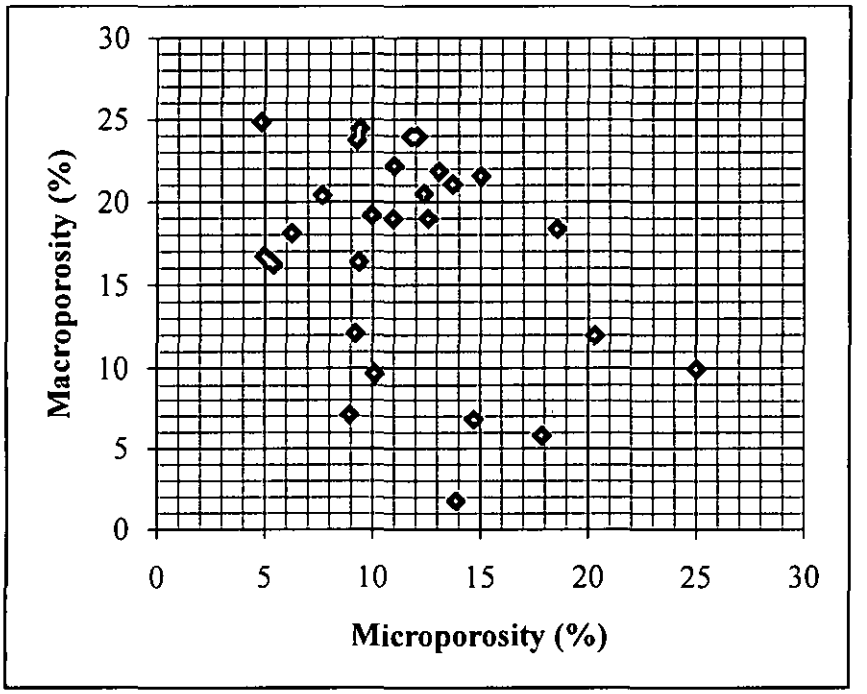

Figure 4.9: The crossplot between microporosity and macroporosity present in the reservoirs. The occurrence of microporosity apparently doesn't follow the occurrence of macroporosity.

Since thin sections are about 30 microns in thickness, pores that are between 10 and 30 microns in diameter may not be visible under transmitted light. To match the data of porosity estimates obtained with thin section images (under transmitted light), quantification of macroporosity was also performed with fluorescence microscopy images taken under incident ultraviolet light in some selected samples. The macroporosity values determined using fluorescence microscopy matched well with the values obtained with transmitted light microscopy.

The total porosity may comprise a significant percentage of microporosity. Miocene carbonate reservoirs of Central Luconia have microporosity in the order of 20 – 40% of the total porosity in most samples, although some samples may have a proportion of microporosity as high as 80% of the total porosity (Figure 4.8). The occurrence of microporosity is apparently not related to the occurrence of macroporosity. As shown in Figure 4.9, microporosity percentages can be as high as 25% in a rock with 10% of macroporosity; similarly a rock may have 25% of macroporosity with 5% microporosity.

4.2.3 Discussion

Baechle et al. (2004) stated that the total porosity measured from core plugs does not entirely relate to fluid flow, because pore bodies connected by very small pore throats do not allow fluid flow and because of the tortuosity effects of the pores. They also stated that carbonate rocks with bimodal pore size distribution, like large vuggy and moldic pore types versus the porosity present within the matrix, could be divided into macro and microporosity. This bimodal distribution of porosity in carbonates will allow studying the abundance and occurrence of microporosity. Several researchers mentioned the importance of using fluorescent resin in the epoxy for thin section impregnation (e.g. Yanguas and Dravis, 1985; Ruzyla and Jezek, 1987). This procedure was found to be effective in enhancing the ability to detect the microporous zones in thin sections under ultraviolet light. In this study, transmitted light microscopy was used to quantify microporosity while fluorescence microscopy was used to detect the microporous zone on the photomicrographs.

Miocene carbonate reservoirs have a significant amount of microporosity that can reach up to 25% by volume or 80% of the total porosity. Rocks with the same amount of microporosity may have different amount and type of macroporosity (Figures 4.5, 4.6, 4.7, 4.9). This observation indicates that the occurrence of microporosity in carbonate reservoirs should be explained in a different manner compared to the occurrence of macroporosity.

4.3 Effects of Microporosity on Permeability and Sonic Velocity

After completing the quantification of microporosity at different depths of the reservoirs, the next step was to observe the effects of microporosity on reservoir properties (e.g. permeability, sonic velocity). This study presents some empirical relationships between microporosity and permeability, and microporosity versus sonic velocity.

4.3.1 Microporosity and Permeability Relationship

Although different permeability values were detected in different samples for the same microporosity value, an overall inverse relationship between microporosity and permeability is observed. This relationship (Figure 4.10) does not follow a linear trend but indicates that for a certain amount of porosity, permeability is reduced with increased microporosity (Rahman and Pierson, 2011) (Appendix B).

However, when microporosity is deducted from the total porosity the relationship between porosity and permeability shows a better correlation (Figures 4.11 and 4.12) (Appendix C). Thus taking microporosity into consideration can reduce the uncertainty in correlation between porosity and permeability (Rahman and Pierson, 2011).

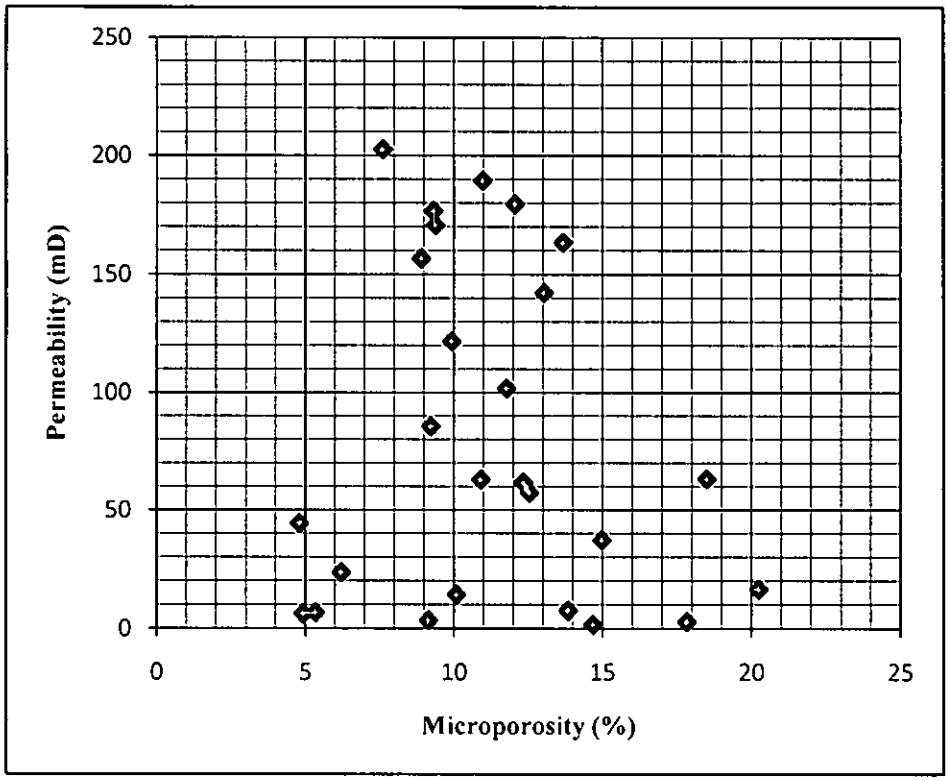

Figure 4.10: Microporosity shows an inverse relationship with permeability.

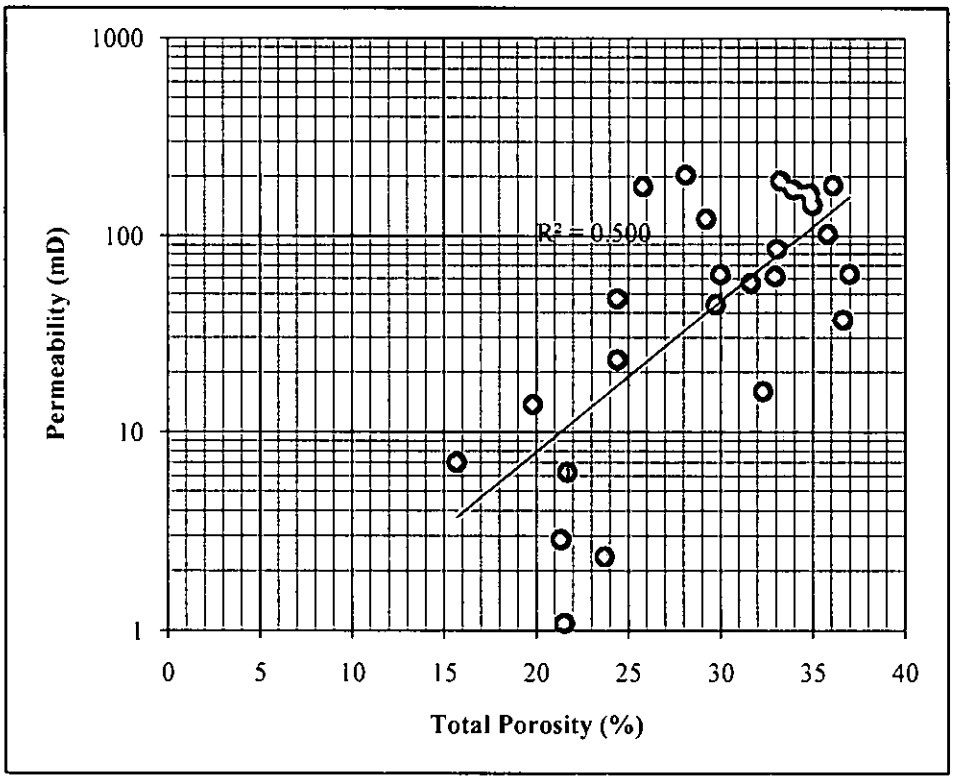

Figure 4.11: The crossplot between total porosity and permeability.

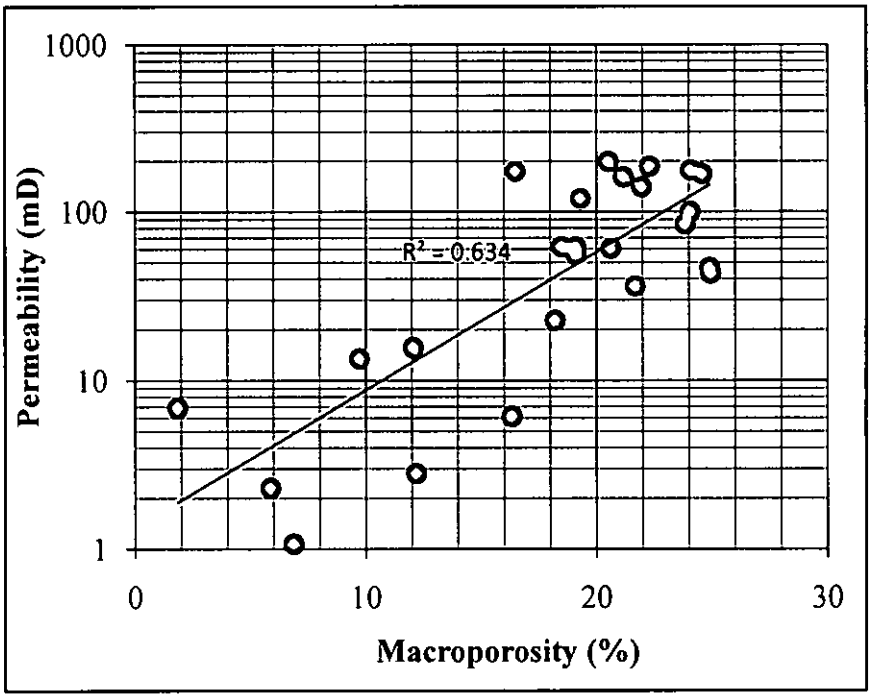

Figure 4.12: A better correlation is observed with permeability when microporosity is deducted from the total porosity.

4.3.2 Microporosity and Sonic Velocity Relationship

It is most unlikely to observe a simple and universal relationship between porosity and elastic properties in carbonate reservoir rocks. Factors other than porosity strongly influence seismic velocities of carbonates (Fournier and Borgomano, 2009). Other than porosity amount some of the factors that influence the elastic properties of carbonates are rock texture, lithotypes, pore stiffness, pore structure, pore aspect ratio etc. Figures 4.13 and 4.14 demonstrate that microporosity reduces the sonic velocity in carbonate reservoir rocks: both P-wave and S-wave velocity (measured along the longitudinal direction of core plugs) decrease with an increase in microporosity in the same reservoir. This suggests that the sonic velocity of a carbonate reservoir rock is lower when the proportion of microporosity is higher (Rahman and Pierson, 2011).

4.3.3 Permeability and Sonic Velocity Relationship

The relationship between permeability and sonic velocity in carbonate reservoir rocks is neither simple nor linear in trend. However, as shown in Figures 4.15 and 4.16,

both S-wave and P-wave velocities are lower at higher permeability. It implies that the reservoir has a lower sonic velocity when there are more interconnections between the macropores (Appendix D).

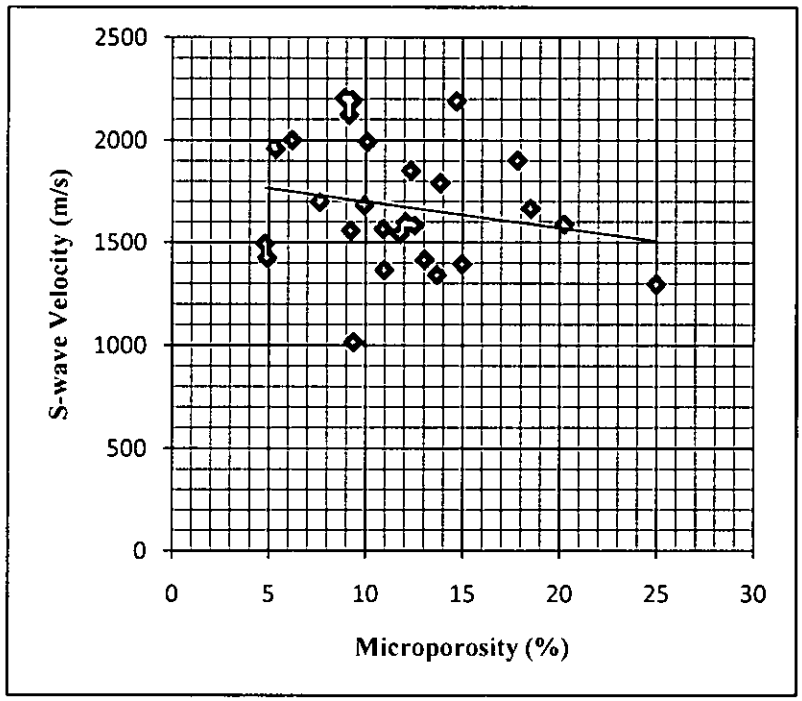

Figure 4.13: S-wave velocity of the carbonate reservoir reduces as microporosity increases.

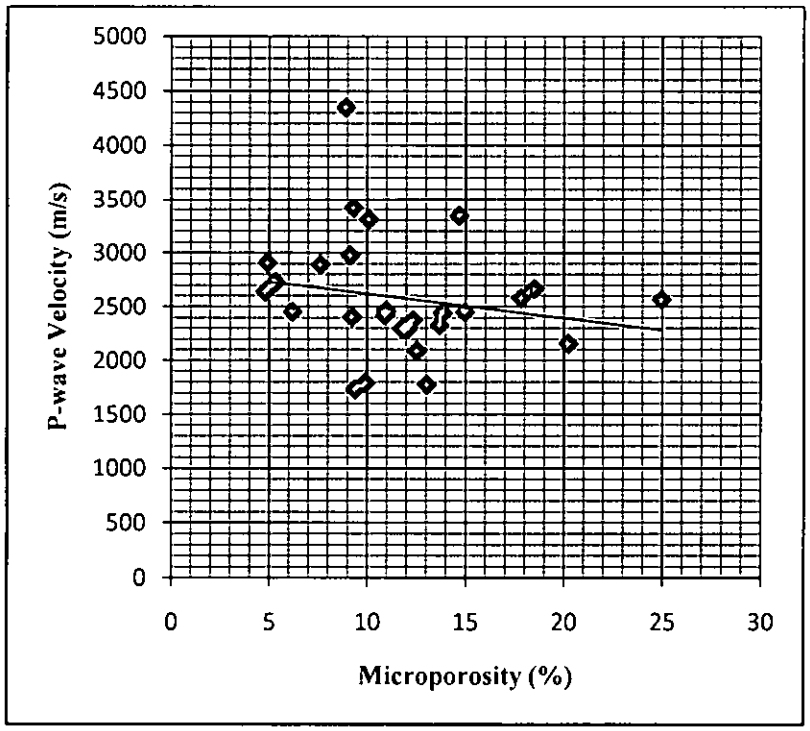

Figure 4.14: P-wave velocity of the carbonate reservoir reduces as microporosity increases.

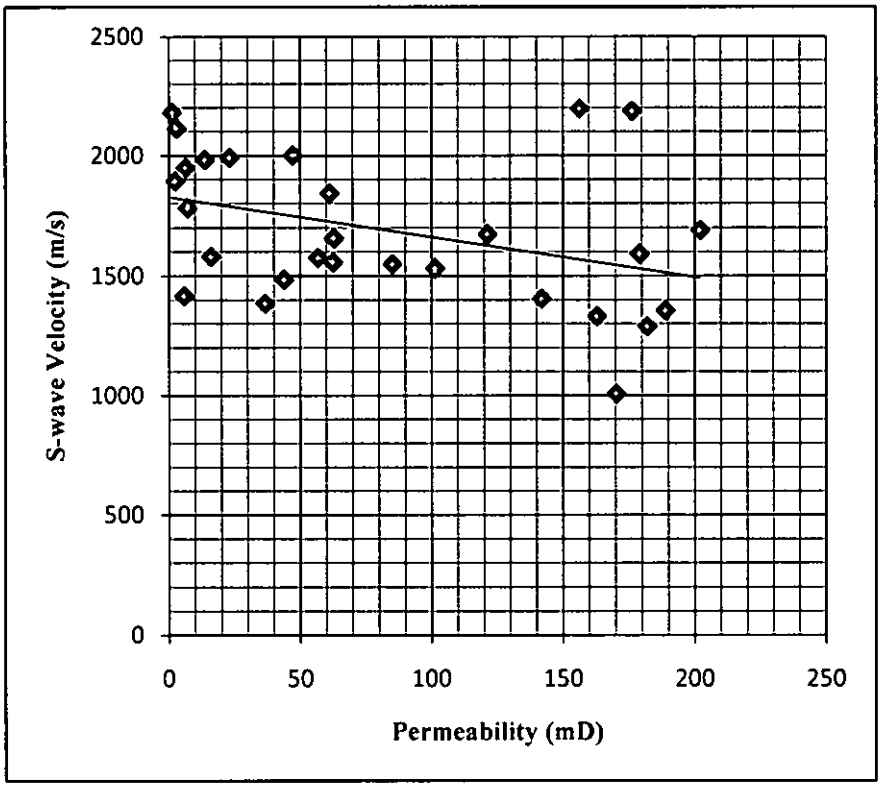

Figure 4.15: S-wave velocity is lower for higher permeability in carbonate reservoirs.

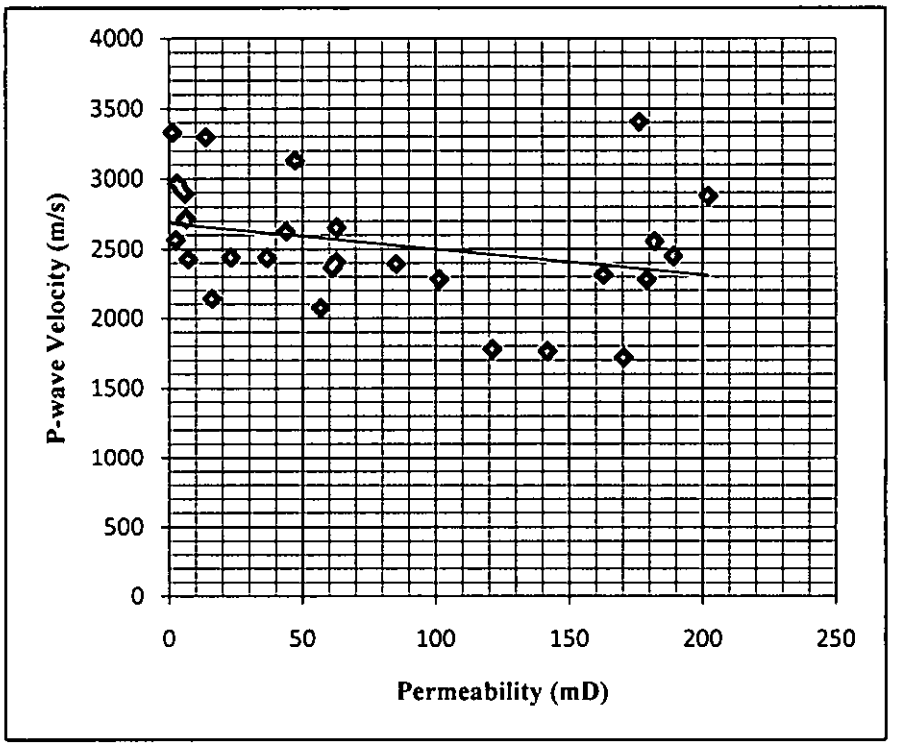

Figure 4.16: P-wave velocity is lower for higher permeability in carbonate reservoirs.

4.3.4 Discussion

The influence of pore types on permeability and acoustic velocities in carbonates has been addressed in numerous studies (Rafavich et al., 1984; Anselmetti and Eberli, 1993, 1997, 1999, 2000; Kenter et al., 1995; Wang, 1997; Sun et al., 2001; Assefa et al., 2003; Eberli et al., 2003; Baechle et al., 2004; Saleh and Castagna, 2004; Weger et al., 2004; Agersborg et al., 2005; Kumar and Han, 2005; Rossebø et al., 2005; Youssef et al., 2008). Both velocity-porosity and porosity-permeability relationships in carbonates are strongly influenced by pore structure (Anselmetti et al., 1998; Anselmetti and Eberli, 1999). Anselmetti and Eberli (1993, 1997, 1999) demonstrated how variations in pore space geometry in carbonates influence acoustic velocities. Anselmetti and Eberli (1999) revealed a strong dependence between sonic velocities and the combined factors of porosity and pore structure in carbonates.

Microporosity has its effects on the reservoir properties of carbonates. These effects are important, particularly in cases where microporosity covers an appreciable fraction of the total porosity. There are numerous studies on the effects of microporosity in carbonate reservoir properties. Weger et al. (2009) demonstrated that combining porosity (macroporosity) and microporosity leads to better estimates of sonic velocity than using total porosity (Figure 4.17). Baechle et al. (2004) stated that it is important to separate the total porosity into macroporosity and microporosity in order to obtain a better correlation for permeability and velocity prediction. In addition Baechle et al. (2004) showed that the correlation coefficient between microporosity and acoustic velocity is much higher and better than between total porosity and acoustic velocity.

Baechle et al. (2008) mentioned that by subtracting microporosity from total porosity, the scatter in a velocity-porosity relationship could be reduced, indicating that the fraction of stiff macropores versus soft micropores is responsible for the variation of velocity at any given porosity. Baechle et al. (2004) mentioned that the image macroporosity (porosity that are estimated from thin section images) is an excellent indicator of permeability, whereas image macroporosity represents the difference between total porosity and microporosity in the reservoir. They also demonstrated that using image macroporosity versus permeability trend reduces the

uncertainty of permeability prediction by more than one order of magnitude. Anselmetti and Eberli (1999) demonstrated that rock samples dominated by microporosity showed lower sonic velocities for a given porosity.

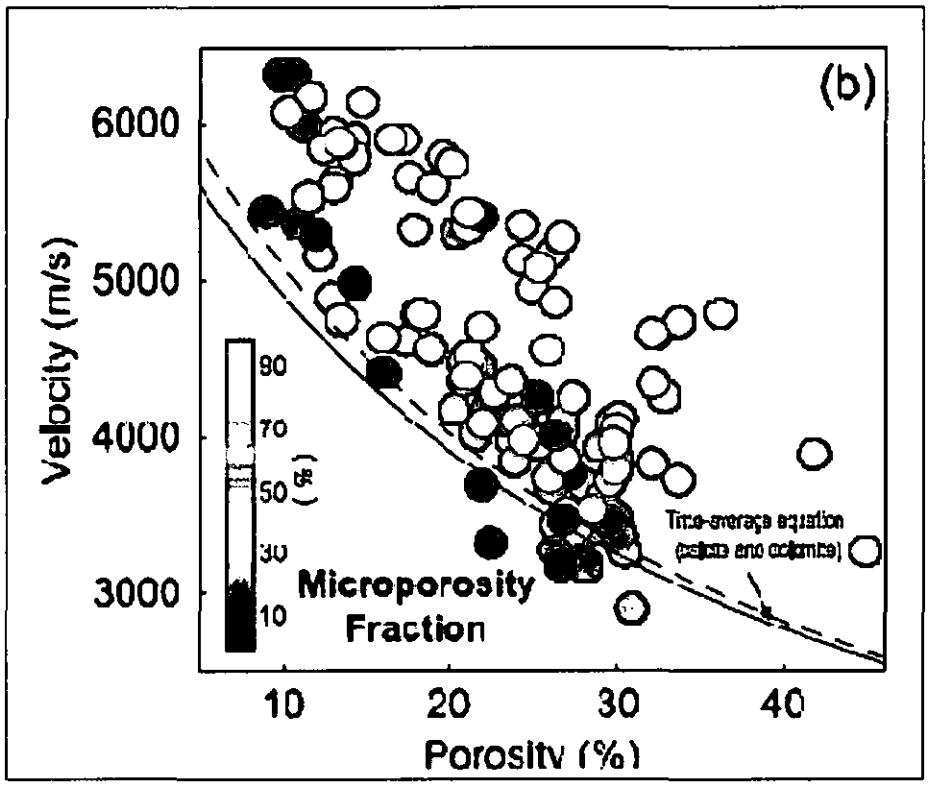

Figure 4.17: Porosity and sonic velocity relationship in carbonate reservoirs (Weger et al., 2009).

4.4 Microtexture and Microporosity Classification of Miocene Carbonates

To classify porosity in carbonate reservoirs, it is necessary to understand the types of texture of the rock. The textures of carbonates can be explained by studying the lithofacies of the rock. The occurrence, abundance and distribution of microporosity are controlled by the micrite microtextures. The study of lithofacies and microtextures of the rock can lead to establishing a microporosity classification scheme relating to the flow related properties in carbonate reservoirs. Moreover, studying diagenesis is important to know the environment of microporosity formation in rocks.

4.4.1 Lithofacies Types

Rock cores covering the reservoirs over a depth interval between 4018ft and 4740ft were studied in terms of lithofacies. Five different lithofacies were identified. To describe lithofacies, standard terminologies used by Shell Sarawak Bhd. were followed.

1) Chalky mouldic limestone (LCM)
2) Argillaceous tight limestone (ALT)
3) Mouldic limestone (LM)
4) Mouldic dolomitic limestone (LDM)
5) Chalky limestone (LC)

These facies classes are grouped based on macroscopic observation of the core plugs and thin section observation under the microscope. These lithofacies have different amounts of porosity and permeability and different pore types. Among these five types of facies, chalky mouldic limestone, chalky limestone and mouldic limestone are excellent reservoir facies in terms of porosity and permeability. Mouldic dolomitic limestone is a moderately good reservoir facies. Argillaceous tight limestone represents a poor quality reservoir facies in terms of porosity and permeability.

Chalky mouldic limestone (LCM) is the best reservoir facies among the five that are defined in the study. This facies has excellent reservoir qualities with an average porosity of 32.71% and a permability of 110.68 mD (Figure 4.18). The texture comprises packstone, pack-wackestone, and some grainstone according to Dunham (1962) classification. Mouldic porosity is the dominant pore type in this type of facies including solution-enhanced pores according to the pore type classification of Choquette and Pray (1970).

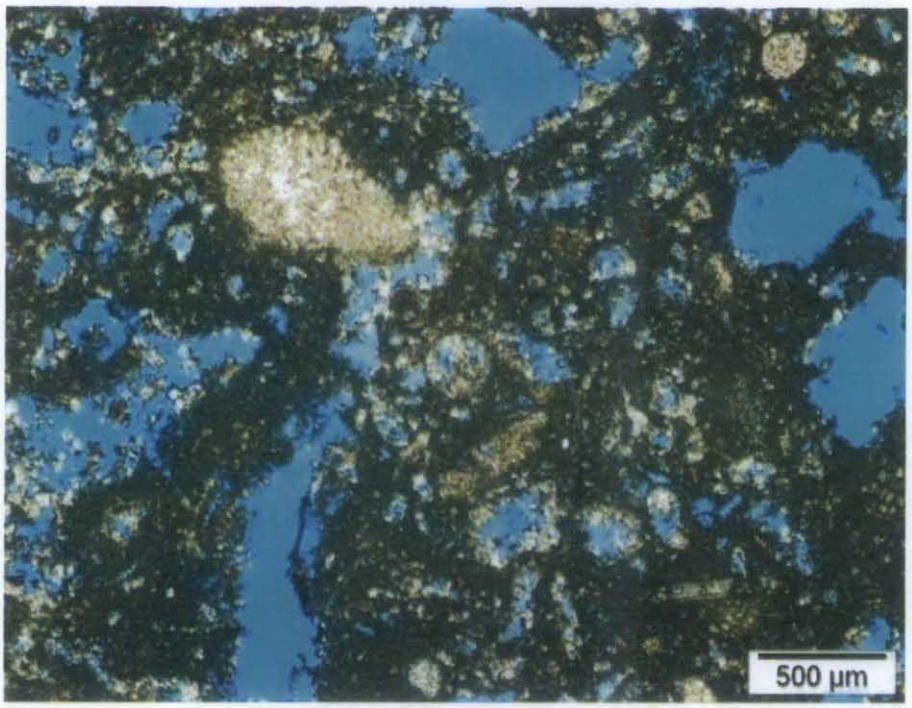

Figure 4.18: Thin section photomicrograph of a chalky mouldic limestone (LCM) at a depth of 4740.1ft. LCM facies has mostly mouldic pores.

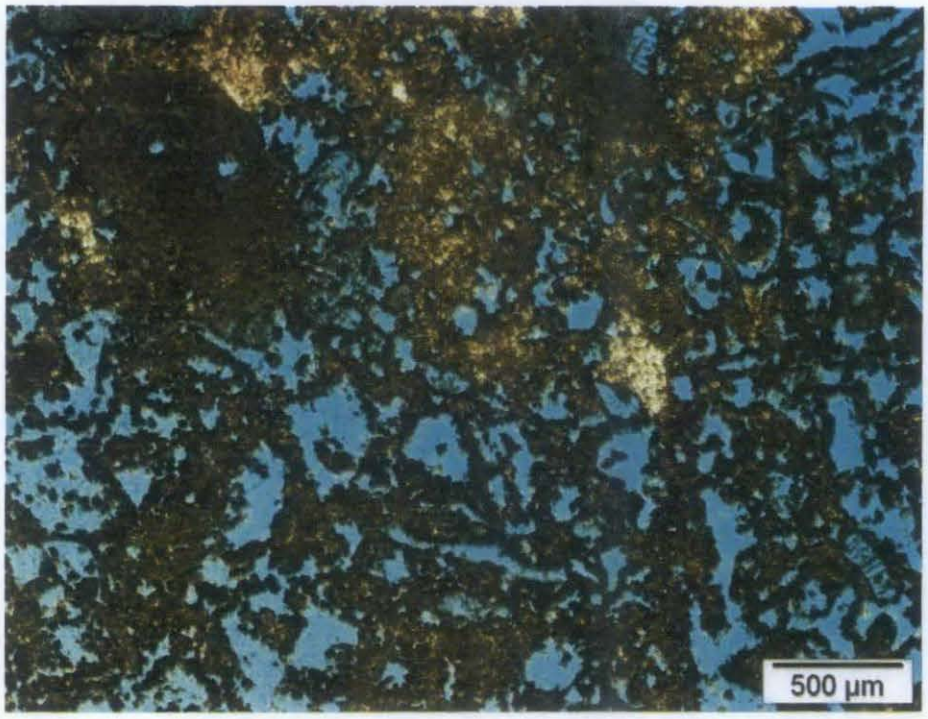

Figure 4.19: Thin section photomicrograph of a chalky limestone (LC) observed at a depth of 4169.7ft. LC facies has good interconnection between the macropores.

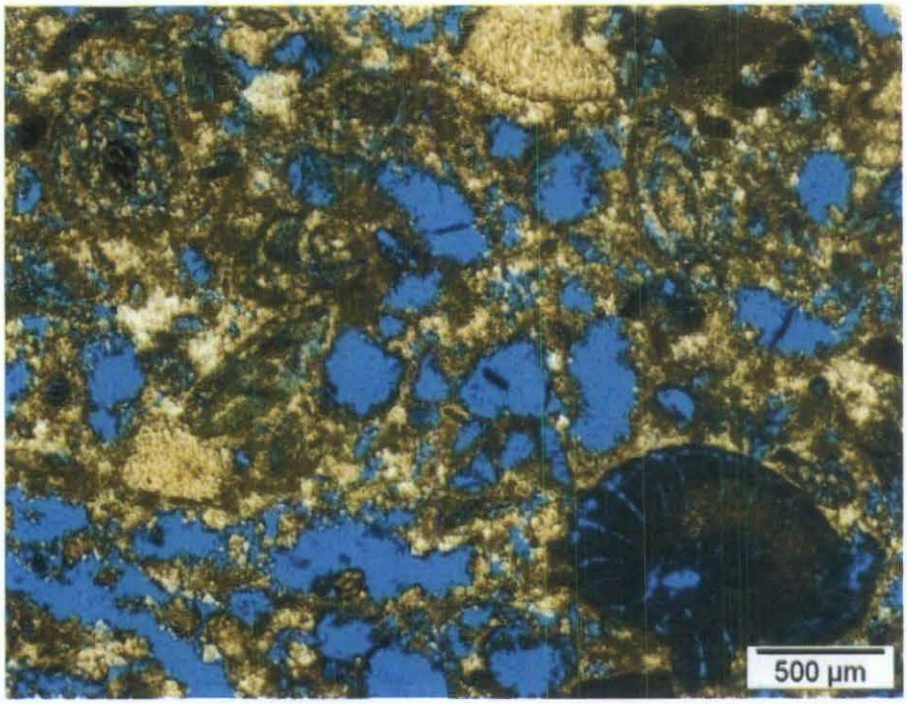

Figure 4.20: Thin section photomicrograph of mouldic limestone (LM) observed at a depth of 4229.5ft. LM facies has mostly mouldic pores.

Chalky limestone (LC) is an excellent reservoir facies in terms of porosity and permeability. The texture of the facies varies from grainstone, grain-packstone, to packstone. This facies has an average porosity of 29.21% and an average permeability of 119.19 mD. The porosity types include mouldic and interparticle porosity. The pores are well connected to each other, providing a very good permeability to the reservoir (Figure 4.19).

Mouldic limestone (LM) has excellent reservoir qualities with an average porosity of 25.51% and a permeability of 73.54 mD. The texture varies from packstone, pack-grainstone, to grainstone. Mouldic porosity is the dominant type of porosity present in this facies (Figure 4.20).

Argillaceous tight limestone (ALT) represents a poor quality reservoir facies. The word tight is used to mention the poor quality lithofacies in terms of porosity and permeability. This facies contains an argillaceous muddy matrix. The texture varies from wackestone, to wacke-mudstone. This facies contains micropores in a muddy matrix, and has a very low amount of macropores. Only few mouldic pores were observed and they were scattered (not connected) around the sample. Therefore this

facies shows a very low permeability that not suitable for hydrocarbon flow (Figure 4.21).

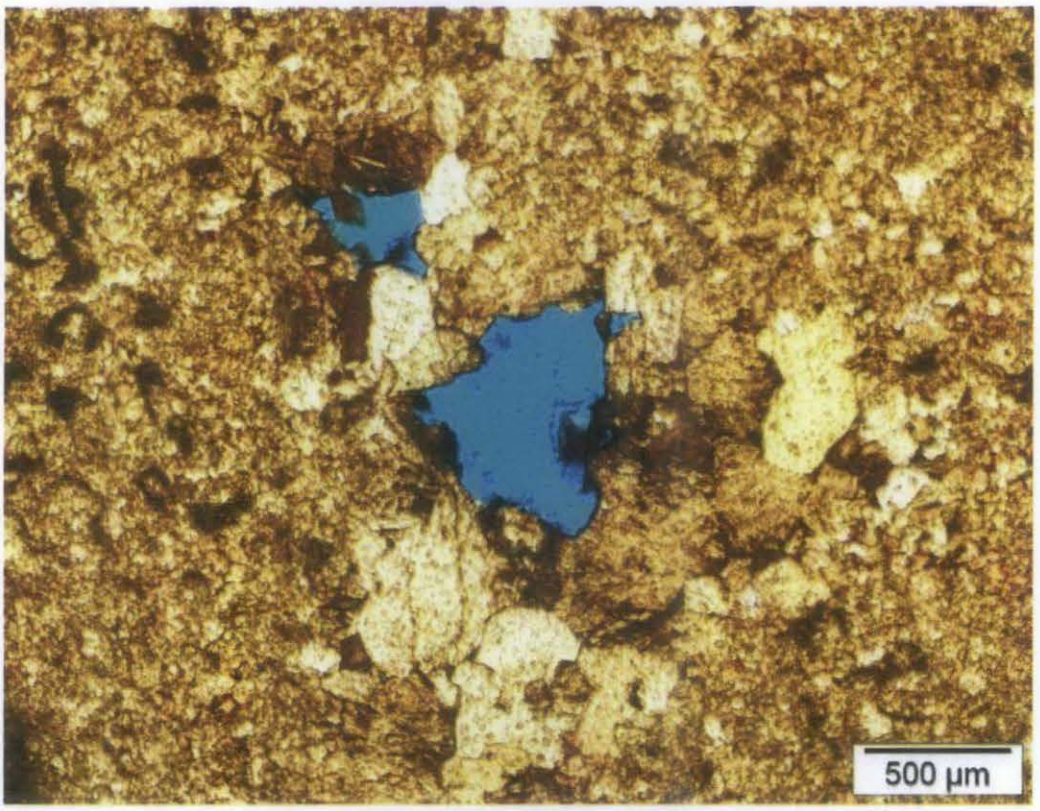

Figure 4.21: Thin section photomicrograph of an argillaceous tight limestone (ALT) observed at a depth of 4568ft. ALT facies has very low amount of macroporosity.

Porosity and permeability measurement of the *Mouldic Dolomitic Limestone (LDM)* facies was not possible due to the very limited number of core plug samples of that particular lithofacies. Furthermore, those plugs were broken and were not suitable for laboratory measurement of porosity and permeability. However, image analysis of thin section pictures show moderately good porosity and good interconnectivity between the pores (Figures 4.22, 4.23).

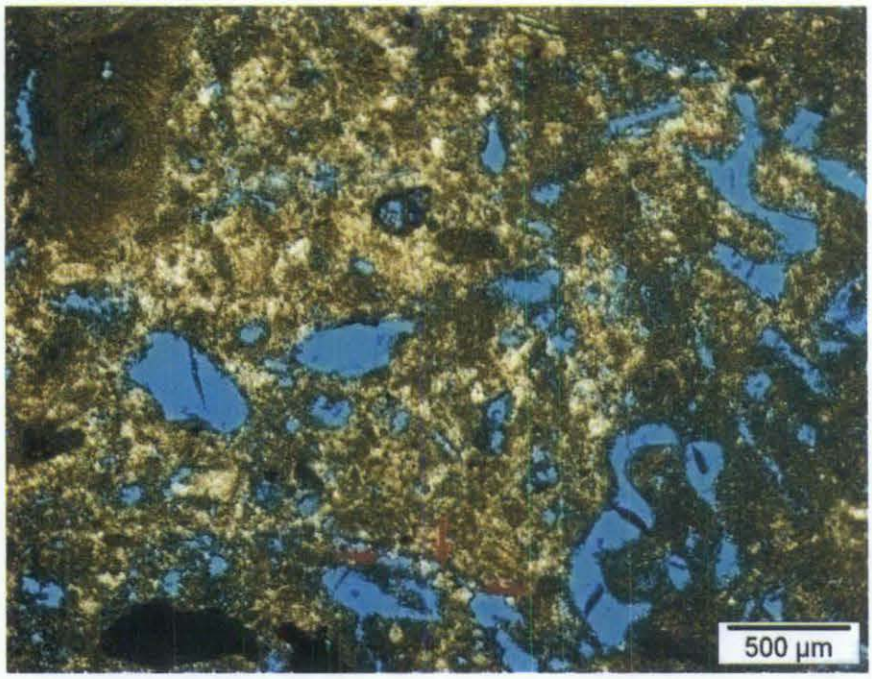

Figure 4.22: This section photomicrograph of a mouldic dolomitic limestone (LDM) facies observed at 4238.9ft. The arrows indicate some of the dolomite rhombs present in this sample.

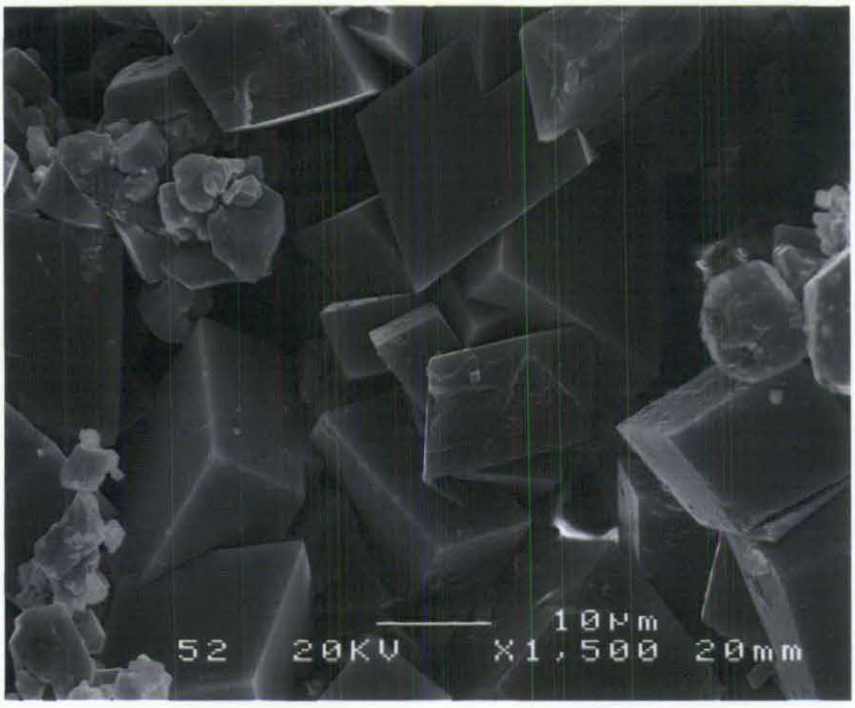

Figure 4.23: SEM photomicrograph of a mouldic dolomitic limestone (LDM) facies.

Figure 4.24 shows lithofacies distribution in the reservoir intervals with the thin section photomicrographs of five different lithofacies. Figure 4.25 shows the occurrence of the different lithofacies with the corresponding microporosity amount in reservoir intervals.

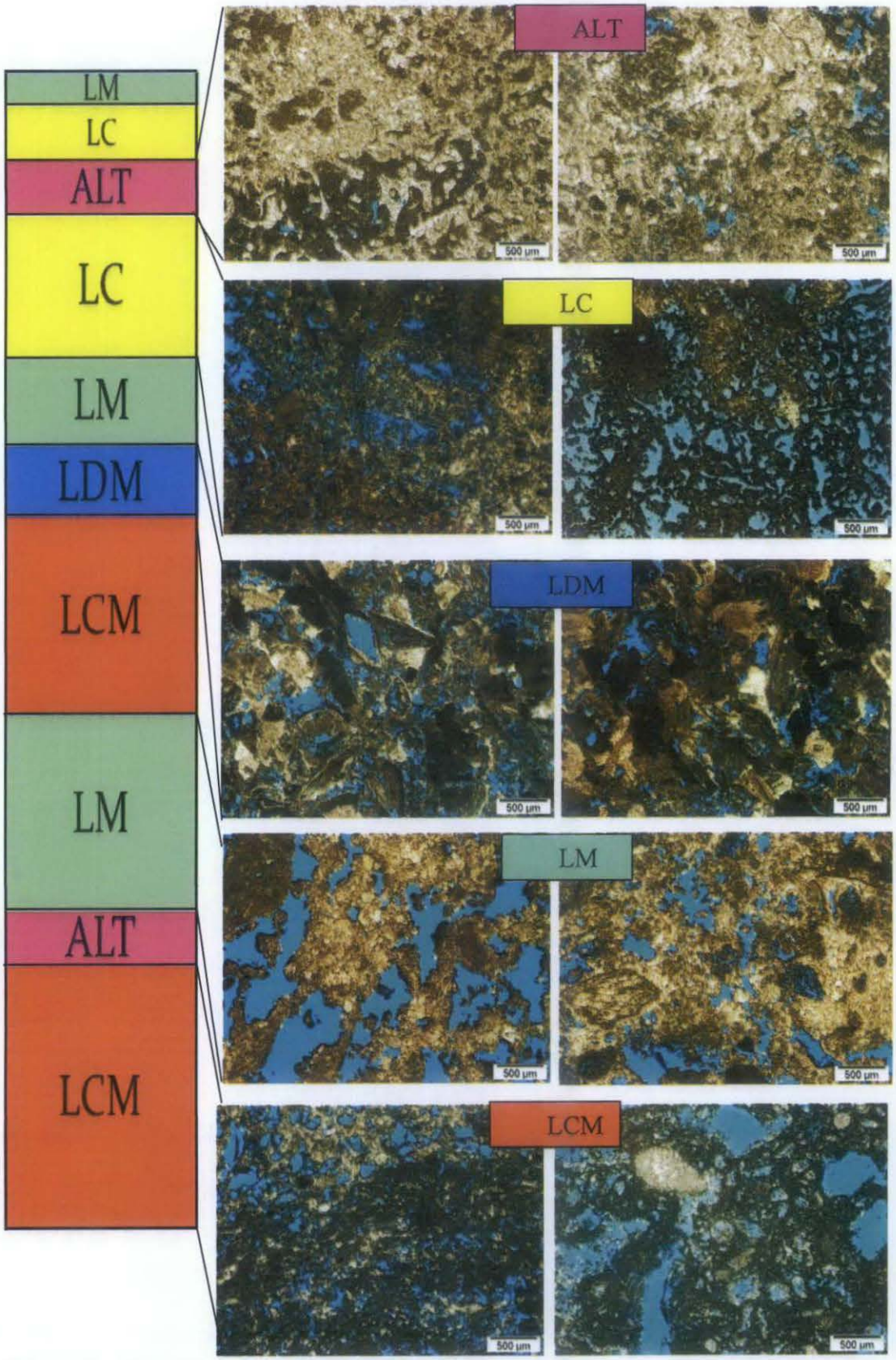

Figure 4.24: Lithofacies distribution in the reservoir intervals. Different lithofacies shows different porosity distributions and textural assembledges..

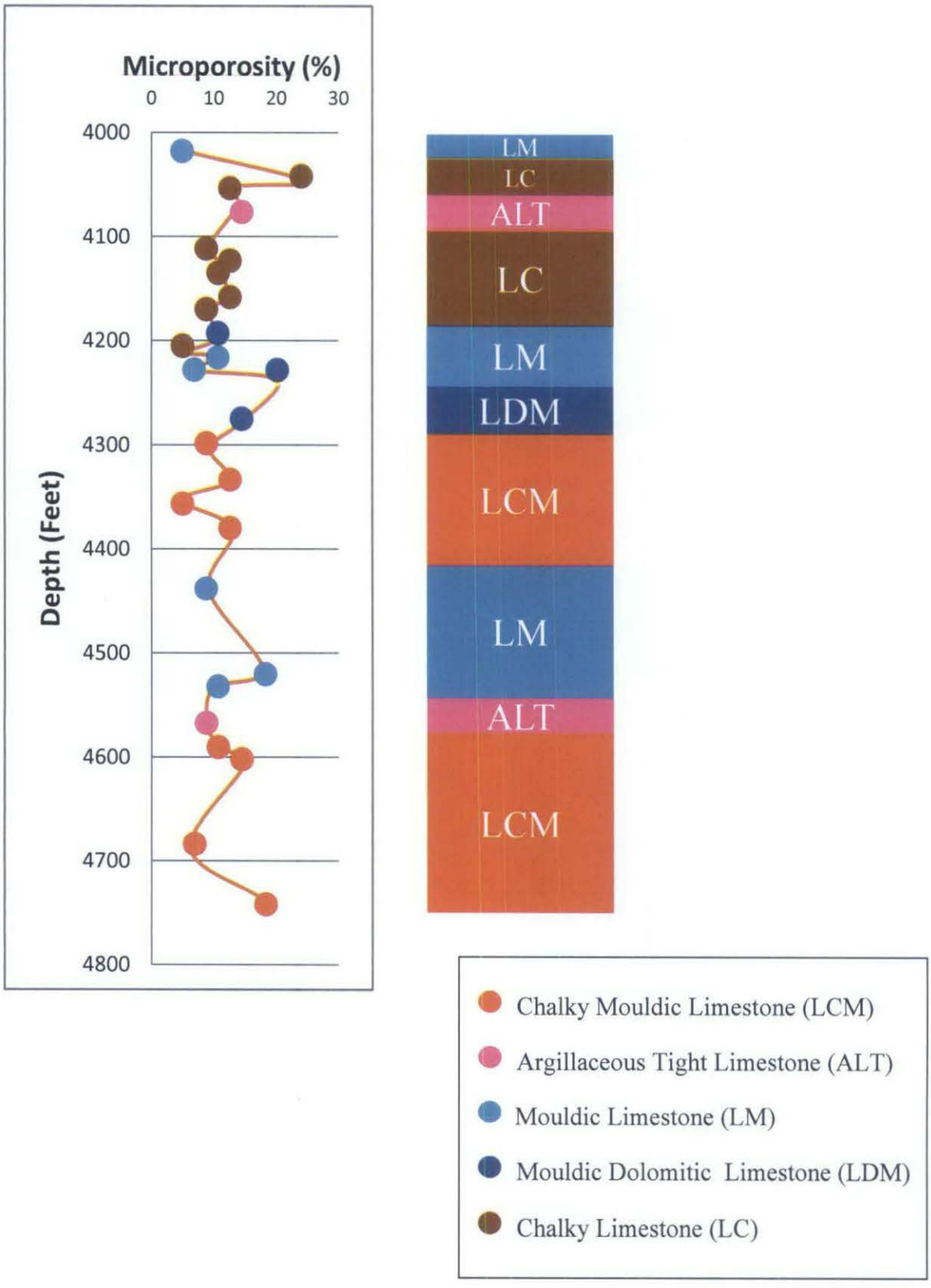

Figure 4.25: Lithofacies distribution with microporosity values at different depths in the reservoirs.

4.4.2 Cathodoluminescence Microscopy

Cathodoluminescence (CL) is the visible light emitted by the surface of a mineral when bombarded with electrons in a vacuum chamber. Manganese is the best studied activator of luminescence, whereas iron is the most common quencher (Emery & Robinson, 1993). The relative concentrations of these cations in carbonates appear to control the luminescence (Pierson, 1981; Fairchild, 1983).

Cathodoluminescence study was carried out to understand the nature of diagenesis in reservoir rocks. The CL study helped to interpret the oxidation state of the calcite cements and to understand the diagenetic environment in the reservoir. 20 samples were analyzed under CL to observe their luminescence. All the analyzed samples showed no luminescence (Figures 4.26, 4.27). The non-luminescent nature indicates a marine origin of the calcite cements (absence of oxygen) or cementation very near to the surface. If the calcite cementation occurs very near to the surface, the reservoir rocks usually show traces of paleosoil or karst in the samples. However these were not observed so frequently in the cored interval of the reservoirs. Therefore the non-luminescent nature of the calcite cements in the reservoir samples seems to indicate cementation of the rock in a marine environment during deposition or soon after deposition.

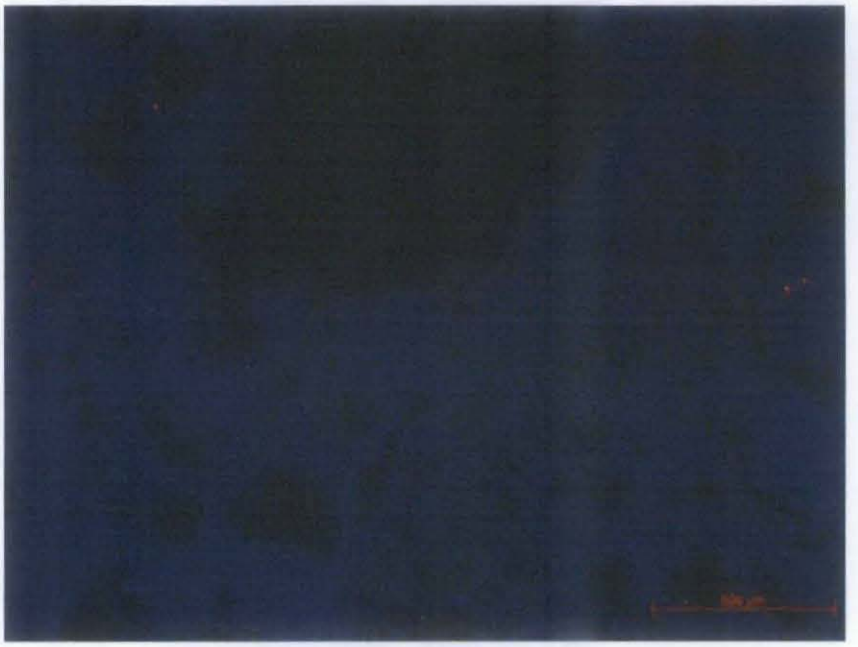

Figure 4.26: The reservoir rock shows a non-luminescent nature during cathodoluminescence study.

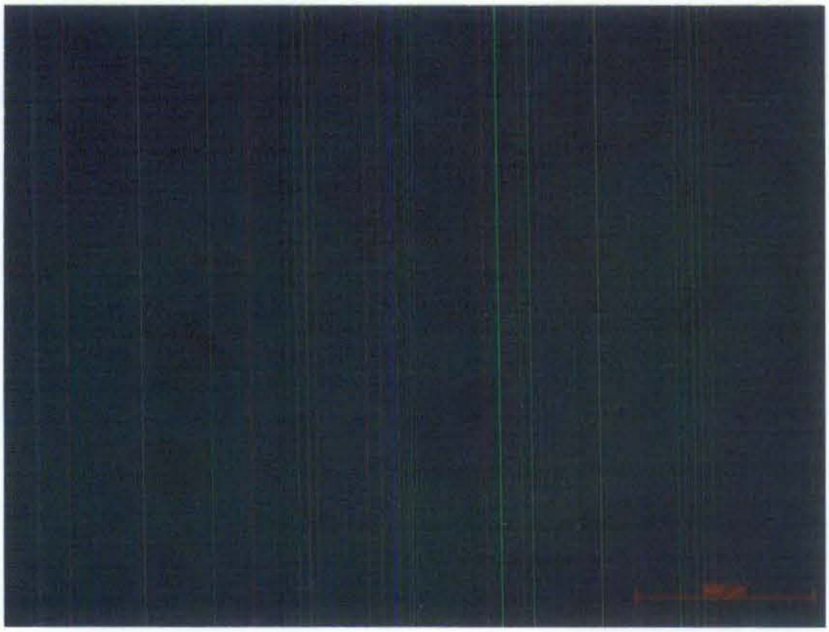

Figure 4.27: Non-luminescent nature of the carbonate reservoir observed at 4567.8 ft.

4.4.3 Stable Isotope Analysis

The stable isotopes of some elements give slightly different thermodynamic properties (Urey, 1947). The isotopes of oxygen (^{17}O , ^{18}O) and carbon (^{13}C) are widely used for study in carbonate stratigraphy and diagenesis. From an analytical standpoint, it is difficult to analyze the rather restricted variations that occur in the absolute concentrations of a given isotope. Stable isotope abundances are therefore measured as differences in the isotope ratios of two substances. Correspondingly stable isotope data are reported using δ notation in which the isotope ratio of a sample is expressed in terms of its deviation, in per mil, from the same ratio in an internationally accepted standard:

$$\delta_A = \left\{\frac{[R_A - R_{STND}]}{R_{STND}}\right\}.10^3$$

Where R_A is the ratio of heavy isotope to the light isotope for phase A ($^{13}C/^{12}C$, $^{18}O/^{16}O$) and R_{STND} is the same ratio for a standard material (Emery and Robinson, 1993).

Ten samples representative of different depths of the reservoir were analyzed and their compositions in carbon and oxygen isotopes were measured (Appendix E). All

values were reported in per mil relative to V-PDB (PDB is the acronym for the Pee Dee belemnite, a standard reference material) by assigning a $\delta^{13}C$ value of +1.95‰ and a $\delta^{18}O$ value of -2.20‰ to NBS19. Reproducibility was checked by replicate analysis of laboratory standards and was found better than ±0.06.

The stable carbon isotope ($\delta^{13}C$) values all plot between +0.82 and -0.82 per mil PDB (Figure 4.28). This suggests a marine signature. It shows that the original signature is present in the limestones despite the diagenetic overprinting. In none of the cements is a contribution of depleted (negative) CO_2 recognizable. Such signatures would be very typical for eogenetic diagenesis.

Most of the values of the stable oxygen signature plot between -4.51 and -5.30 per mil PDB (Figure 4.29). The variation in values likely relates to the relative contribution of diagenetic cements with respect to marine components and is a normal feature. However the higher negative values for these rocks indicate a non-marine cementation/recrystallisation. In the case of a marine dominated diagenesis, the values would be close to zero. As the plotted values are around -5 per mil PDB, it indicates a meteoric water signature during the Miocene or after deposition. This means that it is likely that the limestones were recrystallised and became cemented by meteoric water. This is only possible if they became emergent. Emergence surfaces were observed during the core study (Figure 4.31). The emergence or recurrent emergences were very important since the entire sequence seems to be affected. There is only one value of stable oxygen signature -1.64 per mil at a depth of 4334.8ft that differs from the others. This is much closer to a marine signature. Possibly this sample was shielded (separated, not influenced) from the meteoric fluids. This often happens if a lithology or some components are isolated by clays. Observation of this sample under SEM revealed the presence of more clay minerals in it compared to the rest of the samples (Figures 4.32 and 4.33). Moreover cementation was less severe in this sample. These observations support the interpretation that the sample was isolated by clays and not influenced much by the meteoric fluids. Observation under SEM and the stable isotope analysis suggest that microporosity in the Miocene carbonate reservoirs of Central Luconia were mostly formed during meteoric diagenesis after the deposition of the original marine limestone.

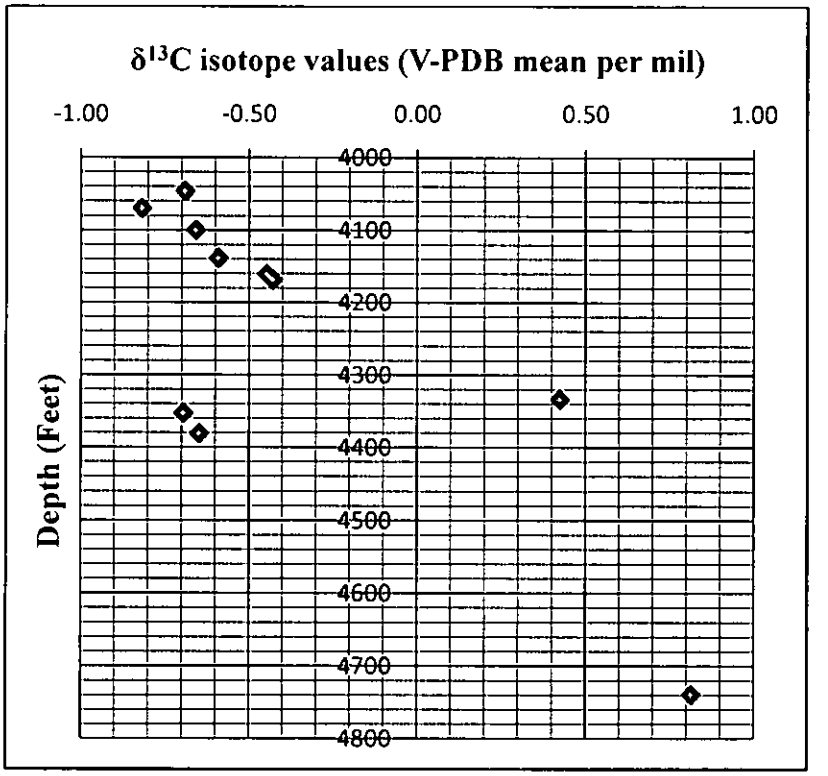

Figure 4.28: $\delta^{13}C$ isotope signatures in terms of depth of the reservoir.

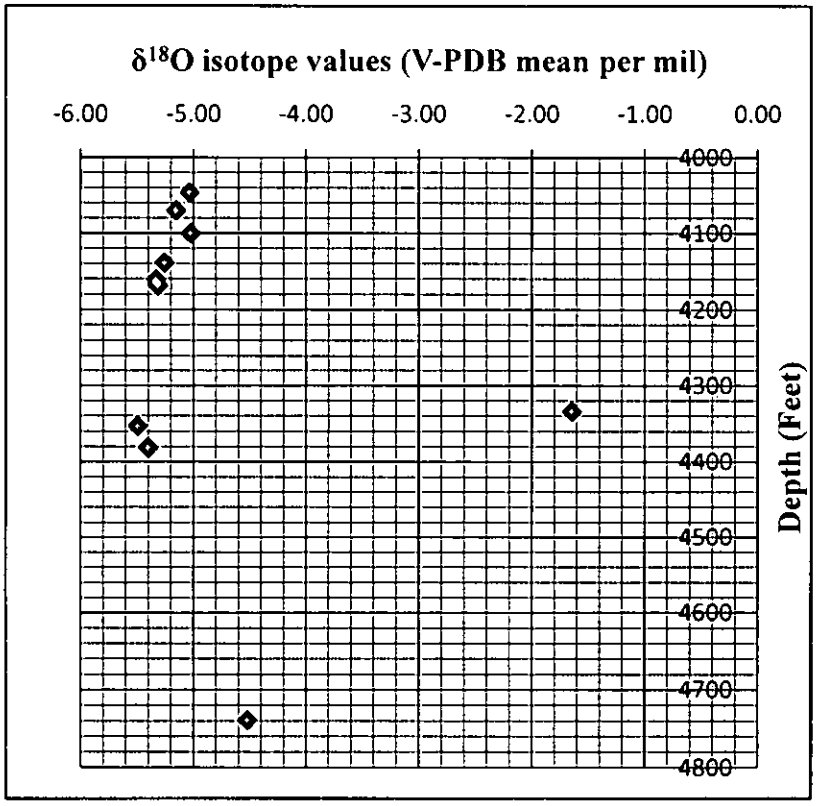

Figure 4.29: $\delta^{18}O$ isotope signatures in terms of depth of the reservoir.

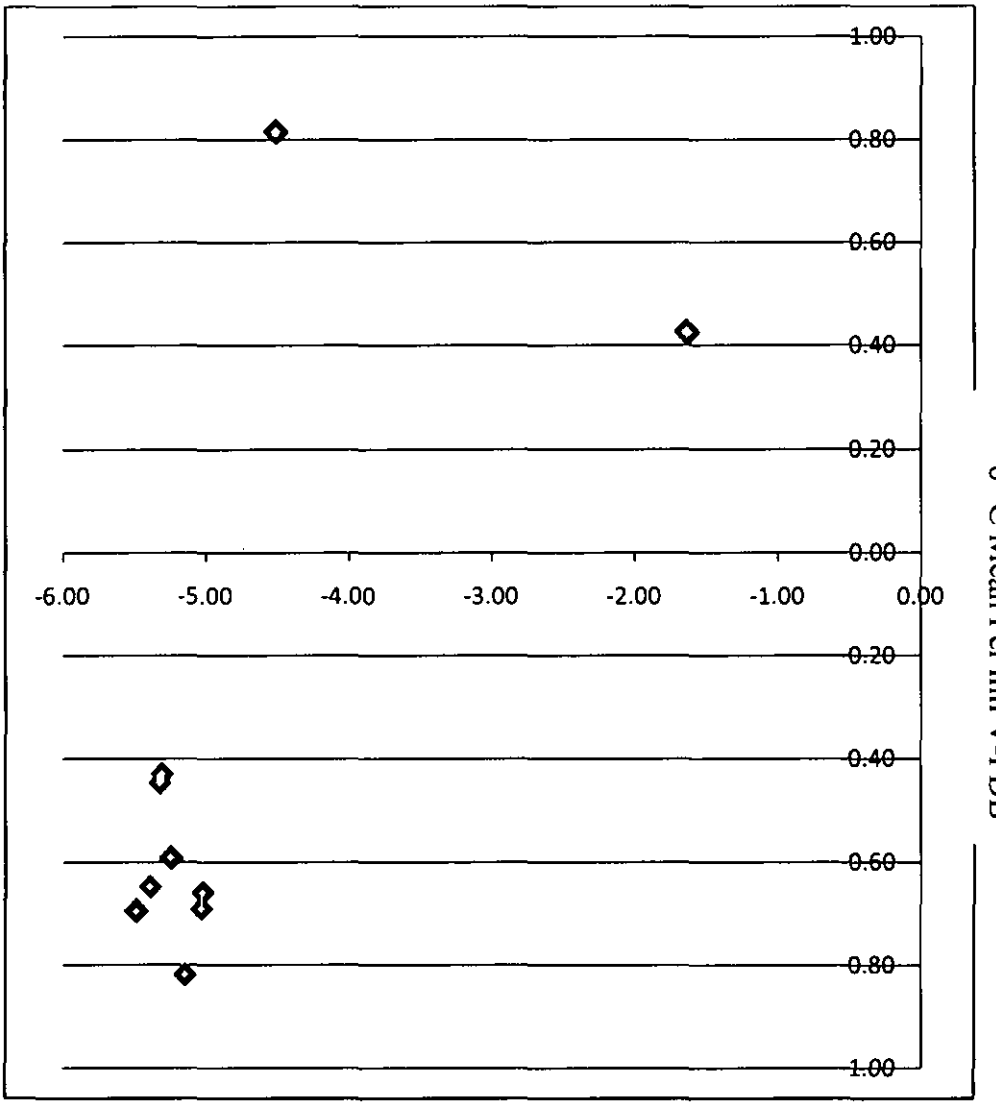

Figure 4.30: Crossplot of $\delta^{18}O$ Vs $\delta^{13}C$ of limestone cement of the reservoir.

Figure 4.31: Surface of Emergence observed in the reservoir. The arrows mark the surface of emergence on the core as shown by the sharp contrast between two lithofacies.

Figure 4.32: Flakes of clay minerals observed at 4334.8ft. The arrows indicate some of the clay mineral flakes.

Figure 4.33: Abundance of clay mineral flakes observed at a depth of 4277 ft. The arrows indicate some of the clay mineral flakes.

4.4.4 Crystallometry of Micrites

Based on the model of Folk's classification (1962), micrite particles are classified in three classes; fine, medium and coarse micrites, with a diameter (or maximum side length of the crystal) of 0.1-3μm, 3-6μm and 6-10 μm, respectively (Rahman et al., 2011). These classes are based on measurements on SEM photomicrographs taken at different magnifications using gold-coated thin sections (Figures 4.34 and 4.35). These classes are entirely dependent on the micrite crystal size irrespective of the mode of deposition or diagenesis of the grains.

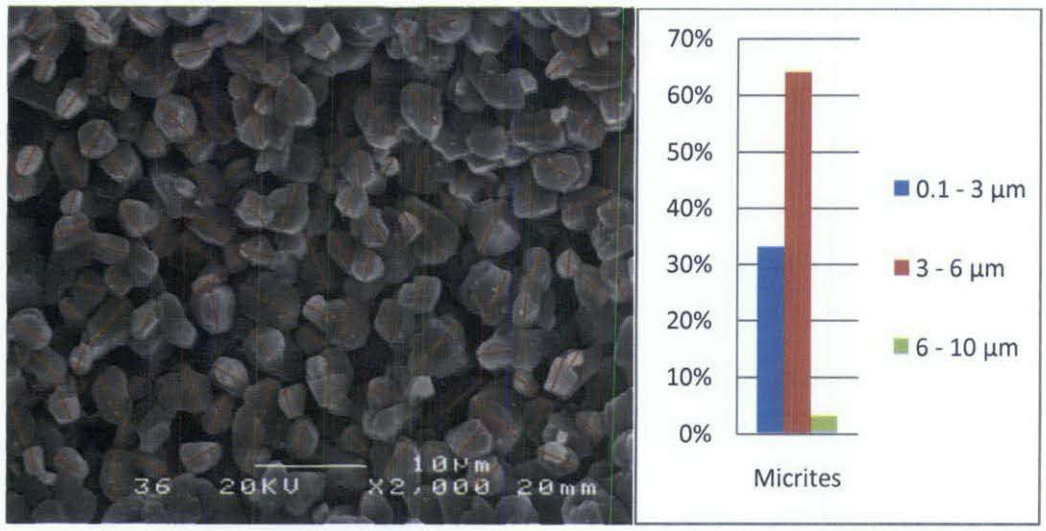

Figure 4.34: Crystallometry of micrites measured at a depth of 4139ft. The bar chart shows the distribution of crystal sizes in terms of their relative percentage on the image.

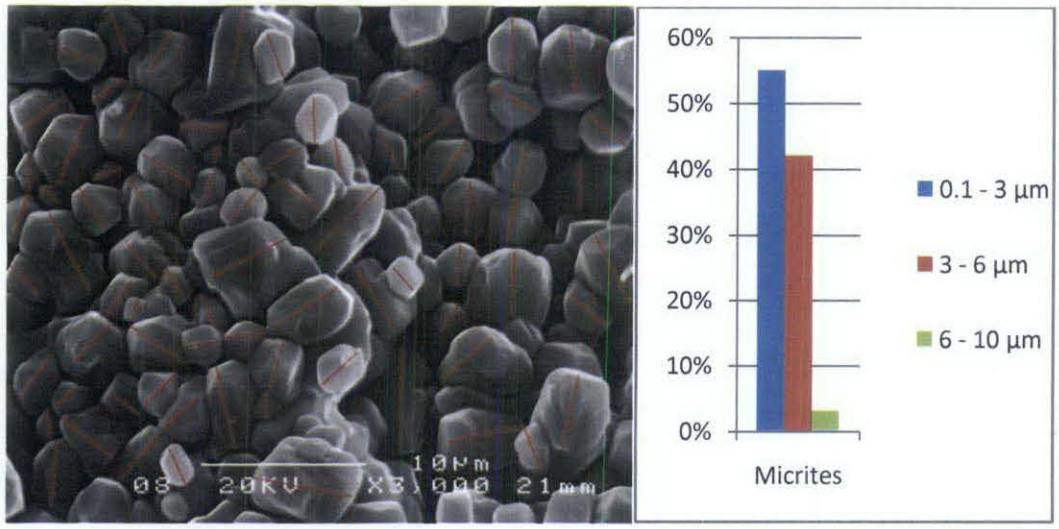

Figure 4.35: Crystallometry of micrites measured at a depth of 4440ft. The bar chart shows the distribution of crystal size in terms of their relative percentage on the image.

4.4.5 Texture and morphology of micrites

Lambert et al. (2006) classified micrite microtexture in the Arab, Kharaib and Mishrif Formations in Jurassic and Cretaceous Middle East reservoirs in three classes. They described the three classes of microtextures as rounded micrites, micro-rhombic micrites, and compact anhedral micrites. Based on Lambert's classification scheme, a more detailed classification is proposed by Periere et al. (2010) that includes six classes of micrite microtextures in Cretaceous limestone from the Arabian Gulf.

These classes are rounded micrites, subrounded micrites, scaleno-micrites, microrhombic to polyhedral micrites, anhedral compact micrites, and fused micrites. This study proposes a classification for the micrite microtextures of the Miocene Carbonate reservoirs of offshore Sarawak, Malaysia. This classification has four classes: rounded micrites, subrounded micrites, microrhombic and polyhedral micrites, and compact anhedral micrites (Rahman et al., 2011).

4.4.5.1 Rounded Micrites

Rounded micrites mainly include subhedral to anhedral micrite particles. They mostly have coalescent and punctic contacts between crystals. Locally a few of the rounded micrite crystals are glued together to form bigger crystals. Gluing of rounded micrites is observed in many instances (Figures 4.36 and 4.37). The gluing of rounded micrites produces bigger grains, resulting in a negative impact on the porosity and permeability of the reservoir. The gluing of the micrites reduces the pore spaces between the crystals.

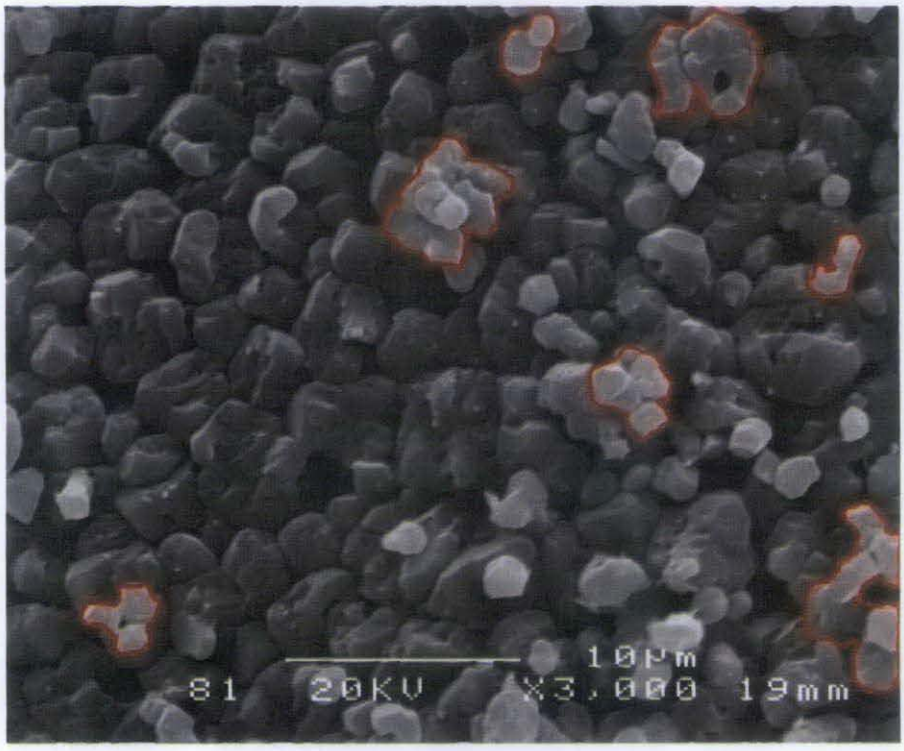

Figure 4.36: Gluing of micrites can block the pores of reservoir rock. Some glued crystals are highlighted with a red outline.

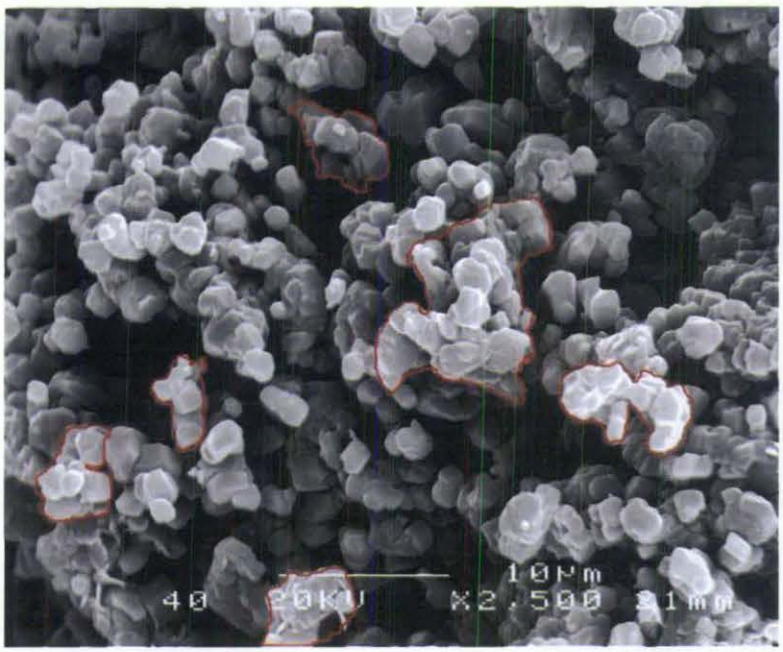

Figure 4.37: Gluing of rounded micrites, as observed at a depth of 4334.5 ft. Some glued crystals are highlighted with a red outline.

The faces of rounded micrites have mostly a convex shape. The rounded micrite microtexture contains mostly medium (4-6µm) and coarse micropores (6-10 µm). More importantly, due to the textural arrangement in rounded micrites, these micropores provide good interconnectivity and thus a positive contribution to the permeability of the reservoir (Figure 4.38) (Rahman et al., 2011; Rahman and Pierson, 2011).

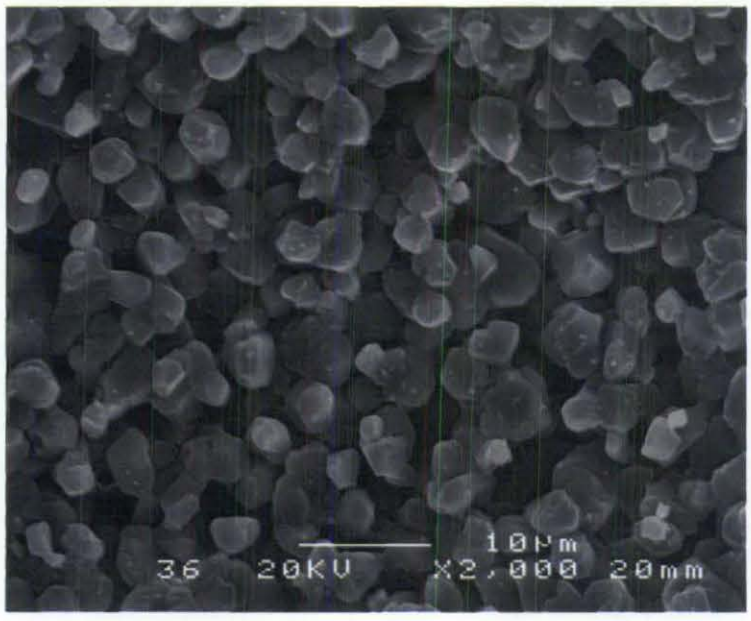

Figure 4.38: Rounded micrites have mostly medium to coarse micropores with good interconnectivity between the pores.

4.4.5.2 Subrounded Micrites

These are subhedral to anhedral micrite particles with mostly straight crystal edges. Subrounded micrites have convex faces and coalescent to punctic contacts between crystals (Figures 4.39 and 4.40). Gluing of crystals is also observed in subrounded micrites. They produce mostly medium (4-6 μm) and fine micropores (2-4μm) (Figure 4.41). Due to the subrounded to angular shape and the textural arrangement of the particles, medium micropores are less connected in subrounded micrites compared to rounded micrites (Rahman et al., 2011; Rahman and Pierson, 2011).

4.4.5.3 Microrhombic and Polyhedral Micrites

Microrhombic and polyhedral micrite particles have well developed clean and regular crystal faces and have punctic contacts (except interlocked crystals) between the crystal faces. The number of crystal faces varies from 6 to more than 20 (Figure 4.42).

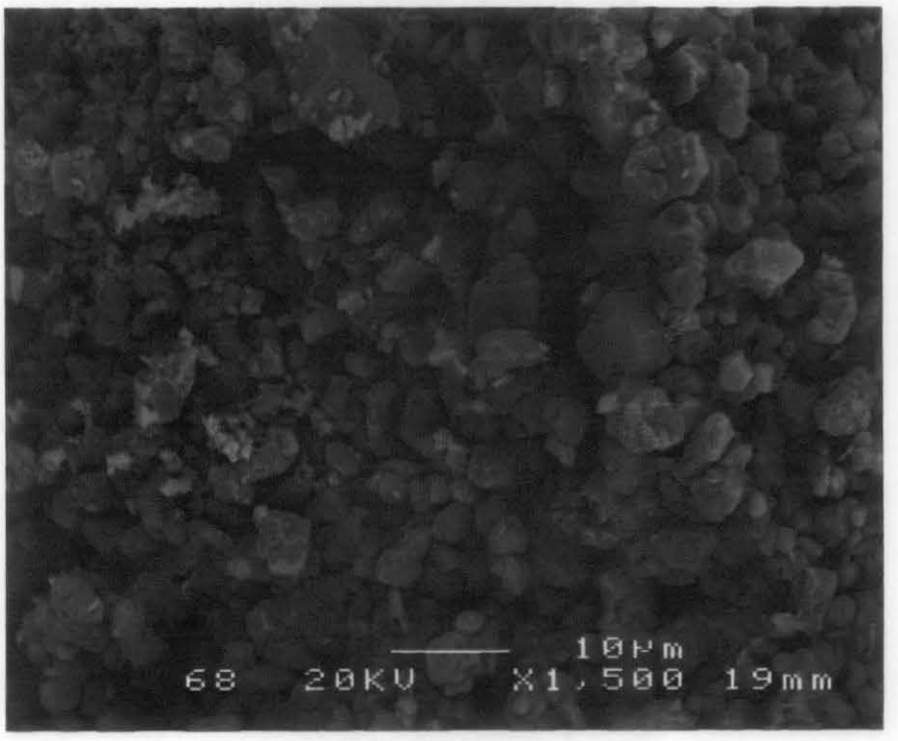

Figure 4.39: Subrounded micrites showing convex faces and coalescent to punctic contacts between the crystals at a depth of 4567.8ft.

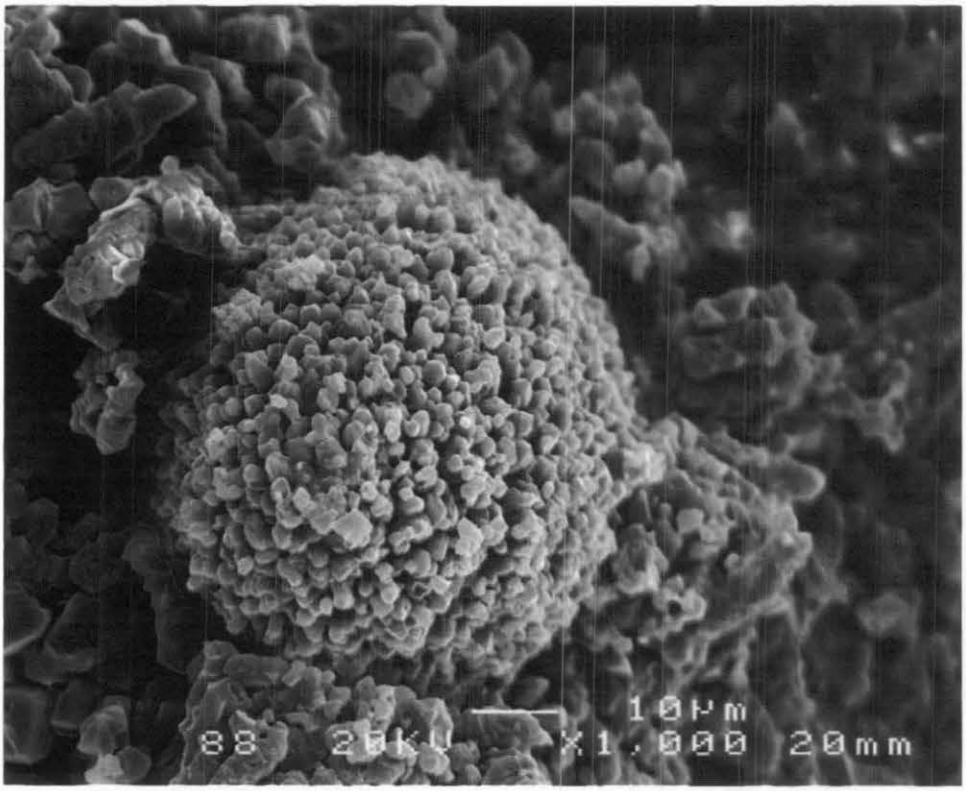

Figure 4.40: Subhedral micrite particles as observed in the micritised shell of a microfossil a common phenomenon observed at different depths of the reservoir.

Microrhombic and polyhedral micrites are mostly characterized by coarse micropores (6-10μm). Where crystals are interlocked, these micrites have less micropores and poor connectivity between the pores (Figure 4.43). However where the crystals show punctic contacts, good interconnectivity exists between the micropores (Figure 4.44). Although these micrites sometimes contain lower amounts of microporosity, due to their morphology and textural arrangements, they show good inter-connectivity between the micropores (Rahman et al., 2011; Rahman and Pierson, 2011).

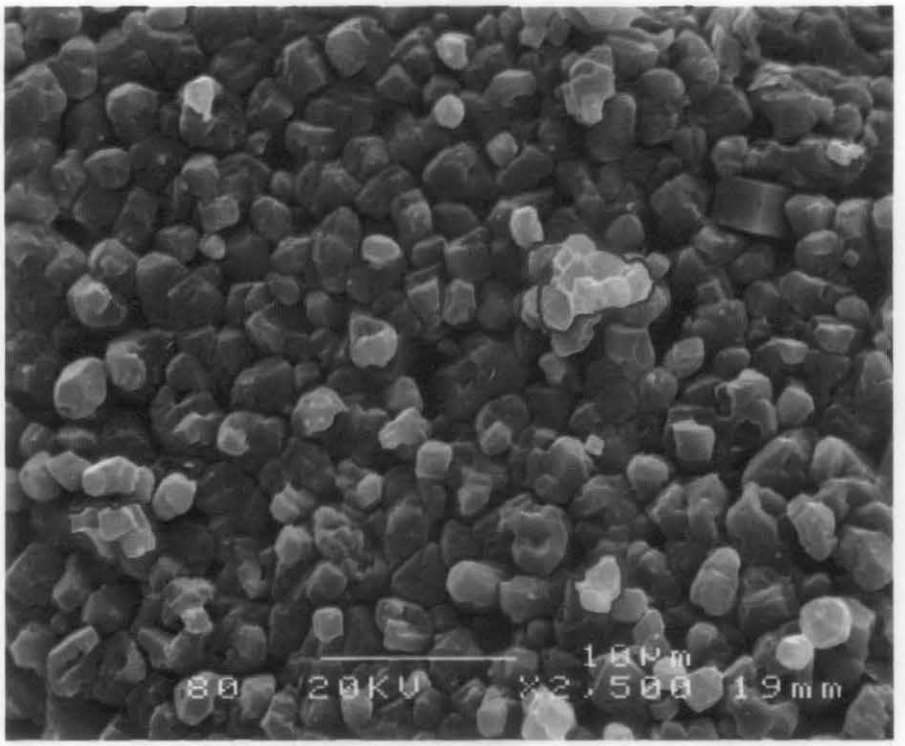

Figure 4.41: Subrounded micrites contain mostly medium micropores and show moderate connectivity between the micropores. Some glued crystals are highlighted with a red outline.

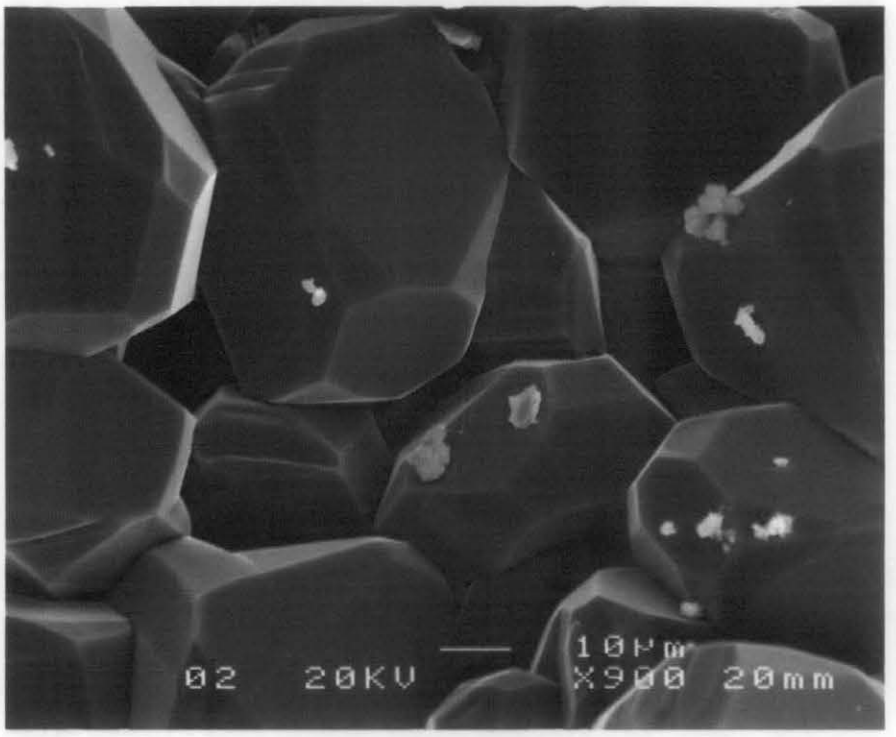

Figure 4.42: Polyhedral micrite crystals showing well-developed crystal faces.

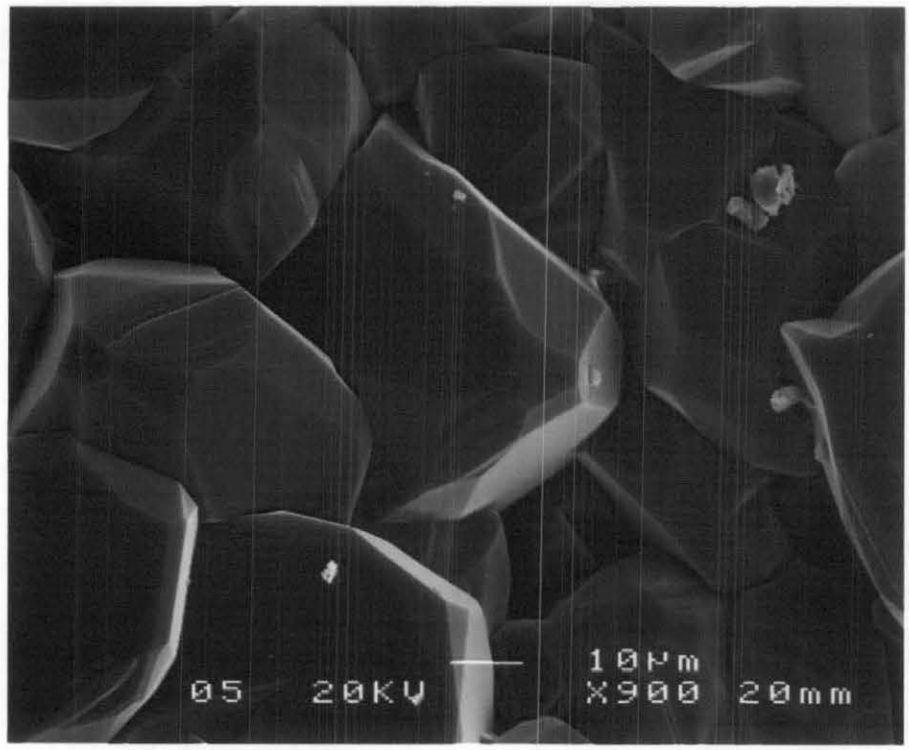

Figure 4.43: Polyhedral interlocked calcite crystals giving less microporosity, observed at a depth of 4101ft.

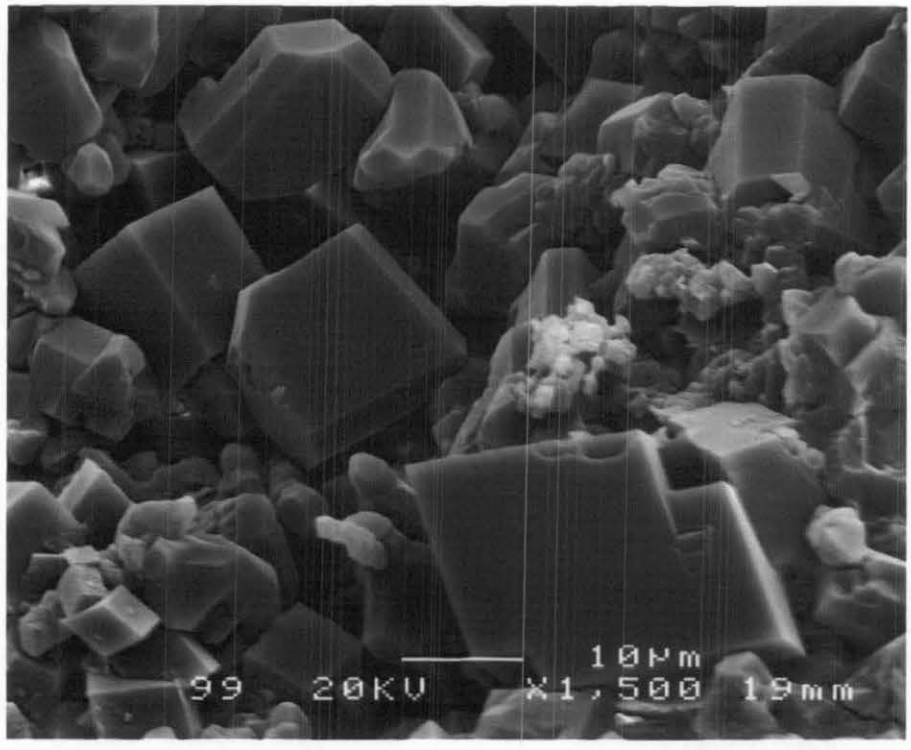

Figure 4.44: Microrhombic to polyhedral calcite and dolomite crystals with punctic contacts have good connectivity between the micropores.

4.4.5.4 Compact Anhedral Micrites

These are anhedral micrites in which intercrystal contacts are usually not distinct. In some instances intercrystal contacts are visible (Figure 4.45), but are commonly irregular. Grain contacts in these micrites are dominantly coalescent. In some cases, some micropores resulting from dissolution of anhedral micrites are observed (Figure 4.46). These are mostly isolated very fine micropores (0.1-2μm) (Rahman et al., 2011; Rahman and Pierson, 2011).

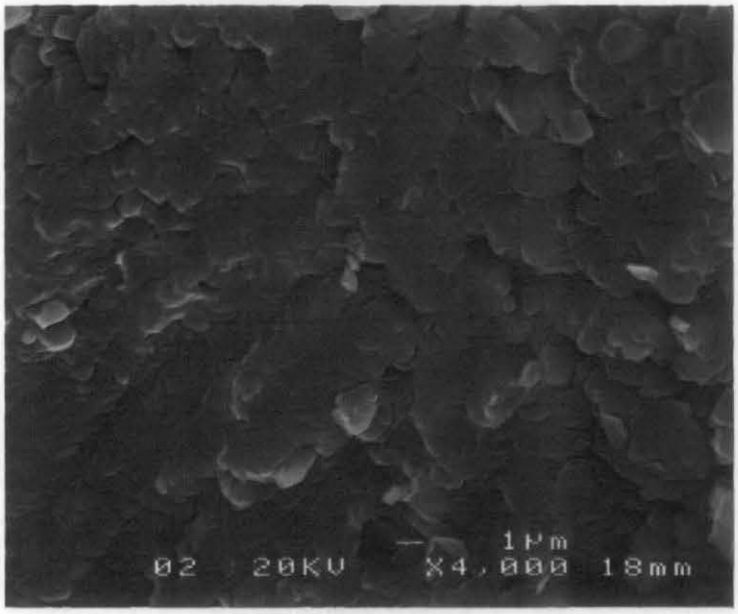

Figure 4.45: Compact anhedral micrites with visible intercrystal contacts at a depth of 4070ft.

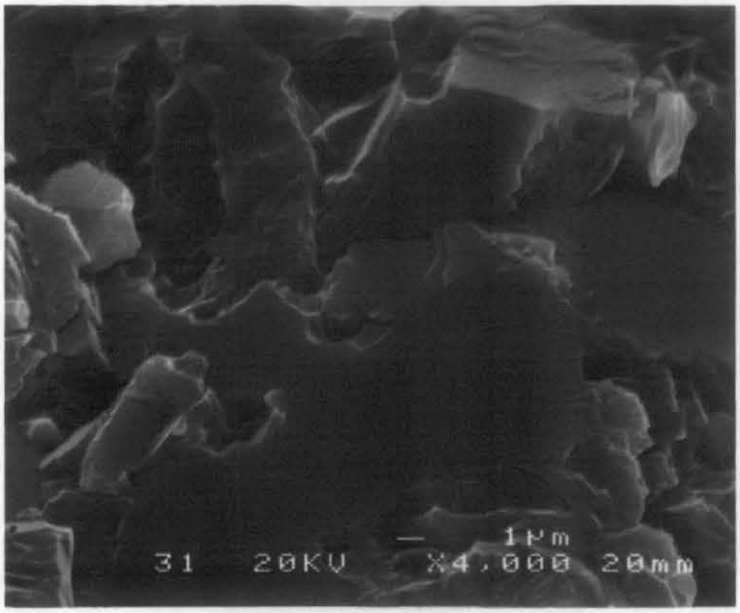

Figure 4.46: Compact anhedral micrites showing isolated fine micropores resulting from dissolution.

4.4.6 Classification of Micropores

The crystallometry, morphometry and texture of micrite particles control the occurrence and distribution of micropores (Rahman et al., 2011). Based on the occurrence and crystallometry of micrites, micropores in the Miocene carbonate reservoirs of Central Luconia, offshore Sarawak are grouped in four classes:

4.4.6.1 Very Fine Micropores

These micropores have a maximum diameter of 0.1 to 2 μm. Very fine micropores are very abundant in compact anhedral micritic textures. They are mostly isolated or have very narrow pore throats when connected (Figures 4.47 and 4.48).

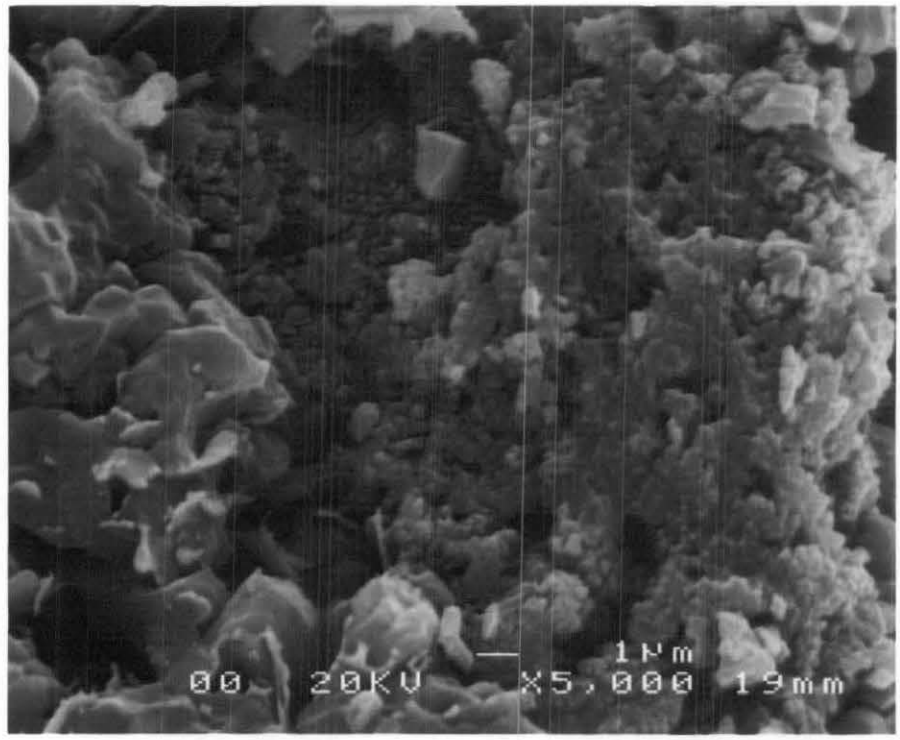

Figure 4.47: Very fine micropores observed in compact anhedral micritic microtexture.

4.4.6.2 Fine Micropores

Micropores with a maximum diameter of 2 to 4 μm are classified as fine micropores. These micropores are dominant in reservoirs with compact anhedral and subrounded micritic microtextures (Figure 4.49 – 4.51). Fine micropores are sometimes connected

through pore throats that are smaller than the diameter of the micropores. However, in many cases, fine micropores are isolated and have little or no interconnections.

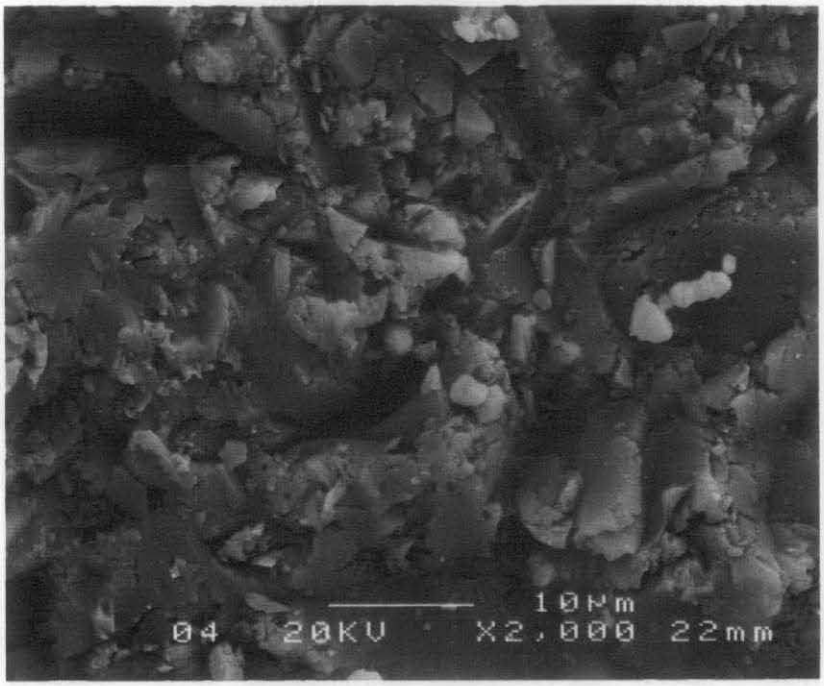

Figure 4.48: Compact anhedral micrites with very fine micropores observed at a depth of 4355.5ft.

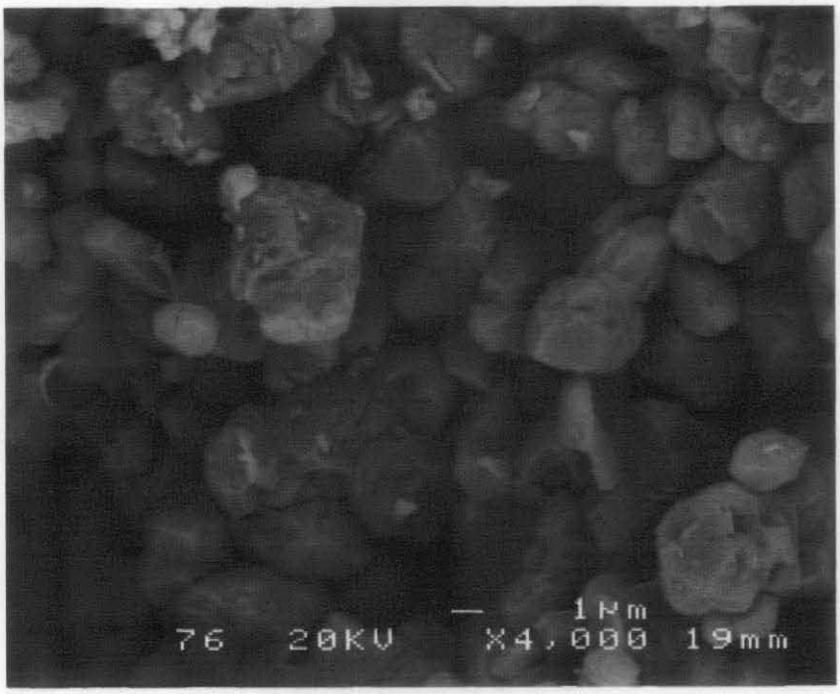

Figure 4.49: Fine micropores observed in subrounded micritic microtexture.

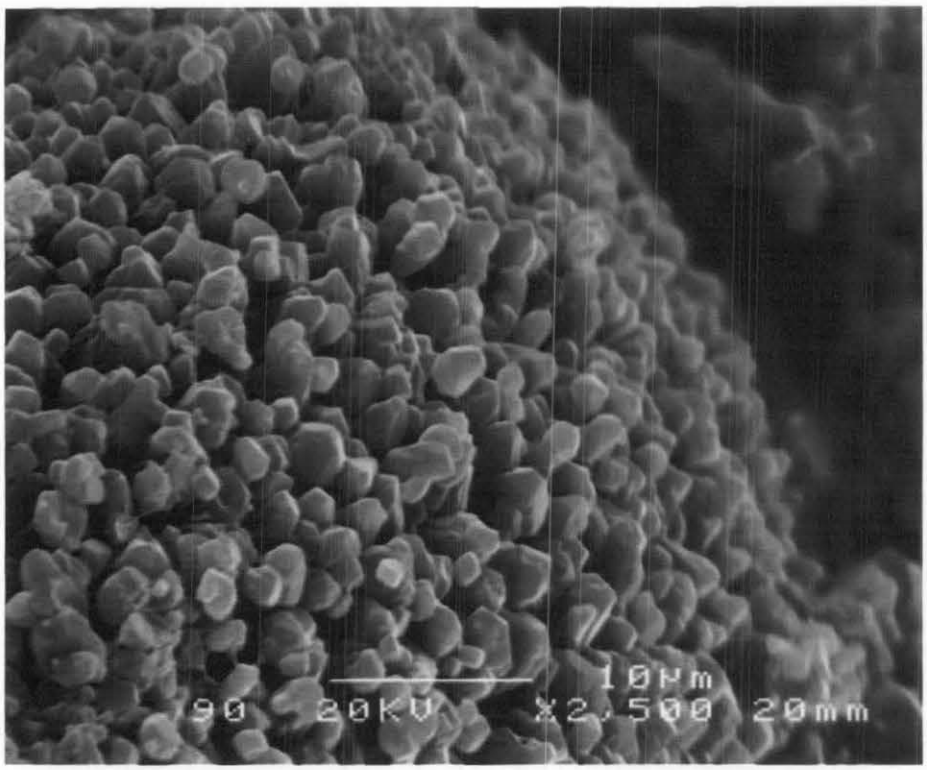

Figure 4.50: Fine micropores with moderate interconnections observed at 4381 ft.

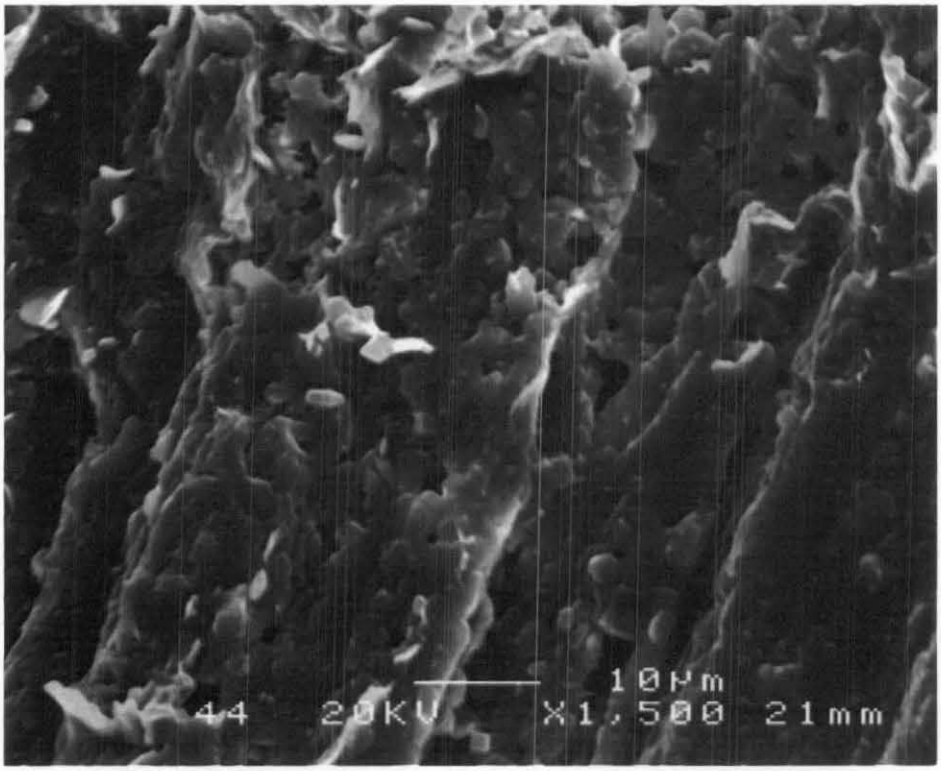

Figure 4.51: Fine micropores observed in compact anhedral micrites at a depth of 4199.5 ft of the reservoir.

4.4.6.3 Medium Micropores

Medium micropores have a maximum diameter of 4 to 6 μm. These micropores are abundant in rounded and subrounded micritic microtexture (Figures 4.52 and 4.53). Medium micropores are well connected in some instances and contribute to the permeability of the reservoir (Figure 4.54).

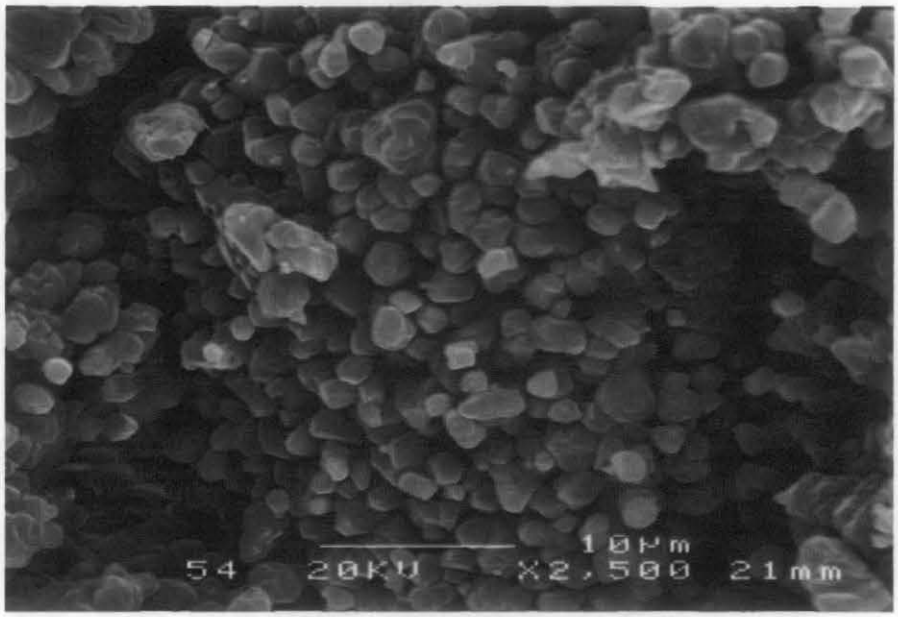

Figure 4.52: Medium micropores observed in subrounded micrite microtexture.

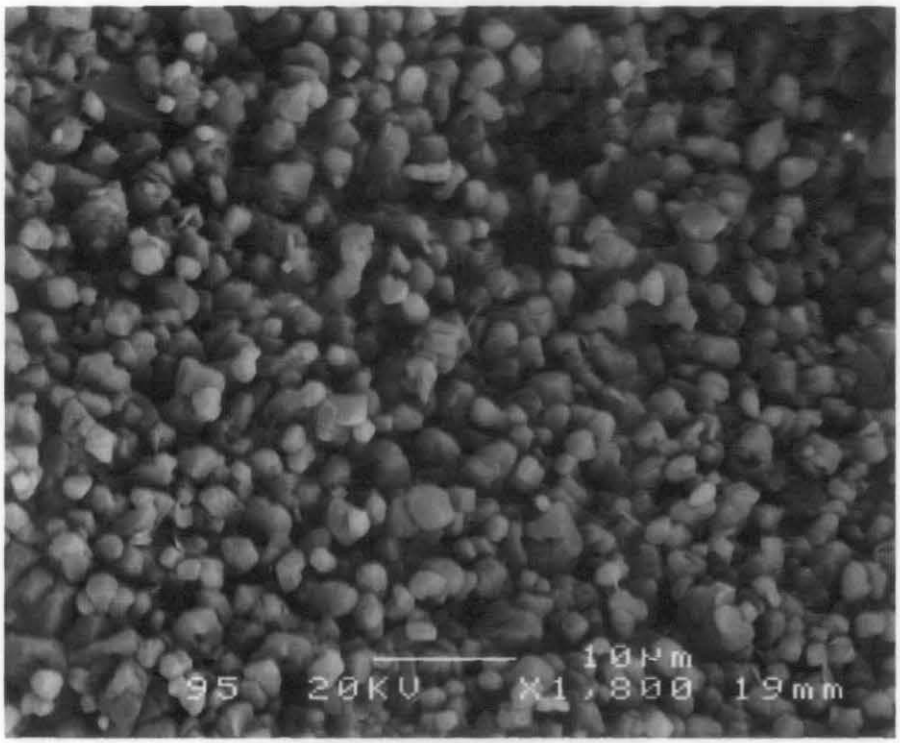

Figure 4.53: Medium micropores observed in rounded micrites at a depth of 4236ft.

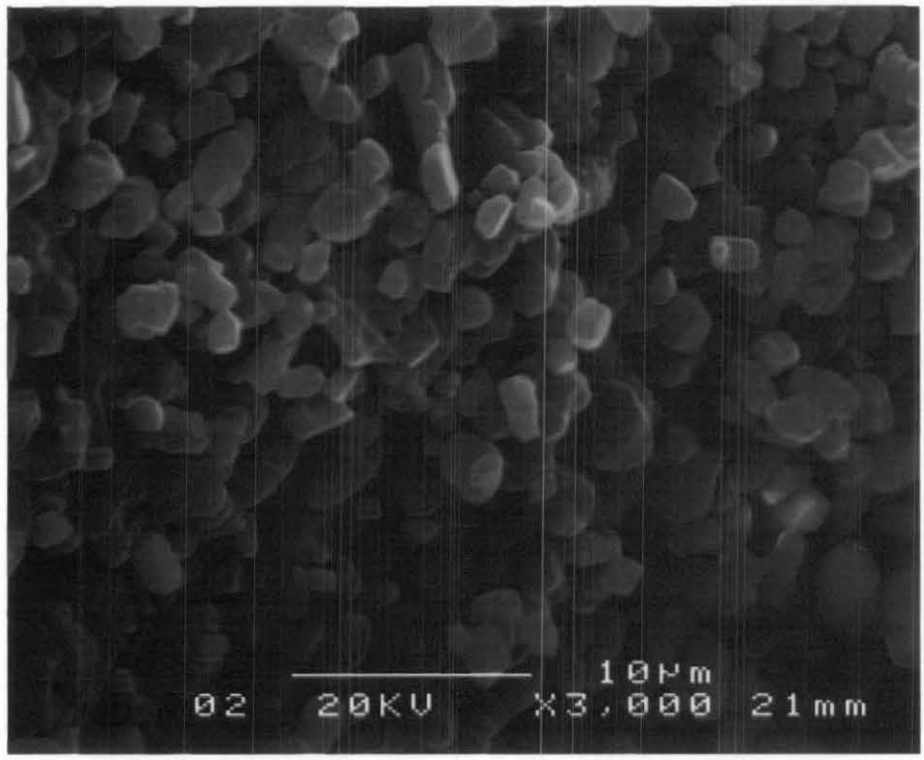

Figure 4.54: Medium micropores showing fairly good interconnection observed at a depth of 4381ft.

4.4.6.4 Coarse Micropores

These micropores have a maximum diameter of 6 to 10 μm in diameter. Coarse micropores are dominant in rounded, microrhombic and polyhedral micrite microtextures (Figures 4.55 and 4.56). When these micropores are connected by larger pore throats, they provide a moderate to fairly good contribution to the permeability of the reservoir. Better interconnections by wide pore throats have been observed when coarse micropores occur in microrhombic and polyhedral microtexture (Figure 4.55).

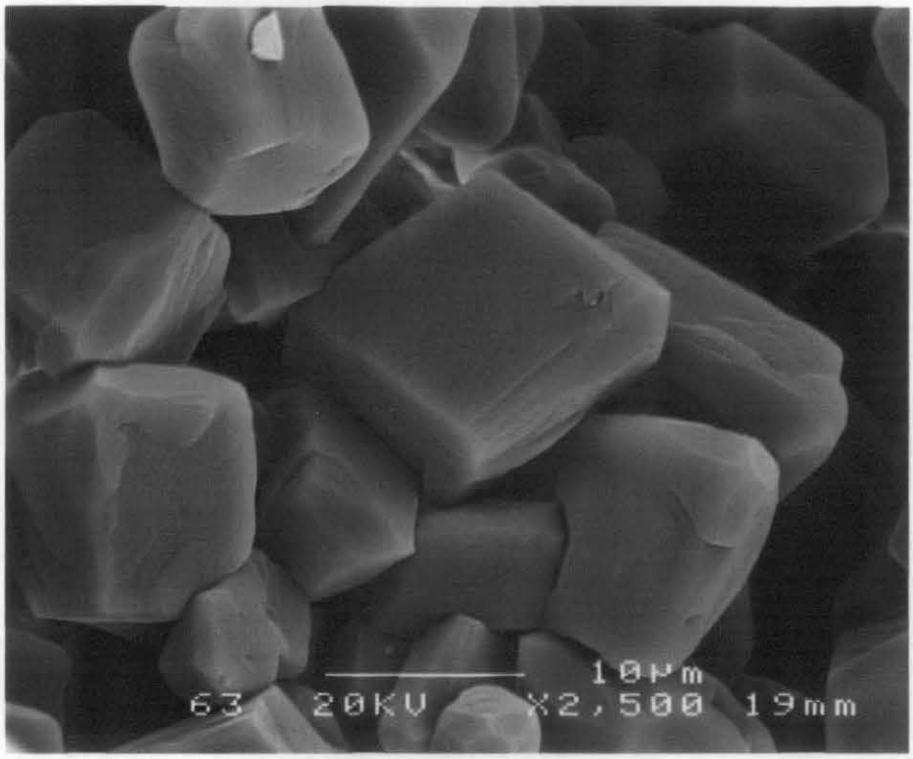

Figure 4.55: Coarse micropores with good interconnection observed in microrhombic and polyhedral micritic microtexture.

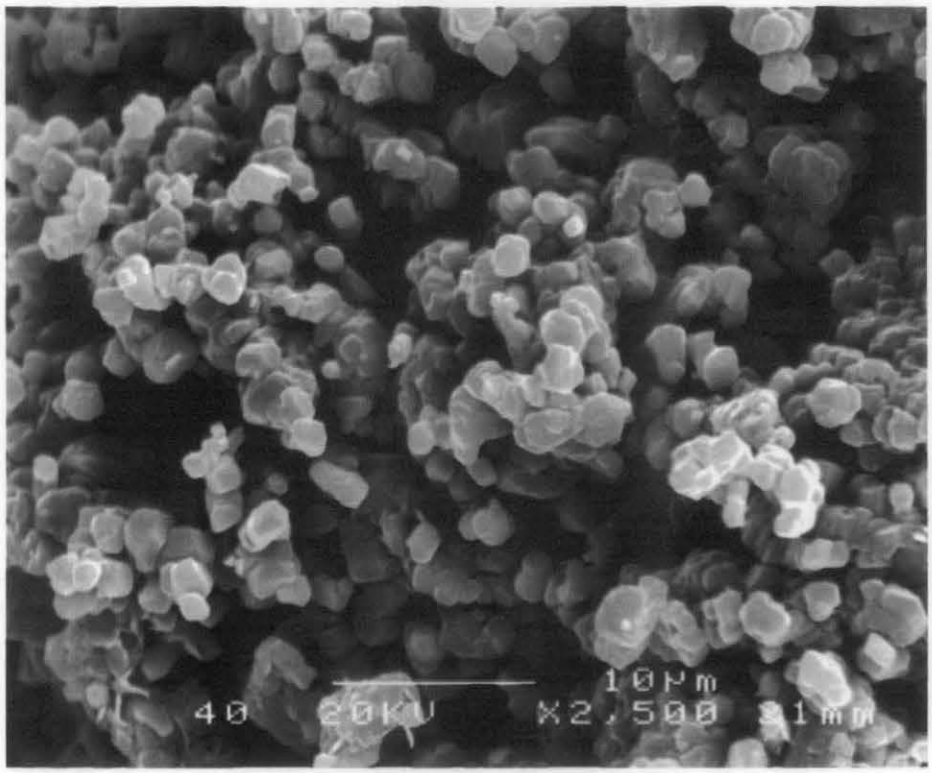

Figure 4.56: Coarse micropores with good interconnection observed in rounded micrites at a depth of 4334.5ft.

Table 4.2: The relationship between micropore classes and micrite microtextures. The cross sign (X) indicates the abundance of a certain type of micropores at certain microtextures (Rahman et al., 2011).

	Rounded Micrites	**Subrounded Micrites**	**Microrhombic and Polyhedral Micrites**	**Compact Anhedral Micrites**
Very fine Micropores (0.1 – 2 μm)				XX
Fine Micropores (2 – 4 μm)		X		X
Medium Micropores (4 – 6 μm)	X	X		
Coarse Micropores (6 – 10 μm)	X		X	

The occurrence and distribution of different sized micropores are closely related to micrite microtexture (Rahman et al., 2011). For example coarse micropores are mostly found in microrhombic and polyhedral micrites and rounded micrites, whereas very fine micropores are mostly observed in compact anhedral micrites. Similarly fine micropores are mostly found in subrounded, and compact anhedral micrites whereas medium micropores are mostly observed in rounded and subrounded micrites. Table 4.2 summarizes the occurrence of different sized micropores of the various microtexture types. Table 4.3 represents the relative contribution of different microtextures to the fluid flow.

Table 4.3: The relative contributions of different types of micrite microtexture on fluid flow. Here C, M, F, and VF stand for coarse (6-10 μm), medium (4 – 6 μm), fine (2 – 4 μm), and very fine (0.1 – 2 μm) micropores respectively.

Microtexture	Micropores Present	Contribution to fluid flow
Rounded Micrites	C, M	Poor
Subrounded Micrites	M, F	Poor to None
Microrhombic and Polyhedral Micrites	C	Moderate
Compact Anhedral Micrites	F, VF	None

4.4.7 Application of Microtexture Classification to Poro-Perm Relationship

As discussed in the Section 4.2.1, the porosity-permeability crossplot does not display a linear distribution of data points. The classification of micrite microtextures on the basis of SEM study was applied to the data. The result shows definite clusters of the types of micrite microtextures that follows the cluster of data points in poro-perm relationship (Figures 4.57 and 4.58).

The clusters in Figure 4.57 suggest that the microtexture classification is effective in explaining the scattered distribution of data points on poro-perm crossplots. For example the data points on the crossplots with microrhombic to polyhedral micrites fall within the area of comparatively higher permeability whereas the cluster of compact anhedral micrites falls in the area of very low permeability. As described earlier in the micrite microtexture description, microrhombic to polyhedral micrites provide good interconnectivity between the micropores and compact anhedral micrites are mostly isolated and do not provide good connectivity between the micropores. The data points with rounded to subrounded micrites fall within the area of moderate permeability with some overlaps. These distributions strongly support the

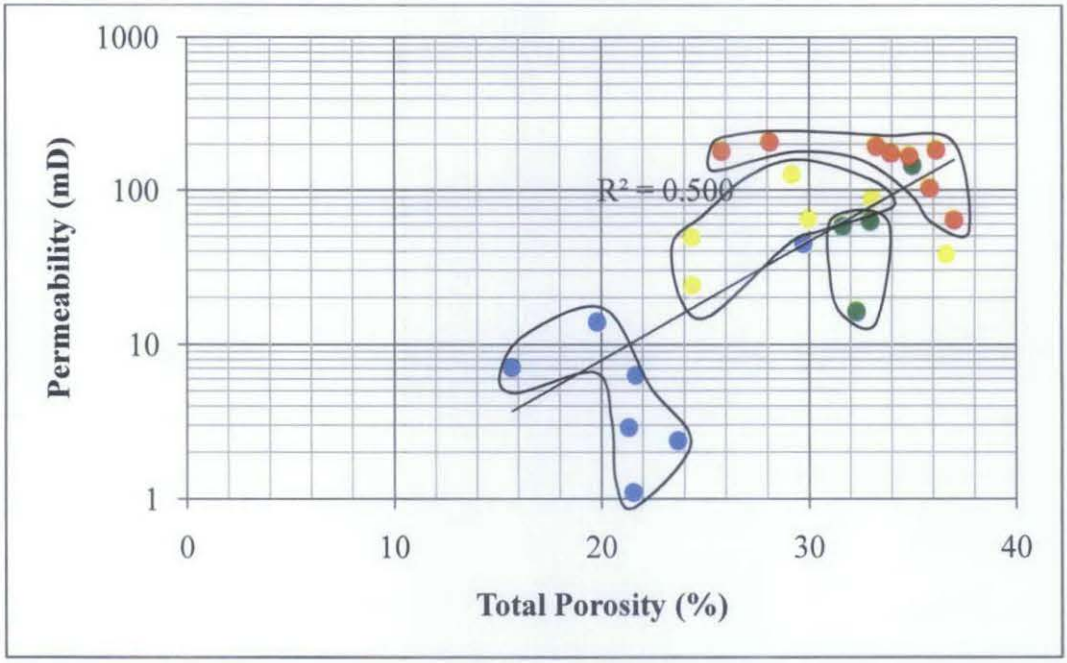

Figure 4.57: Application of microtexture classification to total porosity versus permeability crossplot. The clusters of data points can be grouped following microtexture classification.

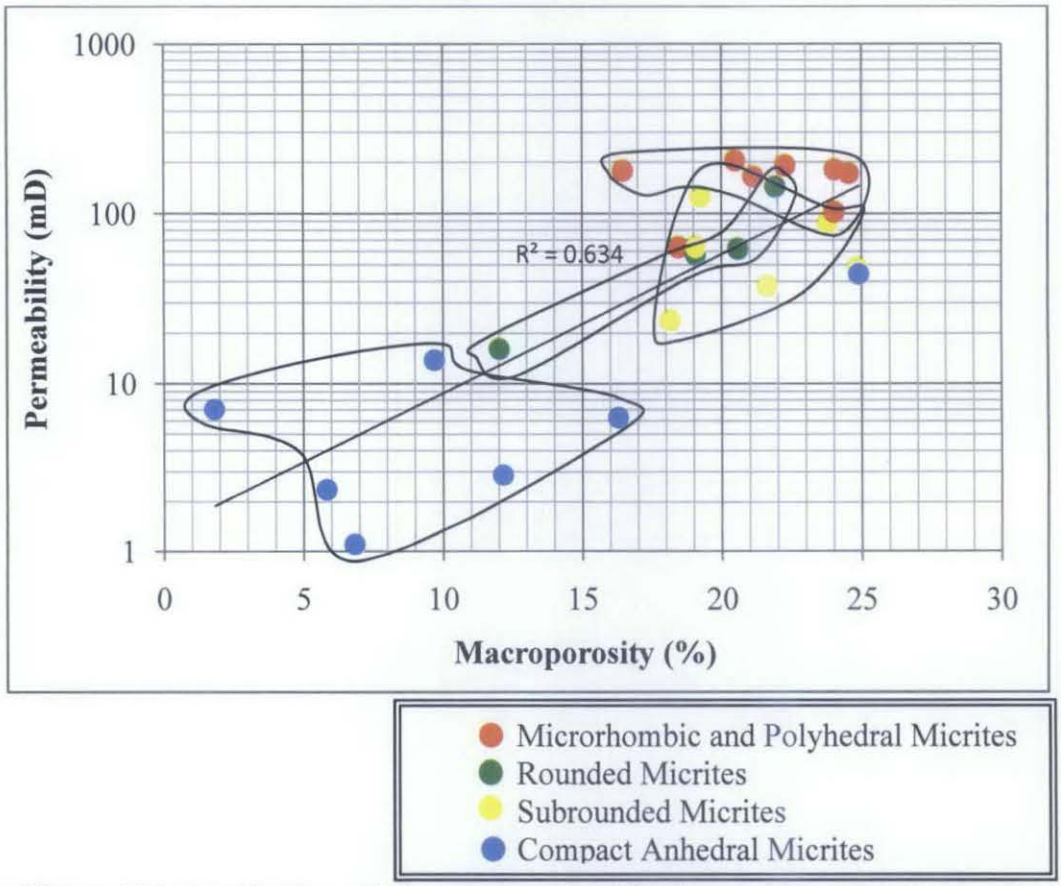

Figure 4.58: Application of microtexture classification to macroporosity versus permeability crossplot. Although the microporosity amounts are deducted from the total porosity, still the microtexture classification fits with the data clusters.

validity and usefulness of the microtextural classification and microporosity classification proposed earlier.

Figure 4.58 shows the data points on macroporosity-permeability crossplot. As described earlier the macropores represent the pores that are 10 μm or larger in diameter. Even though microporosity amount is deducted from the total porosity (in case of macroporosity), the clusters of data points that support the microtexture classification, i.e. microporosity classification and occurrence are still present.

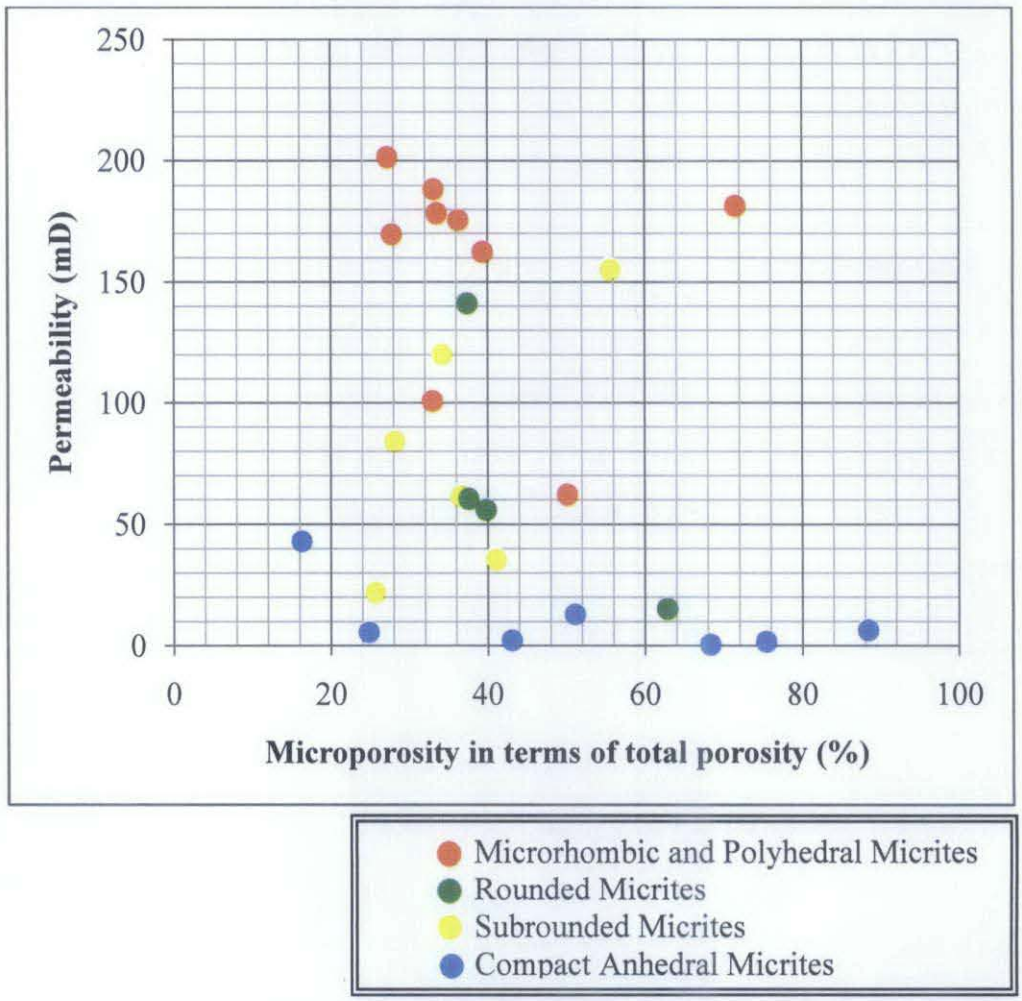

Figure 4.59: The contribution of microporosity in terms of total porosity on different types of micrite microtextures. Microporosity can reach more than 80% of the total porosity in some reservoirs.

Figure 4.59 shows the relative proportion of microporosity in total porosity in different micrite microtextures. The figure shows that the proportion of microporosity in total porosity is very high in compact anhedral micrites (Appendix C). In some cases microporosity may comprise more than 80% of the total porosity in compact

anhedral micrites. This result is quite expected in the sense that compact anhedral micrites are common in argillaceous, muddy lithofacies where micropores are relatively more abundant than macropores. However, it is also observed that microporosity proportion could be high even in highly permeable reservoir rocks. As described earlier in this chapter, microrhombic and polyhedral micrites are mostly characterized by coarse micropores (Table 4.2) and highly permeable rocks have this type of micrite microtexture. It is observed that microporosity proportion could be high (25 – 50% of the total porosity or even more) in microrhombic and polyhedral micrites. This means that microporosity proportion is important not only in low permeability carbonate reservoirs, as highly permeable rocks may also have a high proportion of microporosity as part of the total porosity of the reservoirs.

4.4.8 Discussion

The textural control on porosity was reported by the earliest researchers like Dunham (1962). The presence or absence of mud is very carefully reported in Dunham's classification of texture. He reported two main groups of limestones, mud supported or grain supported. As discussed above, the texture of limestone controls the porosity occurrence. For example, mud supported rocks are expected to have lower amounts of macroporosity compared to the grain supported rocks (in the cases where diagenetic effect is not a major contributor).

The crystallometry and morphometry of micrites are key to study micrite microtextures. Lambert (2006) explained that micrite microtextures (including crystal shapes and contacts) present a wide variability between microporous reservoir facies and non-microporous compact layers. Lambert studied the Arab, Kharaib and Mishrif Formations which are Jurassic and Cretaceous carbonate reservoirs in the Middle East. Three typical end-member microtextures are distinguished by Lambert (2006). These are rounded micrites, micro-rhombic micrites, and compact anhedral micrites (Figure 4.60).

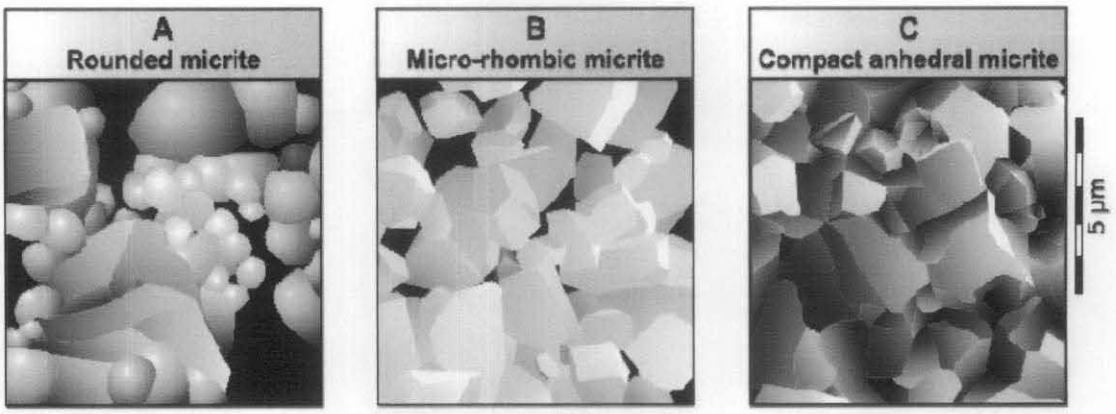

Figure 4.60: Terminology used for microtexture of micrites (Lambert et al., 2006).

In this study, four kinds of micrite microtextures were observed with their distinctive crystallometry and morphometry. The idea that textural studies are the keys to classify porosity in carbonates is fundamental as suggested by many researchers. Earlier researchers on pore type classification like Archie (1952) proposed a limestone classification that consists of two parts, the texture of the matrix, and the character of the visible pore structure. The most widely used carbonate porosity classification (Choquette and Pray, 1970) is based on the textural arrangement of the rock. This classification scheme has two basic parts based on the fabric selectivity or non-selectivity.

The importance of the combined study on rock fabrics and petrophysical properties in carbonates was first raised by Archie (1952). Archie made the first attempt at relating rock fabrics with petrophysical properties in carbonate rocks. Archie (1952) recognized that not all pore spaces can be observed using a 10^x magnification microscope and the surface texture of the rock reflects the amount of matrix porosity. Lucia (1983) proposed a classification for carbonate pore system based on the idea that porosity distribution in carbonate rocks are related to the texture or fabric of the rock. The basic idea is to study the texture of the rock to get an idea of the porosity distribution.

Since this study concentrates on microporosity, the study of microtexture was considered as an important approach to understand microporosity occurrences in the reservoirs. Moreover, pore size is considered as a significant criterion in porosity classification. One of the important objectives of having a porosity classification is to

relate porosity with the flow related properties of carbonates. Archie (1952) stated the importance of pore structure on porosity classification study. Lucia (1995) mentioned that porosity must be classified in terms of both rock fabrics and petrophysical properties.

Lønøy (2006) emphasized the fact that pore-type classification should be able to define the relationship between porosity and permeability in carbonates to reduce the uncertainty in hydrocarbon reserve calculation. Lønøy (2006) proposed a classification scheme that incorporates elements of both rock texture and pore size. These fundamental approaches were taken under consideration while working on microporosity. This study proposes a classification for microporosity of Miocene carbonates of Central Luconia based on the micrite microtextures of the rock and the size of micropores. This classification scheme can explain microporosity of carbonates in terms of flow related properties of the carbonate reservoirs.

CHAPTER 5

CONCLUSIONS

5.1 Conclusions

This study on microporosity of Miocene carbonates used some conventional methods of investigation together with a few new approaches. Microporosity in the Miocene carbonates of Central Luconia was studied using microscopic observations with a transmitted light microscope, fluorescence microscope and scanning electron microscope and by introducing Digital Image Analysis (DIA) technique using the photomicrographs captured under different microscopes. This study raised and demonstrated the fact that microporosity in Miocene carbonate reservoirs can be classified in terms of different micrite microtextures. The classification of micrites allows explaining the clusters of data points in porosity-permeability crossplot. A brief summary of the findings and conclusions of this study are as follows:

1. Detection and Quantification of Microporosity:

a) Miocene carbonates of Central Luconia contain a significant amount of microporosity (sometimes as high as 80 % of the total porosity), which, has a strong impact on fluid flow but also on the petrophysical properties of these carbonate reservoirs.

b) Microporosity can be quantified using Digital Image Analysis (DIA) technique. DIA uses photomicrographs captured with a digital camera using transmitted light, fluorescence light, and scanning electron microscope. The method of quantification of microporosity involves macroporosity estimation using photomicrographs by DIA technique and its comparison with the total porosity measured using core plug with a helium (He) gas porosimeter.

2. Effects of Microporosity on Permeability and Sonic Velocity:

a) Microporosity affects the petrophysical and reservoir properties of carbonates. These relationships are not simple or straightforward because of the heterogeneity of the carbonate reservoir rocks mostly due to complex diagenesis. However some empirical relationships were established in this study on the Miocene carbonate reservoirs of Central Luconia, offshore Sarawak, Malaysia.

b) The relationship between porosity and permeability shows a better correlation when microporosity is deducted from the total porosity present in the reservoirs. Thus taking microporosity into consideration can reduce the uncertainty in predicting the permeability of the Miocene carbonate reservoirs.

c) Microporosity shows an inverse relationship with permeability. The more microporous carbonate reservoirs show a lower permeability.

d) Microporosity reduces the sonic velocity of carbonates. The more microporous carbonate reservoirs show low sonic velocity. Again, an increase in the permeability of the carbonate reservoirs reduces the sonic velocity of the rock; in other words more permeable carbonate reservoirs show low sonic velocity.

3. Occurrence and Classification of Microporosity:

a) Five types of lithofacies were observed in the reservoirs of Central Luconia during the study. These are a) Chalky mouldic limestone (LCM), b) Argillaceous tight limestone (ALT), c) Mouldic limestone (LM), d) Mouldic dolomitic limestone (LDM), and e) Chalky limestone (LC). These lithofacies have their identical texture and porosity types. Three of the lithofacies (LCM, LC, and LM) have excellent reservoir potential in terms of porosity and permeability. These lithofacies types were plotted against the quantified microporosity for each of the samples. This observation suggests that the excellent reservoir facies (LCM) can give very high amounts of microporosity, sometimes as much as 20% of the total rock volume. During this study a

relatively high percentage of microporosity was encountered in excellent reservoir facies. Therefore, the general idea of expecting high microporosity only in tight lithofacies (low porous-permeable rocks) is not necessarily true, especially in Miocene carbonates.

b) The occurrence and abundance of microporosity depends on the crystallometry and morphometry of micrite particles. Based on crystallometry, morphometry and textural arrangements, the micrites in the Miocene carbonate reservoirs of Central Luconia were classified in four different microtextures. These are:

   i) Rounded micrites,

   ii) Subrounded micrites,

   iii) Microrhombic and polyhedral micrites, and

   iv) Compact anhedral micrites.

   Each of these types has its specific crystal shape, contact, morphology, and arrangement.

c) Applying DIA technique on SEM and backscattered SEM photomicrographs, four different classes of micropores were defined. These classes are based on the maximum pore diameter. The classes include:

   i) Very fine micropores (0.1 to 2 μm),

   ii) Fine micropores (2 to 4 μm),

   iii) Medium micropores (4 to 6 μm), and

   iv) Coarse micropores (6 to 10 μm).

d) The cathodoluminescence study showed the core plug samples to be non-luminescent; thus indicating the calcite cementation of the reservoirs in marine environment during deposition or soon after deposition. Carbon ($\delta^{13}C$) and

oxygen ($\delta^{18}O$) isotope signatures indicate that the limestone was deposited in a marine environment and then underwent meteoric diagenesis. The carbon isotope ($\delta^{13}C$) values indicate that most likely the rock has been cemented by some eogenetic diagenesis process, such as meteoric diagenesis. Thus stable isotope signatures revealed the fact that microporosity in Miocene carbonates of Central Luconia is post depositional and developed during diagenesis of the rock.

e) The occurrence, abundance and distribution of different types of micropores are very much related to micrite microtextures. Specific classes of micropores are found in specific micrite microtextures. For example very fine micropores are observed mostly in rocks with compact anhedral micrites; whereas coarse micropores are found in rounded, and microrhombic and polyhedral micrite microtextures.

f) The classification of micropores in terms of their micrite microtextural occurrence allows a more concise definition of micropores that contribute to the permeability of the carbonate reservoirs. The various classes of micropores together with their corresponding micrite microtextures lead to define the potential reservoir rocks in terms of their micrite microtextures. For example, very fine micropores are dominant in compact anhedral micrites whereas coarse micropores occur in rounded, and microrhombic and polyhedral micrites. The coarse micropores are sometimes connected and provide positive contribution to the reservoirs whereas very fine micropores are mostly isolated and even if connected, they associate through very narrow pore throats and do not allow any fluid to flow between the pores. These observations are important to define the potential reservoir rocks in terms of micrite microtextures. These perceptions allow understanding the pore system of the Miocene carbonate reservoirs more precisely and effectively. Thus the classification of micrite microtextures and micropores lead to a better understanding of carbonate reservoirs and can be used as tools for advanced carbonate reservoir characterization.

g) The micrite microtexture classification was applied to the porosity-permeability crossplot during the study. The scattering of data points in the porosity-permeability crossplot can be interpreted using the micrite microtexture classification. The clusters of data points on the porosity-permeability crossplot follow micrite microtexture types. The correlation between porosity and permeability is not straight forward in the Miocene carbonate reservoirs of Central Luconia and the occurrence of microporosity is one of the important factors for that.

5.2 Recommendations for Further Study

While carrying out this study it became clear that there were some potential research areas for further studies. Some of the outcome of this study needs to be validated in other platforms to design an ultimate tool to identify the types and amounts of microporosity from geophysical log data. The recommendations for future studies are as follows:

1) The method of quantification of microporosity using Digital Image Analysis (DIA) can be verified with more data. This may include data from 4 to 6 cored wells from 2 to 3 Miocene carbonate platforms of Central Luconia.

2) The micrite microtextures of another 1 or 2 platforms of Central Luconia can be studied to validate the classification schemes for microtexture and microporosity.

3) A petrophysical study can be conducted applying the microporosity classification on geophysical wireline log signatures. This will allow the quantification of the different types of microporosity on elastic and reservoir properties (e.g. sonic velocity, resistivity, saturation) of the Miocene carbonates and to correct the wireline log values so that the log signatures can accurately and effectively predict the flow-related properties of the Miocene carbonate reservoirs of Central Luconia.

REFERENCES

Addadi, L., & Weiner, S. (1989). Stereochemical and structural relations between macromolecules and crystals in biomineralization. In S. Mann, J. Webb, & R.J.P. Williams (Eds.), *Biomineralization* (pp. 133-156). Weinheim: Vch-Verlag.

Agersborg, R., Johansen, T. A., & Jakobsen, M. (2005). The T-matrix approach for carbonate rocks. *SEG Technical Program Expanded Abstracts, 24,* 1597-1600.

Al-Bazzaz, W.H., & Al-Mehanna, Y. W. (2007). Porosity, permeability, and MHR calculations using SEM and thin section images for characterizing complex Mauddud-Burgan carbonate reservoir: *SPE Asia Pacific Oil & Gas Conference and Exhibition,* (SPE 110730). Jakarta: SPE.

Almasi, M.N., Hoskin, C.M., Reed, J.K., & Milo, J. (1987). Effects of natural and artificial Thalassia on rates of sedimentation. *Journal of Sedimentary Petrology,* 57, 901-906.

Anselmetti, F. S., & Eberli, G. P. (1993). Controls on sonic velocity in carbonates. *Pure and Applied Geophysics, 141,* 287-323.

Anselmetti, F. S., & Eberli, G. P. (1997). Sonic velocity in carbonate sediments and rocks. In I. Palaz, K. J. Marfurt (Eds.), *Carbonate Seismology.* (pp. 53-74). SEG Geophysical Development Series 6.

Anselmetti, F. S., & Eberli, G. P. (1999). The velocity-deviation log: A tool to predict pore type and permeability trends in carbonate drill holes from sonic and porosity or density logs. *AAPG Bulletin, 83,* 450-466.

Anselmetti, F. S., & Eberli, G. P. (2000). Sonic velocity in carbonates; a product of original composition and post-depositional porosity evolution. In K. S. Johnson (Ed.), *Circular - Oklahoma Geological Survey, 101*, 359.

Anselmetti, F. S., Luthi, S., & Eberli, G.P. (1998). Quantitative characterization of carbonate pore systems by digital image analysis. *AAPG Bulletin, 82,* 1815-1836.

Archie, G. E. (1952). Classification of carbonate reservoir rocks and petrophysical considerations. *AAPG Bulletin, 36,* 278-298.

Assefa, S., McCann C., & Sothcott, J. (2003). Velocities of compressional and shear waves in limestones. *Geophysical Prospecting, 51,* 1-13.

Baechle, G. T., Colpaert, A., Eberli, G. P., & Weger, R. J. (2007). Modeling of carbonate pore structure effects on velocity using a dual porosity DEM theory. *SEG Technical Program Expanded Abstracts, 26*, 1589-1593.

Baechle, G. T., Colpaert, A., Eberli, G. P., & Weger, R. J. (2008). Effects of microporosity on sonic velocity of carbonates. *The Leading Edge, 27,* 1012-1018.

Baechle, G. T., Weger, R., Eberli, G. P., & Massaferro, J. L. (2004). The role of macroporosity and microporosity in constraining uncertainties and in relating velocity to permeability in carbonate rocks. *SEG Technical Program Expanded Abstracts, 23*, 1662-1665.

Berger, W.H. (1971). Sedimentation of planktonic foraminifera. *Marine Geology, 11*, 325-358.

Berger, W.H. (1975). Deep-sea carbonates: Dissolution profiles from foraminiferal preservation. *Cushman Foundation Foraminiferal Research Special Publication, 13*, 82-86.

Bosence, D.W. (1985). The morphology and ecology of a mound-building coralline alga (Neogoniolithum strictum) from the Florida Keys. *Palaeontology, v. 28*(1), 189-206.

Brie, A., Johnson, D. L., & Nurmi, R. D. (1985). Effect of spherical pores on sonic and resistivity measurements. *Proceedings of the Society of Professional Well Log Analysts Annual Logging Symposium* (pp. 17).

Budd, D. A. (1989). Micro-rhombic calcite and microporosity in limestons: a geochemical study of the lower Cretaceous Thamama Group U. A. E. *Sedimentary Geology, 63,* 293-311.

Cantrell, D. L., & Hagerty, R. M. (1999). Microporosity in Arab Formation carbonates, Saudi Arabia. *GeoArabia Vol.4*(2), 129-154.

Cerepi, A., Durand, C., & Brosse, E. (2002). Pore microgeometry analysis in lowresistivity sandstone reservoirs. *Journal of Petroleum Science and Engineering, 35,* 205-232.

Chilingarian, G. V., Mazzullo, S. J., Rieke, H. H., Dominguez, G. C. & Samaniego, F. V. (Eds.). (1992). *Carbonate reservoir characterization: a geologic-engeneering analysis, part 1: Developments in Petroleum Science, 30* (pp. 18, 640).

Choquette, P. W., & Pray, L. C. (1970). Geological nomenclature and classification of porosity in sedimentary carbonates. *AAPG Bulletin, 54,* 207-250.

Cloud, P.E. (1962). Carbonate deposition west of Andros Islands, Bahamas. *U.S. Geological Survey Prof. Paper 350* (pp. 138).

Coalson, E. B., Hartman, D. J., & Thomas, J. B. (1985). Productive characteristics of common reservoir porosity types. *South Texas Geological Society Bulletin, 25,* 35-51.

De Groot, K. (1965). Inorganic precipitation of calcium carbonate from sea-water. *Nature, 207,* 404-405.

Degens, E.T. (1979). Why do organisms calcify?. *Chemical Geology, 25,* 257-269.

Dix, G. R. (2001). Origin of Sr-rich magnesian calcite mud in a Holocene pond basin (Lee Stocking Island, Bahamas). *Journal of Sedimentary Research, A71,* 167-175.

Doust, H., & Sumner, H. S. (2007). Petroleum systems in rift basins - a collective approach in Southeast Asian basins. *Petroleum Geoscience, 13,* 127-144.

Dunham, R. J. (1962). Classification of carbonate rocks according to depositional texture. In W. E. Ham (Ed.), *Classification of carbonate rocks, AAPG Memoir 1* (pp. 108-121). Tulsa: AAPG.

Eberli, G. P., Baechle, G. T., Anselmetti, F. S., & Incze, M. L. (2003). Factors controlling elastic properties in carbonate sediments and rocks. *The Leading Edge, 22,* 654-660.

Ehrlich, R., Crabtree, S. J., Horkowitz, K. O., & Horkowitz, J. P. (1991). Petrography and Reservoir Physics I: Objective classification of reservoir porosity. *AAPG Bulletin, 75,* 1547-1562.

Ehrlich, R., Crabtree, S. J., Kennedy, S. K., & Cannon, R. L. (1984). Petrographic image analysis I. Analysis of reservoir pore complexes. *Journal of Sedimentary Petrology, 54,* 1365–1378.

Embry, A.F., & Klovan, J. E. (1971). A late Devonian reef tract on northeastern Banks Island Nordwest Territories. *Bulletin of Canadian Petroleum Geology, 19,* 730-781.

Emery, D., & Robinson, A. (1993). *Inorganic geochemistry application to petroleum geology* (pp. 73-100). Oxford: Blackwell Scientific Publications.

Epting, M. (1980). Sedimentology of Miocene carbonate build-ups, Central Luconia, offshore Sarawak. *Geological Society of Malaysia Bulletin, 12,* 17-30.

Etris, E. L., Brumfield, D. S., Ehrlich, R., & Crabtree, S. J. Jr. (1988). Relations between pores, throats and permeability; a petrographic/physical analysis of some carbonate grainstones and packstones. *Carbonates and Evaporites, 3,* 17-32.

Fairchild. (1983). Chemical controls of cathodoluminescence of natural dolomites and calcites: new data and review. *Sedimentology, 30,* 579–583.

Farrow, G.E. & Fyfe, J.A. (1988). Bioerosion and carbonate mud production on high-latitude shelves. In C.S. Nelson (Ed.), Non-tropical shelf carbonates - modern and ancient. *Sedimentary Geology, 60,* 281-297.

Ferm, J.B., Ehrlich, R. & Crawford, G.A. (1993). Petrographic image analysis and petrophysics: analysis of crystalline carbonates from the Permian Basin, West Texas. *Carbonates Evaporites, 8,* 90-108.

Flügel, E. (1988). Halimeda: paleontological record and paleoenvironmental significance. *Coral Reefs, 6,* 123-130.

Flügel, E. (2004). *Microfacies of carbonate rocks analysis, interpretation and application* (pp. 73-98). Heidelberg: Springer-Verlag Berlin.

Folk, R. L. (1959). Practical petrographical classification of limestones. *AAPG Bulletin, 43,* 1-38.

Folk, R. L. (1962). Spectral subdivision of limestone types. In M. D. Piere (Ed.), *Classification of carbonate rocks, AAPG Memoir 1* (pp. 62-84). Tulsa: AAPG.

Folk, R. L. & Robles, R. (1964). Carbonate sands of Isla Perez, Alacran Reef Complex, Yucatan. *Journal of Geology, 72,* 255-292.

Fortey, N. J. (1995). Image analysis in mineralogy and petrology. *Mineralogical Magazine, 59,* 177-178.

Fournier, F., & Borgomano, J. (2009). Critical porosity and elastic properties of microporous mixed carbonate-siliciclastic rocks. *Geophysics, 74*(2), E93-E109.

Freiwald, A. (1995). Bacteria-induced carbonate degradation: a taphonomic case study of Cibicides lobatulus from a high-boreal carbonate setting. *Palaios, 10,* 337-346.

Futterer, D. K. (1974). Significance of the boring sponge Cliona for the origin of fine grained material of carbonate sediments. *Journal of Sedimentary Petrology, 44,* 79-84.

Gaillard, C., Bernier, P., Gall, J.C., Gruet, Y., Barale, G., Bourseau, J.P., et al. (1994). Ichnofabric from the Upper Jurassic lithographic limestone of Cerin, southeast France. *Palaeontology, 37*, 285-304.

Ginsburg, R.N. (1957). Early diagenesis and lithification of shallow-water carbonate sediments in South Florida. In *Regional aspects of carbonate deposition. SEPM Special Publication 5* (pp. 80-100). SEPM.

Ginsburg, R.N. & Lowenstam, H.A. (1958). The influence of marine bottom communities on the depositional environments of sediments. *Journal of Geology, 66*, 310-318.

Hatfield, K. & Garnham, J. (2001). The application of image analysis to improve permeability prediction. *PETROPHYSICS, 42*, 457-467.

Henrich, R. & Wefer, G. (1986). Dissolution of biogenic carbonates: effects of skeletal structure. *Marine Geology, 71*, 341-362.

Hillis, L. (1959). A revision of the genus Halimeda (order Siphonales). *Publication Institute of Marine Science University of Texas, 6*, 321-403.

Hillis, L. (2001). The calcareous reef alga Halimeda (Chlorophyty, Byropsidales): a Cretaceous genus that diversified in the Cenozoic. *Palaeogeography, Palaeoclimatology, Palaeoecology, 166*, 89-100.

Hillis-Colinvaux, L. (1980). Ecology and taxonomy of Halimeda: primary producer of coral reefs. *Advances in Marine Biology, 17*, 1-327.

Honjo, S. (1969). Study of fine grained carbonate matrix: sedimentation and diagenesis of micrite. *Paleontological society of Japan Special Paper, 14*, 67-82.

Husseini, S. I., & Matthews, R. K. (1972). Distribution of high-magnesium calcite in lime muds of the Great Bahama Bank: diagenetic implications. *Journal of Sedimentary Petrology,* 42(1), 179-182.

Hutchison, C. S. (2005). *Geology of North-West Borneo: Sarawak, Brunei and Sabah* (pp. 421). Amsterdam : Elsevier Academic Press.

Keehm, Y. (2003). Computational rock physics; transport properties in porous media and applications (Doctoral Dissertation thesis, Stanford University), pp. 135. Stanford, CA, United States (USA).

Keim, L., & Schlager, W. (1999). Automicrite facies on steep slopes (Triassic, Dolomites, Italy). *Facies, 41*, 15-26.

Keith, B. D., & Pittman, E. D. (1983). Bimodal porosity in oolitic reservoir effect on productivity and log response, Rodessa limestone (Lower Cretaceous), East Texas basin. *AAPG Bulletin, 67*, 1391-1399.

Kenter, J. A. M., Ivanov, M., Winterer, E. L., Sager, W. W., Firth, J. V., Arnaud, H. M., et al. (1995). Parameters controlling acoustic properties of carbonate and volcanic clastic sediments at sites 866 and 869. In E. L. Winterer (Ed.), *Proceedings of the Ocean Drilling Program, Scientific Results, Leg 143, Northwest Pacific atolls and guyots: College Station* (pp. 287–303). Texas: ODP, Texas A&M University,

Kirkham, A., Juma, M. B., McKean, T. A. M., Palmer, A. F., Smith, M. J., Thomas, A. H., et al. (1996). Fluid saturation prediction in the transition zone carbonate reservoir, Abu Dhabi. *GeoArabia, 1*, 551-566.

Knackstedt, M., Madadi, M., Arns, C., Baechle, G., Eberli, G. & Weger, R. (2008). Carbonate petrophysical parameters derived from 3-D images. *Extended abstracts of AAPG Annual Convention, San Antonio*. San Antonio: AAPG.

Kenter, J. A. M., & Ivanov, M. (1995). Parameters controlling acoustic properties of carbonate and volcaniclastic sediments at Sites 866 and 869. In J. Winterer et al. (Eds.), *Proceedings of the Ocean Drilling Program: Scientific Results*, 143, 287–303.

Kukal, Z., & Saadallah, A. (1973). Aeolian admixtures in the sediments of the N. Persian Gulf. In B.H. Purser (Ed.), *The Persian Gulf* (pp. 115-122). Heidelberg: Springer.

Kumar, M., & Han, D. H. (2005). Pore shape effect on elastic properties of carbonate rocks. *SEG Technical Program Expanded Abstracts, 24*, 1477-1480.

Lambert, L., Durlet, C., Loreau J., & Marnier, G. (2006). Burial dissolution of micrites in Middle East carbonate reservoirs (Jurassic–Cretaceous): keys for recognition and timing. *Marine and Petroleum Geology, 23*, 79-92.

Lindholm, R.C. (1969). Carbonate petrology of the Onondaga Limestone (Middle Devonian), New York: A case for Calcisiltite. *Journal of Sedimentary Petrology, 39*(1), 268-275.

Lindqvist, J. E., & Akesson, U. (2001). Image analysis applied to engineering geology, a literature review. *Bulletin of Engineering Geology and the Environment, 60*, 117-122.

Long, J. V. P. & Agrell, S. O. (1965). The cathodoluminescence of minerals in thin section. *Mineral Magazine, 34*, 318-326.

Lønøy, A. (2006). Making sense of carbonate pore system. *AAPG Bulletin, 90*, 1381-1405.

Loreau, J. P. (1982). Sédiments aragonitiques et leur genese. *Muséum Hist. Natur. Mem., C 47*, 300.

Lowenstam, H.A. & Epstein, S.A. (1957). On the origin of sedimentary aragonite needles of the Great Bahama Bank. *Journal of Geology, 65*, 364-375.

Lowenstam, H.A. & Weiner, S. (1983). Mineralization by organisms and the evolution of biomineralization. In P. Westbroek, & E. W. de Jong (Eds.), *Biomineralization and biological metal accumulation*, (pp. 191-203). Dordrecht: D. Reidel Pub.

Lucia, F. J. (1983). Petrophysical parameters estimated from visual descriptions of carbonate rocks: A field classification of carbonate pore space. *Journal of Petroleum Technology, 216*, 221-224.

Lucia, F. J. (1995). Rock-fabric/petrophysical classification of carbonate pore space for reservoir characterization. *AAPG Bulletin, 79*, 1275– 1300.

Lucia, F. J. (1999). *Carbonate reservoir characterization.* (pp. 226). Berlin: Springer-Verlag.

Matthews, R.K. (1966). Genesis of recent lime mud in southern British Honduras. *Journal of Sedimentary Petrology, 36,* 428-454.

Mohammad Yamon Ali. (1996). The Central Luconia Miocene carbonates and hydrocarbon occurrences from the perspective of exploration and exploitation. *ASCOPE carbonate workshop, Habitat of oil and gas in carbonate sediment of ASEAN region, Jogyakarta.*

Moore, C.H. (1989). *Carbonate diagenesis and porosity: Developments in Sedimentology 46* (pp. 388). New York: Elsevier.

Moore, C.H. (2001). *Carbonate reservoirs. Porosity evolution and diagenesis in a sequence stratigraphic framework. Developments in Sedimentology 55* (pp. 260). Amsterdam: Elsevier.

Moore, C. H. & Shedd, W. W. (1977). Effective rates of sponge bioerosion as a function of carbonate production. *Proceeding of 3rd International Coral Reef Symposium, 2,* 449-505.

Mowers, T. T. & Budd, D. A. (1996). Quantification of porosity and permeability reduction due to calcite cementation using computer-assisted petrographic image analysis techniques. *AAPG Bulletin, 80,* 309-322.

Nelsen, J. E., & Ginsburg, R. N. (1986). Calcium carbonate production by epibionts on Thalassia in Florida Bay, Journal of Sedimentary Petrology, 56, p. 622-628.

Neumann, A. C., & Land, L. S. (1975). Lime mud deposition and calcareous algae in the Bight of Abaco, Bahamas: a budget. *Journal of Sedimentary Petrology, 45,* 763-786.

Neuweiler, F., Reitner, J., & Monty, C. (1997). Biosedimentology of microbial build-ups: IGCP Project No. 380, Proceedings of the 2nd meeting Gottingen/Germany 1996. *Facies, 36,* 195-284.

Noad J. (2001). The Gomantong limestone of eastern Borneo: A sedimentological comparison with the near contemporaneous Lucobnia province. *Palaeogeography, Palaeoclimatology, Palaeoecology, 175,* 273-302.

Periere, M. D., Durlet, C., Vennin, E., Lambert, L., Bourillot, R., Caline, B., et al. (2010). Micrite morphology and crystallometry. keys for understanding reservoir properties in Cretaceous microporous limestones. Examples from the Middle East. *Marine and Petroleum Geology, In press.*

Peszat, C. (1991). Microstructures and origin of the Oxfordian micritic limestones in the southwestern margin of the Swietokrzyskie Mountains (Poland). *Archiwum Mineralogiczne, 47*, 182-188.

Petricola, M. J. C., & Watfa, M. (1995). Effect of microporosity in carbonates: Introduction of a versatile saturation equation: *SPE Middle East Oil Show,* (SPE 29841). Bahrain: SPE.

PETRONAS. (1999). *The Petroleum Geology and Resources of Malaysia* (pp. 371-391). Kuala Lumpur: Petroliam Nasional Berhad (PETRONAS).

Pierson, B. J. (1981). The control of cathodoluminescence in dolomite by iron and manganese. *Sedimentology, 28,* 601-610.

Pilkey, O. H., & Noble, D. (1966). Carbonate and clay mineralogy of the Persian Gulf. *Deep-Sea Research, 13*, 1-16.

Pittman, E. D. (1971). Microporosity in carbonate rocks. *AAPG Bulletin, 55*, 1873-1881.

Poncet, J. (1989). Occurrence of the genus Halimeda Lamouroux, 1812 (green calcareous alga) in Upper Permian sediments of South Tunisia. *Revue de Micropaléontologie, 32*, 40-44.

Rafavich, F., Kendall, C. H. S. C. & Todd, T. P. (1984). The relationship between acoustic properties and the petrographic character of carbonate rocks. *Geophysics, 49*, 1622-1636.

Rahman, M. H. & Pierson, B. J. (2011). Effects of microporosity on permeability and sonic velocity of Miocene carbonates and an approach to relate micrite microtextures with microporosity occurrences in Miocene carbonate reservoirs of offshore Sarawak, Malaysia. *SEG Technical Program Expanded Abstract, 30,* In Press.

Rahman, M. H., Pierson, B. J. & Wan Yusoff, W. I. (2011). A New Approach to Classify Microporosity in Miocene Carbonate Reservoirs of Offshore Sarawak, Malaysia. *SPE Saudi Arabia Section Annual Technical Symposium and Exhibition,* (SPE 149112). Al khobar: SPE.

Reid, R. P., Macintyre, I. G., & Post, J. E. (1992). Mineralized skeletal grains in northern Belize lagoon: a major source of Mg-Calcite mud. *Journal of Sedimentary Petrology, 62*(1), 145-156.

Reitner, J. (1993). Modern cryptic microbialite/metazoan facies from Lizard Island, Great Barrier Reef, Australia, formation and concepts. *Facies, 29,* 3-40.

Reitner, J. & Neuweiler, F. (1995). Mud mounds: a polygenetic spectrum of fine grained carbonate build-ups. *Facies, 32*, 1-70.

Reitner, J., Gautret, P., Marin, F., & Neuweiler, F. (1995). Automicrite in modern microbialite-formation model via organic matrices (Lizard Island, Great Barrier Reef, Australia). *Bulletin of Institute of Oceanography Monaco, 13.*

Reitner, J., Thiel, V., Zankl, H., Michaelis, W., Wörheide, W., & Gautret, P. (2000). Organic and biogeochemical patterns in cryptic microbialites. In R. E. Riding, & S. M. Awramik (Eds.), *Microbial Sediments* (pp. 149-160). Berlin: Springer.

Rossebø, Ø. H., Brevik, I., Ahmadi, G. R., & Adam, L. (2005). Modeling of acoustic properties in carbonate rocks. *SEG Technical Program Expanded Abstracts, 24*, 1505-1508.

Ruzyla, K. & Jezek, D. I. (1987). Staining method for recognition of pore space in thin and polished sections. *Journal of Sedimentary Petrology, 57*, 777-778.

Saleh, A. A., & Castagna, J. P. (2004). Revisiting the Wyllie time-average equation in the case of near-spherical pores. *Geophysics, 69,* 45-55.

Scoffin, T. P. (1970). The trapping and binding of subtidal carbonate sediments by marine vegetation in Bimini lagoon, Bahamas. *Journal of Sedimentary Petrology, 40*, 249-273.

Sharma, R., & Prasad, M. (2009). Characterization of heterogeneities in carbonates. *SEG Technical Program Expanded Abstracts, 28,* 2149-2154.

Simkiss, K., & Wilbur, K. M. (1989). *Biomineralization: cell biology and mineral deposition*, San Diego: Academic Press.

Sippel, R. F. (1968). Sandstone petrology, evidence luminescence petrography. *Journal of Sedimentary Petrology, 38,* 530-554.

Schneider, J. (1977). Carbonate construction and decomposition by epilithic and endolithic micro-organisms in salt- and freshwater. In E. Flügel (Ed.), *Fossil algae. Recent results and developments* (pp. 248-260). Berlin: Springer-Verlag.

Sorby, H. C. (1879). The structure and origin of limestones. *Proceedings of the Geological Society of London, 35*, 59-95.

Stieglitz, R.D. (1972). Scanning electron microscopy of the fine fraction of recent carbonate sediments from Bimini, Bahamas. *Journal of Sedimentary Petrology, 42,* 211-226.

Stockman, K. W., Ginsburg, R. N., & Hinn, E. A. (1967). The production of lime mud by algae in south Florida. *Journal of Sedimentary Petrology, 37,* 633-648.

Sun, Y. F., Massaferro, J. L., Eberli, G. P. & Teng, Y. C. (2001). Quantifying the effects of pore structure and fluid saturation on acoustic wave velocity in carbonates. In Er-Chang Shang, Qihu Li, & T. F. Gao (Eds.). *Theoretical and Computational Acoustics 2001* (pp. 335-347). Singapore: World Scientific.

Swinchatt, J. P. (1965). Significance of constituent composition, texture and skeletal breakdown in some Recent carbonate sediments. *Journal of Sedimentary Petrology, 35,* 71-90.

Torunski, H. (1979). Biological erosion and its significance for the morphogenesis of limestone coasts and for nearshore sedimentation (Northern Adriatic). *Senckenbergiana Maritima, 11,* 193-265.

Urey, H. C. (1947). The thermodynamic properties of isotopic substances. *Journal of Chemical Society (London),* 562-581.

Van den Berg, E. H., Meesters, A. G. C. A., Kenter, J. A. M., & Schlager, W. (2002). Automated separation of touching grains in digital images of thin sections. *Computers & Geosciences, 28,* 179-190.

Van Treeck, P., Schuhmacher, H., & Paster, M. (1996). Grazing and bioerosion by herbivorous fishes-key processes structuring coral reef communities. *Göttinger Arb. Geol. Paläont., 2,* 133-137.

Walter, L. M. (1985). Relative reactivity of skeletal carbonates during dissolution: implications for diagenesis. In N. Schneidermann, & P. M. Harris (Eds.), Carbonate cements. *SEPM Special Publication, 36,* 3-16.

Wang, Z. (1997). Seismic properties of carbonate rocks. *Geophysical Development Series, 6,* 29-52.

Wardlaw, N. C. (1979). The influence of pore structure in rocks on the entrapment of oil. *Canadian Society of Petroleum Geologists Memoir, 6,* 193-208.

Weger, R. J., Eberli, G. P., Baechle, G. T., Massaferro, J. L. & Sun, Y. F. (2009). Quantification of pore structure and its effects on sonic velocity and permeability in carbonates. *AAPG Bulletin, 93,* 1297-1317.

Weger, R. J., Baechle, G. T., Masaferro, J. L. & Eberli, G. P. (2004). Effects of pore structure on sonic velocity in carbonates. *SEG Technical Program Expanded Abstracts, 23,* 1774-1777.

Wilber, J. R. & Neumann, A. C. (1993). Effects of submarine cementation on microfabrics and physical properties of carbonate slope deposits, Northern Bahamas. In R. Rezak, & D. L. Lavoie (Eds.), *Carbonate Microfabrics* (pp. 79–94). New York: Springer.

Wilson, J. L. (1975). *Carbonate facies in geologic history* (pp. 471). New York: Springer.

Wilson, J. L. (1980). Limestone and dolomite reservoirs. In G. D. Hobson (Ed.), *Petroleum Geology, 2*, 1-51.

Witt, W. & Gokdag, H. (1994). Orbitolinid biostratigraphy of the Shuaiba Formation (Aptian), Oman. Implications for reservoir development. In M. D. Simmons (Ed.), *Micropaleontology and Hydrocarbon Exploration in the Middle East* (pp. 221–234). London: Chapman and Hall.

Wolf, K. H. (1965). Gradational sedimentary products of calcareous algae. *Sedimentology, 5*, 1-37.

Wright, J. K. (1992). The depositional history of the Hackness Coral-Sponge Bed and its associated sediments within the Passage Beds Member of the Coralline Oolite Formation (Corallian Group; Oxfordian) of North Yorkshire. *Proceedings of the Yorkshire Geological Society, 49*, 155-168

Wyllie, M. R., Gregory, A. R., & Gardner, G. H. F. (1956). Elastic wave velocities in heterogeneous and porous media. *Geophysics, 21*, 41–70.

Yanguas, J. E., & Dravis, J. J. (1985). Blue fluorescent dye technique for recognition of microporosity in sedimentary rocks. *Journal of Sedimentary Petrology, 55*, 600-602.

Youssef, S., Baurer, D., Han, M., Bekri, S., Rosenberg, E., Fleury, M., et al. (2008). Pore-network models combined to high resolution μ-CT to assess petrophysical properties of homogenous and heterogeneous rocks: *International Petroleum Technology Conference* (IPTC 12884). Kuala Lumpur: IPTC.

PUBLICATIONS

Rahman, M. H. & Pierson, B. J. (2011). Effects of microporosity on permeability and sonic velocity of Miocene carbonates and an approach to relate micrite microtextures with microporosity occurrences in Miocene carbonate reservoirs of offshore Sarawak, Malaysia. *SEG Technical Program Expanded Abstracts, v. 30,* In Press.

Rahman, M. H., Pierson, B. J., & Swennen, R. (2011). The Effects and Classification of Microporosity in Miocene Carbonate Reservoirs in Central Luconia, Offshore Sarawak, Malaysia: Keys for Advanced Reservoir Characterization. *Submitted to First Break*, Under Review.

Rahman, M. H., Pierson, B. J., & Wan Yusoff, W. I. (2011). A New approach to classify microporosity in Miocene carbonate reservoirs of offshore Sarawak, Malaysia. *SPE Saudi Arabia Section Annual Technical Symposium and Exhibition*, SPE 149112. (DOI: 10.2118/149112-MS).

Rahman, M. H., B. J. Pierson and W. I. W. Yusoff, 2011; The classification of microporosity in Miocene carbonates: Examples from Miocene carbonate reservoirs in Central Luconia, offshore Sarawak, Malaysia; Accepted in *International Petroleum Technology Conference (IPTC) to be held on November 15-17, 2011; Bangkok, Thailand.*

Rahman, M. H., Pierson, B. J., & Wan Yusoff, W. I. (2011). Quantification of Microporosity and Its effects on Permeability and Sonic Velocity in Miocene Carbonate Reservoirs, Offshore Sarawak, Malaysia: Submitted to *National Postgraduate Conference 2011 to be held on September 19-20; Universiti Teknologi PETRONAS, Malaysia,* Under Review.

APPENDIX A

DATA SET

Plug No.	Core No.	Tray No.	Depth (Feet)
1	16	2	4740.1
2	16	22	4688.6
3	15	14	4647.9
4	14	17	4606.4
5	14	22	4592.4
6	13	8	4568
7	13	21	4534.1
8	12	5	4516.4
9	10	11	4459.3
10	10	19	4440.2
11	7	6	4382.2
12	7	17	4354.1
13	7	24	4334.8
14	6	13	4303.9
15	6	17	4294
16	6	23	4277.6
17	5	15	4238.9
18	5	19	4229.5
19	5	24	4215.9
20	4	2	4212.2
21	4	7	4199.5
22	4	18	4169.7
23	4	21	4161.6
24	3	6	4139.6
25	3	10	4130.7
26	3	14	4120.7
27	3	17	4111.3
28	3	21	4100.9
29	2	9	4080.1
30	2	13	4070.9
31	2	21	4052.7
32	2	23	4047.5
33	1	6	4018.2

APPENDIX B

MICROPOROSITY VS. PERMEABILITY

Plug No.	Microporosity (%)	Permeability (mD)
1	18.53	62.704
2	6.23	22.998
4	15	36.609
5	10.99	188.88
6	8.93	156.127
7	9.95	121.168
8	17.85	2.333
10	9.17	2.844
11	13.06	141.802
12	4.82	43.788
13	12.56	56.678
14	9.41	170.25
16	14.7	1.083
17	20.27	15.907
18	7.64	202.023
19	10.93	62.479
20	5.36	6.205
21	10.11	13.638
22	9.26	85.033
23	12.08	178.98
24	11.79	101.251
25	12.36	61.12
27	9.34	176.122
30	13.86	6.96
31	13.7	162.874
33	4.94	5.676

APPENDIX C

POROSITY-PERMEABILITY CROSSPLOT

Plug No.	Total Porosity (%)	Macroporosity (%)	Permeability (mD)	Miroporosity In Total Porosity (%)
1	36.99	18.46	62.704	50.09
2	24.416	18.19	22.998	25.52
4	36.649	21.65	36.609	40.93
5	33.256	22.27	188.88	33.05
7	29.228	19.28	121.168	34.04
8	23.706	5.86	2.333	75.30
9		24.87	47.106	
10	21.346	12.18	2.844	42.96
11	34.993	21.93	141.802	37.32
12	29.742	24.92	43.788	16.21
13	31.641	19.08	56.678	39.69
14	33.955	24.55	170.25	27.71
16	21.555	6.86	1.083	68.20
17	32.311	12.04	15.907	62.73
18	28.128	20.49	202.023	27.16
19	30.007	19.08	62.479	36.42
20	21.682	16.32	6.205	24.72
21	19.818	9.712	13.638	51.01
22	33.074	23.81	85.033	28.00
23	36.122	24.04	178.98	33.44
24	35.823	24.03	101.251	32.91
25	32.963	20.6	61.12	37.50
27	25.806	16.47	176.122	36.19
30	15.693	1.83	6.96	88.32
31	34.839	21.14	162.874	39.32

APPENDIX D

MICROPOROSITY, PERMEABILITY, AND SONIC VELOCITY RELATIONSHIP

Plug No.	Microporosity (%)	Vp (m/s)	Vs (m/s)	Permeability (%)
1	18.53	2659	1660	62.704
2	6.23	2445	1995	22.998
4	15	2443	1389	36.609
5	10.99	2455	1360	188.88
6	8.93	4342	2199	156.127
7	9.95	1785	1676	121.168
8	17.85	2571	1897	2.333
10	9.17	2970	2118	2.844
11	13.06	1769	1409	141.802
12	4.82	2632	1488	43.788
13	12.56	2082	1578	56.678
14	9.41	1725	1011	170.25
16	14.7	3336	2184	1.083
17	20.27	2148	1583	15.907
18	7.64	2882	1692	202.023
19	10.93	2413	1560	62.479
20	5.36	2722	1953	6.205
21	10.11	3302	1987	13.638
22	9.26	2398	1552	85.033
23	12.08	2286	1594	178.98
24	11.79	2289	1535	101.251
25	12.36	2370	1846	61.12
27	9.34	3410	2189	176.122
30	13.86	2433	1785	6.96
31	13.7	2321	1336	162.874
32	25.01	2560	1292	181.93
33	4.94	2901	1420	5.676

APPENDIX E

STABLE ISOTOPE DATA

Plug No.	Depth (Feet)	$\delta^{13}C$ Values (V-PDB per mil)	$\delta^{18}O$ values (V-PDB per mil)
1	4740.1	0.82	-4.51
11	4382.2	-0.65	-5.39
12	4354.1	-0.69	-5.48
13	4334.8	0.43	-1.64
22	4169.7	-0.43	-5.30
23	4161.6	-0.45	-5.32
24	4139.6	-0.59	-5.25
28	4100.9	-0.66	-5.02
30	4070.9	-0.82	-5.15
32	4047.5	-0.69	-5.03

APPENDIX F

DIGITAL IMAGE ANALYSIS DATA

Sample No.	Depth (Feet)	Macroporosity Measurement		
		Observation No.	Macroporosity (%)	Avg. Macroporosity (%)
Plg 1	4740.1	1	24.06	**18.46**
		2	17.51	
		3	20.13	
		4	16.23	
		5	16.17	
		6	22.99	
		7	12.34	
		8	17.81	
		9	19.93	
		10	17.40	
Plg 2	4688.6	1	13.44	**18.19**
		2	16.70	
		3	13.46	
		4	18.04	
		5	14.92	
		6	25.87	
		7	16.61	
		8	16.35	
		9	13.33	
		10	18.41	
		11	14.82	
Plg 3	4647.9	1	16.31	**21.07**
		2	18.54	
		3	17.80	
		4	21.09	
		5	21.15	
		6	22.77	
		7	21.71	
		8	22.00	
		9	20.72	
		10	28.40	
		11	21.34	

Sample No.	Depth (Feet)	Macroporosity Measurement		
		Observation No.	Macroporosity (%)	Avg. Macroporosity (%)
Plg 4	4606.4	1	23.51	21.65
		2	20.28	
		3	20.28	
		4	23.77	
		5	21.50	
		6	25.98	
		7	23.07	
		8	18.20	
		9	24.00	
		10	15.91	
Plg 5	4592.4	1	22.79	22.27
		2	32.27	
		3	20.01	
		4	17.85	
		5	16.69	
		6	15.54	
		7	18.28	
		8	20.16	
		9	25.59	
		10	23.51	
		11	32.24	
Plg 6	4568.0	1	4.44	7.16
		2	1	
		3	24.77	
		4	11.89	
		5	1.84	
		6	2.15	
		7	4.02	
Plg 7	4534.1	1	22.37	19.28
		2	34.61	
		3	16.20	
		4	22.17	
		5	11.27	
		6	19.20	
		7	16.88	
		8	24.69	
		9	11.34	
		10	14.07	

Sample No.	Depth (Feet)	Macroporosity Measurement		
		Observation No.	Macroporosity (%)	Avg. Macroporosity (%)
Plg 8	4516.4	1	7.23	**5.86**
		2	6.18	
		3	3.13	
		4	3.27	
		5	8.86	
		6	3.23	
		7	8.16	
		8	11.63	
		9	3.10	
		10	3.83	
Plg 9	4459.3	1	30.24	**24.87**
		2	26.90	
		3	28.76	
		4	23.13	
		5	24.72	
		6	15.00	
		7	17.40	
		8	31.70	
		9	26.18	
		10	24.63	
Plg 10	4440.2	1	10.19	**12.18**
		2	7.88	
		3	7.28	
		4	12.55	
		5	17.60	
		6	18.34	
		7	17.48	
		8	5.86	
		9	12.99	
		10	11.60	

Sample No.	Depth (Feet)	Macroporosity Measurement		
		Observation No.	Macroporosity (%)	Avg. Macroporosity (%)
Plg 11	4382.2	1	32.61	**21.93**
		2	17.22	
		3	22.24	
		4	32.34	
		5	16.12	
		6	26.54	
		7	17.04	
		8	26.22	
		9	29.84	
		10	9.16	
Plg 12	4354.1	1	29.30	**24.92**
		2	19.86	
		3	27.22	
		4	29.72	
		5	27.40	
		6	20.31	
		7	28.66	
		8	23.76	
		9	27.50	
		10	15.51	
Plg 13	4334.8	1	25.67	**19.08**
		2	11.28	
		3	24.89	
		4	23.83	
		5	15.27	
		6	20.59	
		7	22.91	
		8	21.80	
		9	18.60	
		10	11.73	
		11	13.37	
Plg 14	4303.9	1	23.41	**24.55**
		2	30.55	
		3	24.25	
		4	21.91	
		5	20.28	
		6	24.01	
		7	23.79	
		8	25.66	
		9	22.11	
		10	29.54	

Sample No.	Depth (Feet)	Macroporosity Measurement		
		Observation No.	Macroporosity (%)	Avg. Macroporosity (%)
Plg 15	4294.0	1	10	**6.97**
		2	8.31	
		3	5.85	
		4	5.88	
		5	3.63	
		6	9.34	
		7	10.03	
		8	2.75	
Plg 16	4277.6	1	6.50	**6.86**
		2	6.72	
		3	6.70	
		4	3.64	
		5	8.26	
		6	8.74	
		7	3.32	
		8	2.85	
		9	12.65	
		10	9.23	
Plg 17	4238.9	1	15.28	**12.04**
		2	11.23	
		3	7.23	
		4	9.64	
		5	13.36	
		6	12.67	
		7	13.97	
		8	11.24	
		9	12.68	
		10	13.11	
Plg 18	4229.5	1	16.76	**20.49**
		2	18.26	
		3	17.13	
		4	25.56	
		5	14.58	
		6	18.70	
		7	17.72	
		8	28.97	
		9	16.38	
		10	30.88	

Sample No.	Depth (Feet)	Macroporosity Measurement		
		Observation No.	Macroporosity (%)	Avg. Macroporosity (%)
Plg 19	4215.9	1	10.95	**19.08**
		2	17.94	
		3	18.22	
		4	19.87	
		5	24.50	
		6	9.94	
		7	25.99	
		8	19.71	
		9	29.81	
		10	13.88	
Plg 20	4212.2	1	22.33	**16.32**
		2	15.22	
		3	5.88	
		4	19.26	
		5	18.91	
		6	17.64	
		7	15	
Plg 21	4199.5	1	11.63	**9.71**
		2	10.73	
		3	8.10	
		4	9.74	
		5	8.36	
		6	10.88	
		7	8.54	
Plg 22	4169.7	1	22.45	**23.81**
		2	24.23	
		3	24.48	
		4	22.71	
		5	25.18	
		6	22.63	
		7	24.99	
Plg 23	4161.6	1	22.77	**24.04**
		2	25.54	
		3	22.39	
		4	24.09	
		5	25.39	
		6	22.64	
		7	25.44	

Sample No.	Depth (Feet)	Macroporosity Measurement		
		Observation No.	Macroporosity (%)	Avg. Macroporosity (%)
Plg 24	4139.6	1	22.26	**24.03**
		2	24.93	
		3	28.18	
		4	22.86	
		5	21.92	
Plg 25	4130.7	1	20.92	**20.60**
		2	20.70	
		3	18.19	
		4	17.36	
		5	25.82	
Plg 26	4120.7	1	9.19	**11.05**
		2	7.46	
		3	9.43	
		4	12.42	
		5	16.75	
		6	9.55	
		7	12.55	
Plg 27	4111.3	1	17.44	**16.47**
		2	21.39	
		3	16.91	
		4	15.52	
		5	11.07	
		6	18.21	
		7	14.73	
Plg 28	4100.9	1	10.45	**13.81**
		2	15.15	
		3	11.15	
		4	16.49	
		5	15.80	
Plg 29	4080.1	1	9.70	**12.94**
		2	10.29	
		3	19.61	
		4	11.10	
		5	13.98	
		6	11.9	

Sample No.	Depth (Feet)	Macroporosity Measurement		
		Observation No.	Macroporosity (%)	Avg. Macroporosity (%)
Plg 30	4070.9	1	1.16	**1.83**
		2	2.14	
		3	2.08	
		4	2.12	
		5	1.63	
Plg 31	4052.7	1	21.68	**21.14**
		2	18.23	
		3	19.80	
		4	20.40	
		5	25.57	
		6	22.15	
		7	20.13	
Plg 32	4047.5	1	7.31	**9.99**
		2	5.62	
		3	10.12	
		4	13.63	
		5	13.29	
Plg 33		1	21.87	**16.80**
		2	22.62	
		3	16.61	
		4	9.29	
		5	13.59	